ABSTRACT

GIFFEN, NICHOLAS J. Particle Size Segregation In Granular Avalanches: A Study In Shocks. (Under the direction of Michael Shearer.)

In this thesis, we explore properties of shock wave solutions of the Gray-Thornton model for particle size segregation in granular avalanches. In these avalanches, particles segregate by size when subject to shear. As the particles roll across each other, other particles fall into the gaps that form, with smaller particles more likely to fit. These small particles fall to the bottom of the avalanche and force the larger particles upward. These processes are called *kinetic sieving* and *squeeze expulsion*. The Gray-Thornton model is a nonlinear scalar conservation law expressing conservation of mass under shear for the concentration of small particles in a bidisperse mixture. In this model, the velocity (and thus, shear) is a function of the height of the avalanche. We first discuss characteristic surfaces of the model, which are used in combination with shock waves to construct and analyze solutions of the model.

Shock waves are weak solutions of the partial differential equation across which the concentration of small particles jumps. For a linear velocity profile, we give criteria on smooth initial conditions under which a shock wave forms in the interior of the avalanche in finite time. Additionally, numerical simulations show how and when these shocks form, verifying our analysis.

Shocks will often lose stability as they are sheared by the flow of the avalanche. Upon the loss of stability a complex structure develops in which a two-dimensional rarefaction wave interacts dynamically with a pair of shocks. This rarefaction represents a mixing zone in which small and large particles are mixed as they are transported up and down (respectively) through the zone. Under a linear velocity profile, the structure of this region twice changes over time before reaching the boundary of the avalanche. We also present a special case where the structure of the mixing region does not change over time. By introducing a scaling, we can find a similarity solution for this case.

Linear velocity profiles are not always present in granular materials, especially in the case of boundary driven shear. Thus, we analyze shock formation from smooth initial data under a general increasing velocity profile. Additionally, we analyze the short time solution of the mixing zone under an increasing velocity profile. Here, we present several cases, with each case more general than the previous one. For each case, we analyze the structure of the mixing zone as much as possible, and discuss limitations to the more general cases. Numerical simulations show how the mixing region evolves for each case.

We look at the evolution of an avalanche that is uniform in the downslope direction. Analysis of this solution is important because it appears in the most general version of the mixing zone problem.

Particle Size Segregation In Granular Avalanches: A Study In Shocks

by

Nicholas J. Giffen

A dissertation submitted to the Graduate Faculty of
North Carolina State University
in partial fulfillment of the
requirements for the Degree of
Doctor of Philosophy

Applied Mathematics

Raleigh, North Carolina

2010

APPROVED BY:

Ralph Smith	Pierre Gremaud
Alina Chertock	Michael Shearer Chair of Advisory Committee

BIOGRAPHY

Nicholas J. Giffen (Nick) was born October 28, 1983 in Charlottesville, Virginia. He grew up as part of a large, active family, consisting of mom, dad, one sister and five brothers. Never a dull moment to be had in the family, he grew up playing a variety sports in his backyard with his siblings. Throughout high school, Nick played the trombone, and he would eventually take his talents to James Madison University where he began as a music major.

At college, Nick switched majors after his second year, and chose mathematics instead. Upon switching majors, Nick met with Dr. James Sochacki, a professor in the mathematics department, to plan out how he would meet all the requirements for a math major in his final two years of college. Dr. Sochacki would become Nick's advisor, and gave him his first taste of research, a summer project on the chaotic double pendulum. Having felt like he experienced only two years of college, Nick decided to apply to graduate school, and was accepted at N.C. State.

For nearly the first two years, Nick was set on only obtaining his masters, but after taking one semester of partial differential equations with Dr. Michael Shearer, Nick found his calling in the subject, and decided to stay on as a Ph.D. student as an RA under Dr. Shearer.

Nick has accepted a position at Novozymes North America Inc. as a Scientist, specifically in the areas of data analysis and model development. The position, in Franklinton, NC, is close enough to Raleigh that Nick has decided not to move away from the city.

ACKNOWLEDGEMENTS

I would like to thank:

- My advisor Michael Shearer for his patience, encouragement, and wisdom. I have learned a lot from you about math and life, and will apply it in my future experiences.
- My committee members Ralph Smith, Alina Chertock, Pierre Gremaud and Peter Bloomfield for their insightful comments and questions and for all they have taught me.
- All of my friends, in and out of the math department, with whom I have enjoyed many good times.
- The professors at N.C. State that have taught me so much.
- The members of AMGSS and the Daniels Lab group for critiquing my work and presentations, and sharing their knowledge with me.
- The National Science Foundation for providing the funding for this research under grants DMS-0604047 and DMS-0636590.
- The staff members who keep the mathematics department organized and running smoothly.
- The professors at James Madison University in music and math, for providing me with a solid academic foundation, especially Dr. Sochacki.
- The members of my soccer teams for some quality teamwork and fun on the field.
- My family for their love and support. Thanks for always being there when I need you most.

TABLE OF CONTENTS

LIST OF FIGURES

Chapter 1

Introduction to Segregation in Granular Materials

Many of us start our day by pouring ourselves a bowl of cereal for breakfast. Later in the day, we might drive past a sign that reads "fallen rock zone". In the evening, many people take medications in the form of a pill to fight off the accumulation of aches or pains throughout the day. What most of us don't realize, is that each of these common daily events involve a complex area of science called granular materials. The study of granular materials and the theory of their dynamics has become an increasingly important area of study among scientists, engineers, and mathematicians. Developments in the theory of granular materials have helped with advancements in many aspects of our daily lives, from morning to night, from home to work to vacation.

This thesis focuses on particle size segregation in granular materials. Specifically, we consider the concentration shocks that arise from a specific nonlinear, multi-dimensional hyperbolic PDE model for particle size segregation. Analysis and numerical simulations help us address two important shock related problems for the model, and for broader generalizations of the model.

1.1 Overview of Granular Materials

Granular materials are defined as a collection of discrete solid macroscopic particles that are large enough so that they are not subject to thermal motion fluctuations [2]. Therefore, temperature changes do not affect granular materials on the macroscopic level [32]. Interactions between individual grains are energy dissipative; for example, inelastic collisions display this behavior. Some granular materials occur naturally, such as nuts, sand, soil, and rice. Other granular materials are manufactured, such as ball bearings, pharmaceuticals, and beads. A dry granular material is one that is either absent of interstitial fluid, such as air or water, or is modeled as such. A granular material is called noncohesive if there are no attractive forces between particles. Thus, the shape of the system is determined by either external boundaries or gravity.

1.1.1 Properties of Granular Materials

Granular materials can display properties of all three phases of matter: solids (a pile of rocks), liquids (sand flowing through a funnel), and gases (strongly agitated materials). However, granular materials also display properties that are different from those of the three states of matter [36]. For example, a granular material in a static pile will begin to flow like a liquid when tilted beyond a critical angle. As this happens, the liquid-like flow occurs only in the boundary layer. This is different from the behavior of ordinary liquids, where the entire fluid flows. However, flowing granular material can then jam into a solid-like state, such as flow out of a poorly designed hopper. The difference between gaseous-like granular materials and a dense gas is that the collisions in granular materials are inelastic. A dense gas exhibits elastic collisions. Due to the dissipative interactions between individual particles in a granular material, the material will come to rest unless energy is continuously supplied to the system. While solid, liquid, and gas dynamics are described by well-developed theories, much less is understood about the variety of properties displayed by granular materials.

Some basic assumptions about granular materials are made in this thesis. First, gravity

dominates interparticle forces, such as electrostatic, air drag, van de Waals, and capillary forces. Thus, particle sizes must be larger that 500μm [15]. All granular mixtures are dry, noncohesive, and dense, meaning particle interactions occur frequently and simultaneously with multiple neighbors. Contacts in the material are non-collisional, resulting in little to no momentum transfer between particles. Finally, a bidisperse mixture consists only of two types of particles that display a difference in only one physical property, such as size, density, shape or roughness.

1.1.2 Importance of Granular Materials

The flow of granular materials is of importance in many areas of science and industry. Geophysical events such as debris flows [9, 28, 29, 30],[47], rockslides[3, 10], lahars [69], pyroclasitc flows [6, 31], and snow and ice avalanches [35] are all large-scale flows that involve particulate solids in a fluid-like state. The nature of these events may pose a great threat to human life and can cause considerable property damage [25, 26, 27, 52, 61, 62] underscoring the importance of studying such granular flows. Problems that arise in modeling these events include predicting runout distance, velocities, and flow over a complex topography in order to define a safety zone to minimize loss of life and property damage. The fluid-like behavior of these systems in combination with the steep slopes that they occur on have yielded numerous models, physical and scaling laws, and experimental results about the flow of granular materials down an incline.

In addition to the geophysical importance for studying granular materials, the study of their flow also arises in engineering applications involving transport of minerals, pharmaceuticals, and certain foods (such as beans and cereals). The mining and bulk chemical industries also process large amounts of granular materials. In fact, the pharmaceutical, food, and bulk chemical industries produce an estimated one trillion killograms of granular materials per year [60].

1.1.3 History of the Study of Granular Materials

The study of granular materials is documented as early as the first century B.C., when the mention of granular flow was made by Lucretius (ca. 98-55 B.C.) [15] when observing poppy

seeds. One of the first applications of granular flow was the hourglass, which was in common use by the thirteenth century [54]. In the late eighteenth century, C. de Coloumb (1736-1806) wrote a paper in which he proposed the idea of static friction [32]. In his paper, he draws conclusions about the equilibrium of earthen embankments and stability of stone structures, leading to his laws of dry friction between solids. His work would later be extended to granular materials when in 1857 W. Rankine considered theoretical implications of friction in granular materials. Rankine developed the principles of active and passive states of particles [51].

From the beginning of the twentieth century on, granular materials have become an increasingly important field of study. Early hypotheses [16, 18, 37] to explain fluidization often lacked a detailed computation of the flow development, and direct observation of the dynamics of granular avalanches had been difficult to make. The difficulty in describing these granular flows arises from an uncertainty in the constitutive equations. The dense regime cannot rely on a kinetic approach to resolve the constitutive equations due to the multicontact interactions between particles as well as friction.

Savage and Hutter [55] introduced a model for avalanches that is based on the depth averaged Saint-Venant approach [13], where the material is assumed to be incompressible and the mass and momentum equations are presented in depth-averaged form. Given the assumption that the flowing layer is thin (much longer in length than height), the depth-averaging approach works quite well, and the Savage and Hutter model yields evolution equations that are very similar in nature to the shallow water equations. A simple friction law between the bed and the bulk material, as well as the inclination of the surface produces the differences from the shallow water equations. However, this approach only works for smooth, or relatively smooth beds and high inclination angles. Experimental results [1, 11, 12, 24, 64, 68] have shown that if the roughness of the bed is of the order of the particle size, then the onset of flow is not described by the simple friction law. Pouliquen [48] introduced a criterion based on the material thickness and inclination angle to describe the onset of granular flow on a rough incline, and along with Forterre [49], extended his results further by amending the friction law used by Savage and

Hutter.

1.2 Segregation in Granular Materials

The flow of granular materials also leads to an interesting phenomenon in that dissimilar particles mix and segregate. The blending and separating of dissimilar particles is of significant importance in the industries mentioned in §1.1.2. In some cases, such as the mineral processing industry [70] and the pharmaceutical industry segregation is desired. On the other hand, in processes where the goal is to mix two cohesionless materials [20, 45, 59] segregation is to be avoided to achieve the desired mixture. Incorrect blending or separation of dissimilar particles often reduces the product quality, and in some cases, can even lead to safety concerns. For example, incorrect blends can create dosage variations in pharmaceuticals, flavor variations in foods, and even gas flow problems in chemical reactors [65]. An inconsistency in a blend can often lead to the rejection of an expensive batch, causing the manufacturers a significant loss of money and reputation. The importance of mixing and segregation highlights the need to have an effective model that describes these processes in regards to dissimilar particles.

1.2.1 Introduction to Granular Segregation

Particles can segregate based on a number of differences between them, such as density, roughness, shape, size, or some other distinguishing characteristic. The mechanism that drives segregation is either one or a combination of many, including, but not limited to, convection, inter-particle percolation, inertia, collisional condensation, clustering, differential air drag, and kinetic sieving. These driving mechanisms are produced when the system undergoes a physical change, such as stirring, shearing, vibrating, or tumbling, to name a few. The different combinations of mechanisms and dissimilarities can lead to two possible segregation patterns. The two patterns are vertical segregation, with one type of particle above the other, and horizontal segregation, where dissimilar particles are displaced side by side.

1.2.2 Kinetic Sieving

Consider a system with particles of two different sizes. Experiments and simulations have shown that under shear, vertical segregation with large particles on top of small particles occurs through a process known as kinetic sieving. This process occurs in slow, dense, dry granular flows, which drives particle size segregation based on the combination of percolation (void filling) and squeeze expulsion. This mechanism is often observed when cohesionless mixtures of different sized particles flow down a rough incline. Here, velocity-induced shear is the physical force that drives the mechanism of kinetic sieving. Void filling occurs when the particles roll and tumble over each other, creating fluctuations in the local void ratio. As gaps form in between particles the small particles tend to fall down in between and fill the gaps. The larger particles are pushed upward by squeeze expulsion, which occurs due to an imbalance in contact forces on a particle which squeezes it up or down. Combining the two, the net percolation velocity of both large and small particles is obtained. This mechanism was identified and quantified in the classic paper of Savage and Lun [56].

1.2.3 Granular Segregation Models

Bridgewater and his colleagues [4, 8, 14] laid the foundation for many theoretical and experimental results in segregation of dry granular materials. Specifically, Drahun and Bridgewater [14] studied the effects of segregation when pouring particles onto a heap. Particle size, density, and shape, as well as free fall height onto the heap were studied for their effects on segregation. Later, Bridgewater developed a continuum approach to investigate particle mixing and segregation over time in an annular shear cell [5]. Savage and Lun [56] introduced the idea of kinetic sieving and provided evidence that it was the driving mechanism behind segregation in shear induced granular flow. Their experiment consisted of an incline chute that material flowed down with a transparent side wall for observation. At the end of the chute, collection bins allowed them to separate the material into at most five distinct layers, where the concentration of small particles was then measured in each layer. Their model utilizes an approach based on statistical

mechanics to introduce the idea of kinetic sieving. They provide a comparison between their theory and their experimental results as well as the experimental results from Bridgewater and colleagues [5].

While the Savage and Lun model has the desired feature of predicting steady-state particle size distribution in a steady uniform flow, one of the drawbacks of their model is that it predicts segregation by kinetic sieving even when gravity is not present. This is a shortcoming in the model, since the percolation of small particles downward by void filling is a gravity driven process. While segregation may occur when there is no gravity, it is driven instead by spatial gradients in the fluctuation energy of dissimilar particles [33, 71]. In 2005, Gray and Thornton introduced a model that was closely linked to Savage and Lun's, but provided a means to introduce gravity into the model [23]. This model is the focus of the work in this thesis.

1.3 Summary of Thesis Chapters

This thesis considers concentration shocks of particle size in granular materials. The formation and stability of these shocks along with the subsequent evolution of unstable concentration shocks are the main topics touched on in this work. Specific analysis, simulations, and numerical solutions are all tied together throughout the thesis to confirm all results.

The model developed by Gray and Thornton [23] is considered for particle-size segregation in granular materials. Chapter 2 deals with the introduction, derivation, and formulation of the model. Modifications are developed to fit the model to generalize the problems of shock formation and shock breaking. A discussion of the numerical method employed in our MATLAB code for the model concludes the chapter.

In Chapter 3 we provide a discussion about characteristics and shocks in the Gray-Thornton model. Additionally, at the end of the chapter we prove a general result regarding the stability of particle-size concentration shocks. In Chapter 4, we address the problem of shock formation under a constant shear rate. Criteria for the formation of shock waves in two-dimensional flow is presented, following a procedure employed by Lax [38] and later brought to use on

multidimensional conservation laws by Conway [7] and Majda [40]. The main difference in the use here, is due to shear within the flow which gives rise to the non-constant coefficients in the PDE. A full analysis of the two-dimensional version of the Gray-Thornton model completely characterizes shock formation from smooth initial data. Numerical simulations and subsequent analysis are used in combination to further verify the analysis. The first part of Chapter 5 deals with the problem of shock wave breaking after a concentration shock loses stability in the case of two dimensional flow under constant shear. The resulting mixing zone has a structure that evolves in three stages. In the first stage, we construct the solution exactly, while the second and third stage constructions consist of shocks and rarefactions that are pieced together to form the mixing region. The latter two stages are constructed through explicit evolution of the first stage, and numerically in the unknown parts of the region. The second part of Chapter 5 concerns a special case of the mixing zone problem, where a piecewise quadratic concentration shock breaks. Chapter 6 talks about a scaling for the Gray-Thornton model, specifically applied to the piecewise quadratic case from Chapter 5.

The next chapter explores generalizations in both shock formation and shock breaking. The shock formation generalization in Chapter 7 is analogous to the work in Chapter 4. However, in this chapter the velocity profile, shear rate, and segregation flux are generalized. We provide characterization of shock formation in three of four possible cases. The fourth case is strictly dependent on initial conditions, and is not addressed here. The latter portion of the chapter concerns generalizations of the shock breaking problem from Chapter 5.

Chapter 2

The Gray-Thornton Model

Gray and Thornton [23] formulated a PDE conservation law as a model for particle-size segregation using binary mixture theory [46, 67], which allows for every point in the material to be occupied by large and small particles. As a result, velocities, pressures, and densities of both phases can be defined everywhere in the material. Individual constituent momentum balances are used to encapsulate the effects of gravity and the resulting modeling is able to compute the temporal and spatial evolution of particle size distribution in a three-dimensional dry granular flow. The main assumptions made by the Gray-Thornton model are that the mixture is bidisperse, all particles have the same bulk density, the bulk flow is incompressible, normal accelerations can be neglected, and diffusive remixing is negligible. In a later paper, Gray and Chuganov include diffusive remixing [21].

2.1 Derivation and Formulation

The variable of interest in the Gray-Thornton model is the concentration of small particles (the ratio of the volume of small particles to the total volume of small and large particles). This variable φ is a function of space in three dimensions (x, y, z) and time t. The volume fraction of large particles will then be $1 - \varphi$. The model is developed within the framework of a granular avalanche, with x being the downslope direction, z normal to the slope, and y in the

cross-slope direction. The slope is at an angle ζ to horizontal. The bulk velocities in the x, y, and z-directions are given by u, v, and w, respectively.

Another assumption is that segregation occurs only in the direction normal to the base of the avalanche z. Therefore, the velocity in the z direction has two components: the bulk velocity and the segregation velocity. The equations for the normal constituent velocities are simply derived from the conservation of momentum equation for each constituent.

$$\rho^\nu \frac{D_\nu \mathbf{u}^\nu}{Dt} = -\nabla p^\nu + \rho^\nu g + \beta^\nu, \quad \nu = s, l, \tag{2.1}$$

where s and l represent the small and large particles, $\mathbf{u} = (u, v, w)$, and $D_\nu/Dt = \partial/\partial t + \mathbf{u}^\nu \cdot \nabla$ is the material derivative. The partial densities, velocities, and pressures are given by ρ^ν, $\mathbf{u}^\nu$, and p^ν, respectively. The gravitational acceleration is given by g, and the interaction force (the force exerted by the other constituent on phase ν) is given by β^ν. In mixture theory, variables are either intrinsic or partial. In this case, an intrinsic variable is independent of the volume fraction of small or large particles. On the other hand, a partial variable is related to an intrinsic variable through a linear volume fraction scaling. The velocity field is the only exception, and is identical in both the partial and intrinsic cases. The bulk density and pressures are related to the constituent quantities by

$$p = p^s + p^l \tag{2.2}$$

and

$$\rho = \rho^s + \rho^l \tag{2.3}$$

In mixture theory, partial variables are related to their physical, or intrinsic, counterparts. In standard mixture theory, the partial and intrinsic velocity fields are identical, while the other fields are related by linear volume fraction scalings

$$\rho^\nu = \varphi^\nu \rho^{\nu *}, \quad p^\nu = \varphi^\nu p^{\nu *}, \quad \mathbf{u}^\nu = \mathbf{u}^{\nu *}, \quad \nu = l, s \tag{2.4}$$

where the superscript * denotes an intrinsic variable and where $\varphi^s = \varphi$ and $\varphi^l = 1 - \varphi$. The forces β^s and β^l are equal in magnitude, opposite in direction, and the intrinsic densities are equivalent and constant, thus equal to the bulk density.

Under the assumption that the normal acceleration is negligible, the sum of the momentum balance components (2.1) for each constituent implies

$$\frac{\partial p}{\partial z} = -\rho g \cos\zeta. \tag{2.5}$$

Since ρ is constant, integrating through the depth of the avalanche h shows the bulk pressure is hydrostatic:

$$p = \rho g(h - z)\cos\zeta. \tag{2.6}$$

When the small particles percolate between the large particles, they support less than their share of the overburden pressure, meaning the large particles must carry more of the load. Therefore, a new pressure scaling is introduced

$$p^l = f^l p, \quad p^s = f^s p \tag{2.7}$$

where f^l and f^s determine the proportion of the hydrostatic load carried by large and small particles respectively. Equation (2.2) implies $f^l + f^s = 1$.

Experimental observations of the kinetic sieving process suggest an analogy with the percolation of fluids through porous solids, thus, Darcy's law motivates an interaction drag of the form [46]

$$\beta^\nu = p\nabla f^\nu - \rho^\nu c(\mathbf{u}^\nu - \mathbf{u}), \quad \nu = l, s \tag{2.8}$$

where c is the coefficient of inter-particle drag and $\mathbf{u} = (\rho^l \mathbf{u}^l + \rho^s \mathbf{u}^s)/\rho$.

The normal constituent velocities w^v are obtained by substituting equations (2.5)-(2.8) into the normal components of (2.1) and using the assumption that the normal acceleration terms

are negligible, to get

$$\varphi^\nu w^\nu = \varphi^\nu w + (f^\nu - \varphi^\nu)(g/c)\cos\zeta, \quad \nu = l, s. \tag{2.9}$$

The significance of f^ν is now clear, for if $f^\nu > \varphi^\nu$ then particles rise and if $f^\nu < \varphi^\nu$ then particles fall. When the two quantities are equal, there will be no motion of particles relative to the bulk. Therefore, the funcion f^ν must satisty the constraint that if only a single type of particle is present, it must support the entire load, i.e.

$$\begin{aligned} f^l &= 1, \quad \text{when } \varphi^s = 0, \\ f^s &= 1, \quad \text{when } \varphi^s = 1. \end{aligned} \tag{2.10}$$

The simplest nontrivial functions that satisfy (2.10) and $f^l + f^s = 1$ are $f^l = \varphi^l + B\varphi^s\varphi^l$ and $f^s = \varphi^s - B\varphi^s\varphi^l$. Substituting these into (2.9) gives

$$w^l - w = q\varphi^s, \quad w^s - w = -q\varphi^l, \tag{2.11}$$

where q is the mean segregation velocity given by $q = (B/c)g\cos\zeta$. These equations show that the large particles move upward with a velocity proportional to the local concentration of small particles and the small particles move downward with a velocity proportional to the local concentration of large particles. There is no segregation when $\varphi^s = 0$ or $\varphi^s = 1$, in other words, when the local concentration consists entirely of all small particles or all large ones. The downslope and cross-slope constituent velocities are equal to the bulk downslope and cross-slope velocities. Consequently, only vertical segregation is induced.

In addition to satisfying conservation of momentum, large and small particles must also satisfy the conservation of mass equation

$$\frac{\partial \rho^\nu}{\partial t} + \nabla \cdot (\rho^\nu \mathbf{u}^\nu) = 0, \quad \nu = s, l. \tag{2.12}$$

Using (2.12) for small particles, along with the formulae for the constituent velocities, the PDE model for the concentration of small particles φ^s becomes

$$\frac{\partial \varphi^s}{\partial t} + \frac{\partial}{\partial x}(\varphi^s u) + \frac{\partial}{\partial y}(\varphi^s v) + \frac{\partial}{\partial z}(\varphi^s w) - \frac{\partial}{\partial z}\left(q\varphi^s\varphi^l\right) = 0. \tag{2.13}$$

Since φ^s is the concentration of small particles, let $\varphi^s = \varphi$ and $\varphi^l = 1 - \varphi$. Using the incompressibility assumption ($\nabla \cdot \mathbf{u} = 0$), (2.13) becomes

$$\frac{\partial \varphi}{\partial t} + u\frac{\partial \varphi}{\partial x} + v\frac{\partial \varphi}{\partial y} + w\frac{\partial \varphi}{\partial z} - \frac{\partial}{\partial z}(q\varphi(1-\varphi)) = 0. \tag{2.14}$$

To be consistent with avalanche models, the variables are nondimensionalized by standard avalanche scalings $x = L\tilde{x},\ z = H\tilde{z},\ (u, v) = U(\tilde{u}, \tilde{v}),\ w = (HU/L)\tilde{w},\ t = (L/U)\tilde{t}$, where U is a typical downslope velocity magnitude, L a typical avalanche length which is much larger than the typical thickness H. The Gray-Thornton model becomes:

$$\frac{\partial \varphi}{\partial t} + u\frac{\partial \varphi}{\partial x} + v\frac{\partial \varphi}{\partial y} + w\frac{\partial \varphi}{\partial z} + S_r\frac{\partial}{\partial z}(\varphi(\varphi - 1)) = 0, \tag{2.15}$$

where $S_r = \dfrac{qL}{HU}$ is the nondimensional proportionality constant. Thus, the mean segregation velocity is constant in the Gray-Thornton model, an idea that is challenged through experimental results in a Couette cell by Daniels and Golick [19] who show the mixing and segregation rates (both of which would be described by S_r) are different. In the absence of gravity, the parameter $S_r = 0$, and no segregation is present, a feature absent from the model proposed by Savage and Lun [56].

2.2 Modifications of the Gray-Thornton Model

The work presented in this thesis explores different physical assumptions of granular flow. Accordingly, the Gray-Thornton model must be modified to accompany these changes. In each case, we consider avalanche flow down an inclined plane in two dimensions. In the first set of

assumptions, the parallel bulk velocity is assumed to be linear, thus yielding a constant shear rate throughout the layer. The flux function is given in (2.15). We consider an initial boundary value problem in §4 with smooth initial data in order to address the problem of shock formation. Additionally, we address the problem of shock wave breaking in §5 under these assumptions. The next set of assumptions considers a nonlinear, increasing velocity profile. Under this circumstance, the shear rate becomes depth-dependent, and for the shock formation problem (see §7.1) we consider a general convex flux. In the other parts of §7 we address the more general versions of shock wave breaking. Although in each case we consider an increasing, nonlinear velocity profile, we also consider relaxing conditions in the Gray-Thornto model in the following ways:

- Constant (S_r) or depth-dependent ($S(z)$) shear rate
- Specific flux ($f(\varphi) = \varphi(\varphi - 1)$) or general convex flux $f(\varphi)$
- Specific ($\varphi_- = 1,\ \varphi_+ = 0$) or general ($\varphi_- > \varphi_+$) concentrations of φ on either side of a shock

2.2.1 Linear Velocity Profile

Consider a two-dimensional chute with parallel upper and lower boundaries, filled with granular material. Assume a linear bulk velocity, consistent with avalanche flow down an incline. Further, assume that the initial concentration of small particles φ_0 is smooth. There is no bulk velocity in the direction normal to the parallel boundaries and, due to the two-dimensional nature of the problem, the model is independent of y. Further, we assume any effect of sidewalls is negligible. Scaling x and t in the model effectively sets the segregation constant $S_r = 1$. Thus, equation (2.15) becomes

$$\frac{\partial \varphi}{\partial t} + u(z)\frac{\partial \varphi}{\partial x} + \frac{\partial}{\partial z}(\varphi(\varphi - 1)) = 0. \tag{2.16}$$

Here, $u(z) = \alpha + 2(1 - \alpha)z$ is a linear velocity profile where α is a parameter that allows the velocity profile to vary from plug flow ($\alpha = 1$) to simple shear ($\alpha = 0$). We consider the case

of simple shear ($\alpha = 0$), and use the scaling $z = \frac{1}{2}\tilde{z},\ x = \frac{1}{2}\tilde{x},\ t = \frac{1}{2}\tilde{t}$. Dropping the tilde notation, (2.16) remains the same, but with $u(z) = z$. We take the upper and lower boundaries to be $z = \pm 1$. The lower boundary ($z = -1$) consists only of small particles, while the upper boundary ($z = 1$) consists only of large particles. This is consistent with no flux boundary conditions. By characterizing the initial data $\varphi_0(x, z)$ in the case of avalanche flow with a linear velocity profile, the problem of shock formation from this initial boundary value problem is completely determined. Further, if a shock does form, this formulation of the model is used to determine the resulting mixing region should the shock lose stability under this geometry.

2.2.2 Nonlinear Velocity Profile

In the case of two-dimensional planar flow in a moving frame where the bulk velocity is nonlinear, we consider three cases in which we modify the PDE.

Case 1: Simple shear. In this case, (2.15) is exactly the same as (2.16), however, $u(z)$ is any monotonically increasing function. This corresponds to the shock breaking example in §7.2.1. We can take φ_- (the concentration of small particles to the left of an interface) to be greater than φ_+, where both φ_- and φ_+ are constant, not necessarily 1 and 0 respectively.

Case 2: Depth-dependent segregation rate. In this case, changes are made to the Gray-Thornton model to account for the depth-dependent segregation rate. The segregation parameter S_r can no longer be assumed to be constant, and instead is taken to be proportional to the derivative of the bulk velocity. Based on this additional generalization, equation (2.15) now becomes

$$\frac{\partial \varphi}{\partial t} + u(z)\frac{\partial \varphi}{\partial x} + \frac{\partial}{\partial z}\left(sa(z)\varphi(\varphi - 1)\right) = 0 \tag{2.17}$$

where $a(z) = |u'(z)|$ is a positive function of the height z. The parameter $s > 0$ sets the segregation rate. For simplicity, in the rest of this work will define $S(z) = sa(z)$.

Case 3: General convex flux. Finally, in addition to the generalization of the bulk velocity profile, we consider a generalization of the flux function $f(\varphi) = \varphi(\varphi - 1)$ used by Gray and Thornton. This is generalized by taking $f(\varphi) : [0, 1] \to \mathbb{R}$ to be convex (i.e. $f''(\varphi) > 0$) where the flux vanishes when the mixture contains a local concentration of all small or all large particles (i.e. $f(0) = f(1) = 0$). Thus, (2.15) becomes

$$\frac{\partial \varphi}{\partial t} + u(z)\frac{\partial \varphi}{\partial x} + \frac{\partial}{\partial z}\left(S(z)f(\varphi)\right) = 0. \tag{2.18}$$

By once again considering smooth initial data $\varphi_0(x, z)$, we tackle the shock formation problem using the assumptions from this case in §7.1. We can resolve three of four possible scenarios, with the final case remaining an open problem.

In both cases 2 and 3, we consider two sub-cases that involve the initial data.
(i) In this sub-case, $\varphi_- = 1$ and $\varphi_+ = 0$. This sub-case is simpler than the following sub-case since the flux term is identically zero in these regions, thus φ_- and φ_+ are solutions to (2.18).
(ii) In this sub-case $\varphi_- > \varphi_+$ are both constant. However, they are not necessarily solutions to (2.18) and thus evolve over time. Shock wave breaking is addressed for both of these sub-cases with numerical simulations in §7. However, the first sub-case can be taken farther to show analytically that a mixing solution exists (but no explicit solution is found), whereas in the second sub-case, only a numerical simulation shows the existence of a mixing zone. This sub-case is considered the generalized shock wave breaking problem.

2.2.3 Uniformity Downslope

To address the case 2(ii) in §2.2.2, we consider the regions where φ_- and φ_+ are constant (and thus uniform in the downslope direction). Consider the two dimensional (x, z) plane where the initial data is uniform in the downslope direction. Then since segregation only occurs in the normal direction, the solution will remain uniform in the downslope direction for all time. This

means we can drop the x-term from (2.17) to get

$$\frac{\partial \varphi}{\partial t} + \frac{\partial}{\partial z}\left(S(z)\varphi(\varphi - 1)\right) = 0. \tag{2.19}$$

Understanding the evolution of constant initial data φ_0 using (2.19) helps us understand how the initially constant regions φ_- and φ_+ evolve near an interface separating the two constant values when studying the problem of shock wave breaking using equations (2.17) and (2.18). We present the full solution to this problem, with general initial data $\varphi_0(z)$ that is uniform in x in §7.3.

2.3 Numerical Simulations of (2.18)

Numerical simulations are used throughout this work to compare explicit or numerical solutions with high resolution simulations. The method chosen employs a forward march in time, upwind difference for linear transport downslope (i.e in the x-direction), and Godunov's method [17] for the nonlinear flux term to describe the vertical transport of particles in the z-direction. The method, a MATLAB code written by Rowe [53] and modified to suit the problems in this work, uses a uniform grid on a rectangle $a \leq x \leq b$, $c \leq z \leq d$ with grid spacing $\Delta x = \Delta z = 1/N$, where $N + 1$ is the number of gridpoints in the z-direction. Let $x_i = i\Delta x,\ z_j = j\Delta z$ be the gridpoints and $t_k = k\Delta t$ be a uniform sequence of times. We choose Δt so that the Courant-Friedrichs-Lewy (CFL) condition is satisfied [39]. Thus, the time step is chosen small enough so that the known information does not leave the grid cell for a single time step. If we let $\varphi(x_i, z_j, t_k) = \varphi^k_{i,j}$, then the forward march in time in the x-direction is given by

$$\varphi^{k+1}_{i,j} = \varphi^k_{i,j} - \Delta t\left(u(z_j)\frac{V}{\Delta x} + S(z_j)\frac{F_l - F_r}{\Delta z}\right). \tag{2.20}$$

Here, V is the upwind method [39]. The sign of V depends on the sign of the velocity profile $u(z_j)$:

$$V = \begin{cases} \varphi^k_{i,j} - \varphi^k_{i-1,j}, & u(z_j) \geq 0, \\ \varphi^k_{i+1,j} - \varphi^k_{i,j}, & u(z_j) < 0. \end{cases} \tag{2.21}$$

The variables F_l and F_r are the left and right numerical fluxes determined from the flux function $f(\varphi)$:

$$F_l = \begin{cases} \min\limits_{\varphi_{i,j} \leq \varphi \leq \varphi_{i,j+1}} f(\varphi), & \varphi_{i,j} \leq \varphi_{i,j+1}, \\ \max\limits_{\varphi_{i,j} \leq \varphi \leq \varphi_{i,j+1}} f(\varphi), & \varphi_{i,j} > \varphi_{i,j+1}, \end{cases} \tag{2.22}$$

$$F_r = \begin{cases} \min\limits_{\varphi_{i,j-1} \leq \varphi \leq \varphi_{i,j}} f(\varphi), & \varphi_{i,j-1} \leq \varphi_{i,j}, \\ \max\limits_{\varphi_{i,j-1} \leq \varphi \leq \varphi_{i,j}} f(\varphi), & \varphi_{i,j-1} > \varphi_{i,j}. \end{cases} \tag{2.23}$$

Since we require $f(\varphi)$ to be a convex function, this allows us to simplify $\min f(\varphi)$ and $\max f(\varphi)$ as

$$\max_{\varphi_l \leq \varphi \leq \varphi_r} f(\varphi) = \max\{f(\varphi_l), f(\varphi_r)\}, \tag{2.24}$$

$$\min_{\varphi_l \leq \varphi \leq \varphi_r} f(\varphi) = \begin{cases} \min\{f(\varphi_l), f(\varphi_r)\}, & f'(\varphi_l) f'(\varphi_r) \geq 0, \\ \min\limits_{\varphi_l < \varphi < \varphi_r} f(\varphi), & f'(\varphi_l) f'(\varphi_r) < 0. \end{cases} \tag{2.25}$$

When the flux function from (2.16) is used, (2.25) becomes

$$\min_{\varphi_l \leq \varphi \leq \varphi_r} f(\varphi) = \begin{cases} \min\{f(\varphi_l), f(\varphi_r)\}, & f'(\varphi_l) f'(\varphi_r) \geq 0, \\ -1/4, & f'(\varphi_l) f'(\varphi_r) < 0. \end{cases} \tag{2.26}$$

Chapter 3

Characteristics and Shocks

The Gray-Thornton PDE

$$\varphi_t + u(z)\varphi_x + f(\varphi)_z = 0, \quad -\infty < x < \infty, \ -1 < z < 1, \ t > 0. \tag{3.1}$$

is a scalar equation in conservation form, so the theory of scalar conservation laws can be applied to construct solutions. In particular, characteristic surfaces and shock waves together are used to construct and analyze the solutions of the PDE. Additionally, a theorem is presented that describes the stability of shock waves (in the sense of hyperbolic PDE [57]).

3.1 Characteristics

Characteristics for the PDE (3.1) are curves for which the solution φ is constant. A characteristic curve $x = x(t), z = z(t)$ passing through the point (x_0, z_0) at a time $t = t_0$ will satisfy the initial value problem

$$\frac{dx}{dt} = u(z); \qquad \frac{dz}{dt} = f'(\varphi); \qquad x(t_0) = x_0; z(t_0) = z_0. \tag{3.2}$$

Note that φ is constant along characteristics. For $u(z) \neq 0$, the system can be solved by eliminating t:

$$u(z)\frac{dz}{dx} = f'(\varphi). \tag{3.3}$$

By making a change of variables, if we set

$$\psi(z) = \int_0^z u(\zeta)d\zeta \tag{3.4}$$

then provided $f'(\varphi) \neq 0$, (3.3) becomes a curve in (x, z) given by

$$\psi(z) - \psi(z_0) = f'(\varphi)(x - x_0). \tag{3.5}$$

Taking $f(\varphi) = \varphi(\varphi - 1)$ (the flux function used by Gray and Thornton) leads to an equation for φ along each characteristic:

$$\varphi = \frac{1}{2}\left(1 + \frac{\psi(z) - \psi(z_0)}{x - x_0}\right). \tag{3.6}$$

To get characteristic curves in space-time for (3.1) just integrate (3.2):

$$x(t) = \int_{t_0}^t u(z(t))dt + x_0, \qquad z(t) = f'(\varphi)(t - t_0) + z_0. \tag{3.7}$$

In the case of a granular avalanche down an incline, the parallel bulk velocity $u(z)$ is assumed to be linear and characteristic curves are parabolic in space-time. More specifically, for $u(z) = z$,

$$x(t; t_0) = \frac{1}{2}f'(\varphi)(t - t_0)^2 + z_0(t - t_0) + x_0, \qquad z(t; t_0) = f'(\varphi)(t - t_0) + z_0. \tag{3.8}$$

In other words, for each value of φ and t, (3.8) is a contour of φ parameterized by t_0. For example, if $f(\varphi) = \varphi(\varphi - 1)$, then (3.8) satisfies (3.6) with $\psi(z) = z^2/2$.

3.2 Shocks

Shock wave solutions of (3.1) are weak solutions of the PDE in which $\varphi(x,z,t)$ is discontinuous across an interface, given here by a curve $z=\hat{z}(x,t)$. From the divergence theorem, we obtain the Rankine-Hugoniot jump condition (as in [63]) which relates the normal speed of a shock wave to the jump in φ and the flux of φ across the wave. Using (2.18) we see in (t,x,z) space that if

$$F=(\varphi,u(z)\varphi,S(z)f(\varphi)) \tag{3.9}$$

then

$$\nabla\cdot F=\varphi_t+u(z)\varphi_x+(S(z)f(\varphi))_z=0. \tag{3.10}$$

Therefore, from the divergence theorem,

$$\int_U \nabla\cdot F dx=0=\int_{\partial U} F\cdot n dS \tag{3.11}$$

where $n=(z_t,z_x,-1)$. Thus, $[F\cdot n]=0$, giving

$$\hat{z}_t[\varphi]+u(\hat{z})\hat{z}_x[\varphi]-S(\hat{z})[f(\varphi)]=0. \tag{3.12}$$

Here, square brackets indicate the jump between the left and right-hand limits so that $[h]=h_+-h_-$. By letting $\varphi_\pm(x,t)=\varphi(x,\hat{z}(x,t)\pm,t)$ denote the one-sided limits of φ and dividing by $[\varphi]$, equation (3.12) becomes (dropping the hat notation):

$$z_t+u(z)z_x=S(z)G(\varphi_+,\varphi_-);\qquad \text{where } G(\eta,\nu)=\begin{cases}\dfrac{f(\eta)-f(\nu)}{\eta-\nu},\ \eta\neq\nu\\[2ex] G(\eta,\eta)=f'(\eta),\ \eta=\nu\end{cases} \tag{3.13}$$

This equation is a nonlinear conservation law coupled to the weak solution $\varphi(x,z,t)$. If $\varphi_\pm$ are known, then (3.13) can be solved using the method of characteristics to get the evolution of the

interface $\hat{z}(x,t)$. It is important to note that if $f(\varphi) = \varphi(\varphi - 1)$, then (3.13) becomes

$$z_t + u(z)z_x = S(z)(\varphi_- + \varphi_+ - 1). \tag{3.14}$$

Further, if $\varphi_- = 1$ and $\varphi_+ = 0$ (regions of all small and large particles respectively), then (3.14) becomes Burgers' equation. For $u'(z) > 0$ an initially decreasing interface $z = \hat{z}(x,t)$ evolves as it would in Burgers' equation. However, since we are studying concentrations of small particles, φ is actually the variable of interest rather than $\hat{z}$. Thus, for regions where $\dfrac{d\hat{z}}{dx} > 0$, the interface $\hat{z}(x,t)$ is unstable, as shown as a theorem in §3.3.

To determine the stability of $\hat{z}(x,t)$ with an initial condition, the Lax entropy condition [38] ensures that the solution can be continued at least for a short time with the same structure. Thus, the solution $\varphi(x,z,t)$ evolves, as does the shock with it. The Lax entropy condition guarantees that characteristic surfaces emanating from the shock would cross, resulting in a multi-valued solution in the overlapping region. Wellposedness is obtained from constructing a shock in this region that satisfies (3.13). This construction corresponds to *structural* stability (short-time persistence), and is standard in hyperbolic equations literature [57] when solutions are constant along characteristics. This is opposed to *asymptotic* or long-time stability which appears often in dynamical systems.

3.3 Shock Stability

For stable shocks, the characteristic surfaces in space-time overlap, meaning that the single-valuedness of the solutions is recovered by continuing the shock into this region. In the sense of a bi-disperse mixture of small and large particles, the shock will be stable if there is a greater density of large particles above the shock interface than below. This result is proved in [58] for $f(\varphi)$ quadratic, convex, and with $f(0) = f(1) = 0$. Let $z = \hat{z}(x,t)$ be a smooth interface with $\varphi_\pm$ as described before.

Theorem 3.3.1 *The interface $z = \hat{z}(x,t)$ is dynamically stable if $\varphi_+ < \varphi_-$ and unstable if $\varphi_+ > \varphi_-$.*

Proof: To show the characteristic surfaces overlap, the speeds of the characteristics and shock normal the shock are calculated at a time $t = t_0$. Suppose $z = \hat{z}(x_0, t_0)$ is the shock $\mathcal{S}$ at $t = t_0$ being parameterized by x_0. Let characteristics originating at $(x, z) = (x_0, \hat{z}(x_0, t_0))$ with $\varphi = \varphi_\pm$ be denoted $x_\pm(t; x_0), z_\pm(t; x_0), t > t_0$, forming characteristic surfaces. Then from each $(x_0, z_0) \in \mathcal{S}$, the normal component of the tangents $\partial_t(x_\pm(t; x_0), z_\pm(t; x_0))$ at $t = t_0$ is given by

$$\lambda_\pm = (x', z') \cdot \hat{N} \tag{3.15}$$

where $x'(t), z'(t)$ are given by the characteristic equations. Thus,

$$\lambda_\pm = \frac{1}{\sqrt{1 + \hat{z}_x^2}}(-\hat{z}_x, 1) \cdot (u(\hat{z}), S(z)f'(\varphi_\pm)). \tag{3.16}$$

Similarly, the velocity of the shock at a fixed $x = x_0$ is given by $(\dot{x}, \dot{z}) = (0, \hat{z}_t)$. Thus, the speed in the normal direction to the shock surface $(x, \hat{z}(x,t), t)$ is

$$\sigma = \hat{N} \cdot (\dot{x}, \dot{z}) \tag{3.17}$$

which becomes

$$\sigma = \frac{1}{\sqrt{1 + \hat{z}_x^2}}(-\hat{z}_x, 1) \cdot (0, -u(\hat{z})\hat{z}_x + S(z)G(\varphi_+, \varphi_-)) \tag{3.18}$$

with $\hat{z}_t$ coming from (3.13). Since f is convex, then for $\varphi_+ < \varphi_-$ it results that $f'(\varphi_+) < G(\varphi_+, \varphi_-) < f'(\varphi_-)$. The inequalities are reversed if $\varphi_+ > \varphi_-$. A simple comparison of the speeds (3.16),(3.18) completes the proof. ■

Chapter 4

Shock Formation

The formation of shocks from smooth initial data in nonlinear hyperbolic systems is well documented for a single space dimension [34]. However, in multiple space dimensions, analysis is restricted mainly to scalar equations, [7, 40]. The novelty here is that shock formation is discussed in great depth for an equation with one non-constant coefficient, the parallel bulk velocity $u(z)$. Consider the initial value problem

$$\varphi_t + u(z)\varphi_x + f(\varphi)_z = 0, \quad -\infty < x < \infty,\ -1 \le z \le 1,\ t > 0 \tag{4.1a}$$

$$\varphi(x, z, 0) = \varphi_0(x, z) \quad -\infty < x < \infty,\ -1 \le z \le 1, \tag{4.1b}$$

with φ_0 smooth. By characterizing the initial data, we can show whether a shock forms on the interior of this domain. Since solutions of scalar conservation laws remain bounded, a singularity in the solution involves the gradient becoming unbounded. For a nonlinear, scalar equation in multiple space dimensions with constant coefficients, a simple Ricatti equation governs the evolution of the magnitude of the gradient [40]. However, since equation (4.1) has a non-constant coefficient, the evolution is more complex.

It should be noted that shock waves also form at the horizontal boundaries $z = \pm 1$. Physically, this corresponds to a region of large particles (which we call a *layer*) forming at $z = 1$

which occurs as soon as the first large particles reaches that boundary. A similar layer develops at $z = -1$ with small particles. Such a layer can be a part of a continuous solution in which $\varphi = \varphi(x, z, t)$, but only if there is a layer already present initially. However, if the layer is not present initially, then a boundary shock develops between the layer and the interior region. The discussion of shock formation excludes these boundary shocks, and only focuses on formation in the interior of the region, away from these boundary regions.

4.1 Analysis of interior shock formation

The defining feature of shock formation in particle-size segregation is a jump in the concentration φ of small particles. Thus, it is sufficient to look at $\nabla\varphi$ when discussing shock formation of such systems. To discuss shock formation in the interior of the physical domain, a simple renaming of variables is introduced. Letting $(v, w) = (\varphi_x, \varphi_z)$ and differentiating (4.1a) successively with respect to x and z, the resulting system becomes

$$\frac{dv}{dt} = -f''(\varphi)vw \tag{4.2a}$$

$$\frac{dw}{dt} = -u'(z)v - f''(\varphi)w^2. \tag{4.2b}$$

Here, $\frac{d}{dt} = \partial_t + u(z)\partial_x + f'(\varphi)\partial_z$ is the convective derivative along a characteristic (3.2) on which φ is constant. System (4.2) is autonomous only in the case of simple shear, i.e., when $u(z)$ is linear (for the non-autonomous case, see §7.1). System (4.2) can be treated for general $f(\varphi)$ by scaling $f''(\varphi)$. As a result, the phase portrait may look different from Figure 4.1, but will still display the similar features. Figure 4.1 utilizes the specific conditions $u(z) = z, f(\varphi) = \varphi(\varphi-1)$, system (4.2) becomes:

$$\frac{dv}{dt} = -2vw \tag{4.3a}$$

$$\frac{dw}{dt} = -v - 2w^2. \tag{4.3b}$$

Three properties of (4.3) are:

(1) The system is invariant under $t \to t/\alpha,\ v \to \alpha^2 v,\ w \to \alpha w$ for any $\alpha \neq 0$. In particular (with $\alpha = -1$), $v(t)$ is even, and $w(t)$ is odd if $w(0) = 0$.

(2) The system has a first integral, with solutions lying on the conic sections

$$w^2 + \kappa v^2 + v = 0, \tag{4.4}$$

where κ is a constant of integration. For $\kappa > 0$, the curves are ellipses, and hyperbolae for $\kappa < 0$. If $\kappa = 0$, this is simply the parabola $v = -w^2$. The (v, w) phase portrait is shown in Figure 4.1.

(3) The solution to (4.3) with initial conditions $v(0) = v_0, w(0) = w_0$ is

$$v(t) = \frac{v_0}{q(t)}, \quad w(t) = \frac{w_0 - v_0 t}{q(t)} \tag{4.5}$$

with $q(t) = 1 + 2w_0 t + v_0 t^2$. Since $q(t)$ is quadratic in time, then the smallest positive zero (if any exists) will be the time at which $\nabla\varphi = (v, w)$ develops a finite time singularity. The zeros of $q(t)$ are

$$t_\pm(v_0, w_0) = \begin{cases} \dfrac{w_0}{v_0} \pm \dfrac{1}{v_0}\sqrt{w_0^2 + v_0}, & \text{if } v_0 \neq 0 \\ -\dfrac{1}{2w_0} & \text{if } v_0 = 0, w_0 \neq 0. \end{cases} \tag{4.6}$$

This results in four different cases.

(a) If $v_0 > 0$, then $t_- < 0 < t_+$.

(b) If $-w_0^2 \leq v_0 \leq 0$, and $w_0 < 0$ then $0 < t_+ \leq t_-$.

(c) If $-w_0^2 \leq v_0 \leq 0$, and $w_0 > 0$, then $t_\pm < 0$.

(d) If $v_0 < -w_0^2$, then $t_\pm$ are complex.

In cases (a) and (b), the phase portrait is unbounded and involves finite time blow-up; $t_+ > 0$ is the smallest time for which $q(t) = 0$, meaning a shock has formed. Conversely, for bounded trajectories as in cases (c) and (d), solutions decay algebraically to the origin as

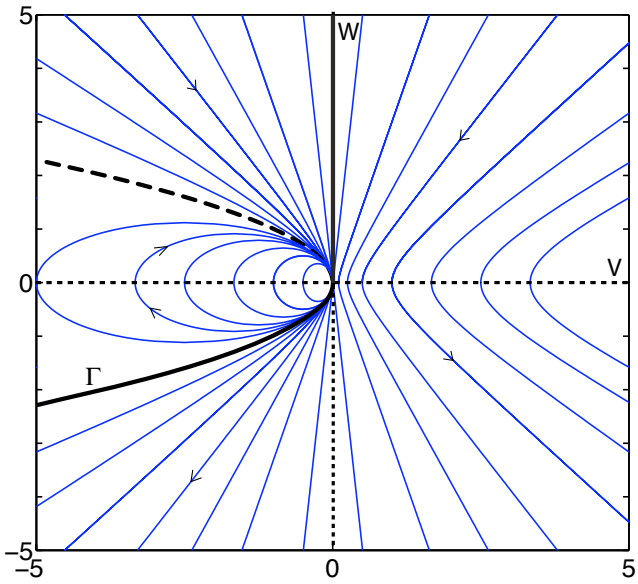

Figure 4.1: Phase portrait for system (4.3).

$t \to \infty$; the roots $t_\pm$ are either complex or negative. Since blow-up of $\nabla\varphi$ on characteristics is determined by these solutions, precise conclusions can be drawn for shock formation based solely on the gradient of the initial data $\nabla\varphi_0 = (v_0, w_0)$. Let Γ be the union of the curve $\{(v_0, w_0) : v_0 = -w_0^2, w_0 < 0\}$ with the positive w_0 axis $\{(0, w_0) : w_0 \geq 0\}$, and let $\mathcal{D}$ be the region to the right of Γ in the (v, w) plane. Then finite time shock formation can be characterized for the initial value problem on the entire plane

$$\varphi_t + z\varphi_x + (\varphi(\varphi - 1))_z = 0, \quad -\infty < x, z < \infty, \ t > 0 \tag{4.7a}$$

$$\varphi(x, z, 0) = \varphi_0(x, z) \quad -\infty < x, z < \infty. \tag{4.7b}$$

with the following theorem.

Theorem 4.1.1 *Let $\varphi_0 \in C^1(\mathbb{R}^2)$, with $0 \leq \varphi_0(x, z) \leq 1$ for all $(x, z) \in \mathbb{R}^2$. If $\nabla\varphi_0(x, z) = (v_0, w_0)$ lies in $\mathcal{D}$ for any (x, z), then the solution $\varphi(x, z, t)$ of the initial value problem (4.7)*

develops a singularity: $\sup_{(x,z)} |\nabla\varphi(x,z,t)| \to\infty$ *as* $t \to t^*-$ *in finite time* t^* *given by*

$$t^* = \inf\{t_+(\nabla\varphi_0(x,z)) : \nabla\varphi_0(x,z) \in \mathcal{D}\} \tag{4.8}$$

Proof: If $(v_0, w_0) \in \mathcal{D}$, then $t_+ > 0$ is real, and t_- is either negative or greater than t_+. Individual contours evolve according to (3.2), and the normal $(v, w) = \nabla\varphi$ evolves along characteristic curves (on which φ is constant) according to (4.3). Consequently, the singularity $|\nabla\varphi| \to \infty$ develops at the smallest value of t_+, evaluated on the initial data, as in (4.8). ■

The theorem can be interpreted by dividing $\mathcal{D}$ and its complement in the (v_0, w_0) plane into four regions in which the behavior of the characteristics acts differently.

(i) $v_0 > 0, w_0 > 0$. In this case, the trajectory lies on the hyperbola given by (4.4) with $\kappa = \kappa_0 < 0$. From Figure 4.1, the phase portrait clearly shows that $|\nabla\varphi| = |(v, w)|$ decreases, meaning contours are spreading out. Once the trajectory crosses the v-axis at $t = w_0/v_0$ from (4.5), contours of φ become vertical in (x, z), tip over, and begin to compress as $\nabla\varphi = (v, w)$ has now entered the fourth quadrant of the phase portrait.

(ii) $v_0 > 0, w_0 < 0$. Here, $|\nabla\varphi| = |(v, w)|$ increases corresponding to a compressing of the contours of φ. Eventually, $v(t)$ and $w(t)$ blow-up in a finite amount of time, given by the positive zero of $q(t)$ in (4.6). At this time, $\varphi(x, z, t)$ develops a jump discontinuity at this value of (x, z).

Cases (i) and (ii) together show that $|\nabla\varphi| \to \infty$ along the characteristic as t increases if $\varphi_x = v > 0$ initially. Physically, a region of more small particles has developed below a region with a higher concentration of large particles; subsequent segregation sharpens the profile of φ, eventually forming a shock.

(iii) $-w_0^2 < v_0 < 0, w_0 < 0$. In this case, the trajectory lies on a hyperbola given by (4.4) with $\kappa = \kappa_0 < 0$. However, this time the trajectory lies in the third quadrant, since $v_0 < 0$. Once again, $|\nabla\varphi| = |(v, w)|$ increases, with blowup time given by t_+, the smaller of the two

positive zeros of $q(t)$ in (4.6). Here, the contours always have a negative slope as they get closer together, quickly forming a shock.

(iv) In the remaining portion of the (v, w) plane for which $w_0 > -\sqrt{v_0},\ v_0 < 0$, the contours may switch from having negative slope (if $w_0 < 0$) to a positive one (when $w > 0$). In this case, $|\nabla\varphi|$ increases before decreasing to zero, corresponding to an initial compression of the contours, before they expand. However if $w_0 > 0$, then $|\nabla\varphi|$ decreases monotonically to zero. In other words, the contours start expanding and continue to do so. Note that anywhere in this region $|\nabla\varphi| = |(v, w)| \to 0$ as $t \to \infty$, meaning $(\varphi_x, \varphi_z) \to (0, 0)$, or in other words, the solution $\varphi(x, z, t)$ is smoothening out and tending toward a constant.

4.2 Shock formation example

The phase portrait and subsequent analysis of the shock formation time given by (4.6) and (4.8) from Theorem 4.1.1 paint a complete picture of intetrior shock formation for smooth initial data. Consider the following initial data:

$$\varphi_0(x, z) = \pm 0.1 \tan\left(\frac{\pi}{2}z\right) + \frac{1}{2} \pm x. \tag{4.9}$$

This initial condition represents initial data from each of the four quadrants of the phase portrait, depending on the choices of sign, which represent each of the four cases (i-iv) of §4.1. The initial gradient

$$\nabla\varphi_0 = (v_0, w_0) = \left(\pm 1, \pm 0.1\frac{\pi}{2}\sec^2\left(\frac{\pi}{2}z\right)\right) \tag{4.10}$$

is used to find the solution along each trajectory (4.5), as well as the blow-up time (4.8).

(i) In the first case, the gradient is positive in both the v and w directions, meaning the positive sign is chosen in both components of (4.10). As described in case (i) from §4.1 the interior contours initially expand and have a negative slope in the (x, z) plane. At

$$t = w_0/v_0 = 0.1\frac{\pi}{2}\sec^2\left(\frac{\pi}{2}z\right) \tag{4.11}$$

each contour becomes vertical, tips over and the slope of the contour becomes positive as $\nabla\varphi$ crosses the v-axis and enters the fourth quadrant. The first slope to do so is the slope given by the minimum value of t in (4.11); this occurs at $z = 0$ with $t \approx 0.157$. Now that the trajectories have entered the fouth quadrant, they compress until a shock forms. Using (4.6) and (4.8), the shock formation time becomes

$$t^* = \inf_z \left\{ t_+(z) = 0.1\frac{\pi}{2}\sec^2\left(\frac{\pi}{2}z\right) + \sqrt{\left(0.1\frac{\pi}{2}\sec^2\left(\frac{\pi}{2}z\right)\right)^2 + 1} \right\}. \tag{4.12}$$

The infimum is actually achieved at the minimum value, which again occurs at $z = 0$ at a time of $t^* \approx 1.169$. Thus, an interior shock has first formed at this time t^* at the point $(x, z) = (0, 0)$.

(ii) In this case, contours that initially start out with all positive slope in (x, z) and an initial gradient pointing toward the fourth quadrant. Here, contours simply compress until they form a shock, which occurs rapidly using the initial data in this example. Fourth quadrant initial data are represented by taking the positive sign for v_0 and the negative sign for w_0 from (4.10). The blow-up time now becomes

$$t^* = \inf_z \left\{ t_+(z) = -0.1\frac{\pi}{2}\sec^2\left(\frac{\pi}{2}z\right) + \sqrt{\left(0.1\frac{\pi}{2}\sec^2\left(\frac{\pi}{2}z\right)\right)^2 + 1} \right\}. \tag{4.13}$$

With an unbounded x domain, the infimum occurs as $x \to \infty, z \to \pm 1$, yielding $t^* = 0$. However, using a bounded domain $-1 \le x, z \le 1$, the infimum occurs at $x = \pm 1,\ z \approx \pm 0.874$, giving a blow-up time of $t^* \approx 0.121$. A stable shock has completely formed leaving a fully segregated material at the maximum value of (4.13); this is when $z = 0$ at a time of $t^* \approx 0.855$. In other words, shocks forms quickly at the outer ends of the domain $x = \pm 1$ where the initial gradient is the steepest, and move in toward and meet at the middle at $x = 0$, resulting in complete segregation with large particles above small ones.

(iii) Taking the negative sign for both v_0 and w_0 puts the initial data in the third quadrant of the phase portrait. Where the gradient is steep initially, with x and z near ± 1, the initial data lie to the right of Γ in region $\mathcal{D}$ from §4.1 and a shock eventually forms. On the other

hand, in areas of shallow initial gradient, the initial data falls to the left of Γ where trajectories head toward the origin and contours expand. The initial data in the third quadrant that lie on Γ is given by $v_0 = -w_0^2$. Solving this equation using (4.10) yields $z_0 \approx \pm 0.741$ which subsequently gives $x_0 \approx \mp 0.732$. In other words, in areas where $|x_0| \gtrapprox 0.732$ a shock forms, and no shock forms from initial data in the complementary region. The initial shock formation time is found using the same procedure as case (ii), yielding the same values $t^* = 0$ on an unbounded domain, and $t^* \approx 0.121$ on the domain $-1 \le x, z \le 1$. Unlike case (ii), a shock does not completely segregate small and large particles, and instead the interior mixing region after an initial compression until $t = w_0/v_0 \approx 0.157$ tilts over and expands.

(iv) In the simplest of the four cases where v_0 uses the negative sign in (4.10) and w_0 the positive, contours expand as $|\nabla\varphi| \to 0$. As seen from Figure 4.1 the gradient remains bounded (and decrese monotonically) as trajectories head toward the origin. The only shocks that form are the shocks propagating inward from the boundary (not interior shocks).

This example, with initial φ_0 given by (4.9) and initial gradient $\nabla\varphi_0$ by (4.10) encompasses all the possible outcomes for shock formation using (4.1) with $u(z) = z$ and $f(\varphi) = \varphi(\varphi - 1)$. The initial data determines not only if a shock forms, but at what specific time the shock will form. Analysis of the the third quadrant distinguishes between initial data where interior shocks form, and initial data where a smooth mixing region occurs. The time to complete segregation is found in the second quadrant. The behavior of (4.1) is well understood from analysis of the four cases in this example, and is verified using numerical simulations in §4.3.

4.3 Shock formation simulations

The results from §4.2 are illustrated in the first set of numerical simulations in this section. Subsequent simulations are just to verify and confirm the behavior found in §4.1 and §4.2. The finite difference code, written initially by Rowe [53] and modified for these specific examples, employs an upwind differencing in x, and a first order Godunov method in z with an explicit time step (see §2.3). The computational domain is $-3 \le x \le 3$, $-1 \le z \le 1$ with results

plotted on the smaller, bounded domain $-1 \leq x \leq 1,\ -1 \leq z \leq 1$. The smaller domain means that time can be computed up to $t = 2$ so that effects of the lateral boundaries at $x = \pm 3$ are not noticed. Boundary conditions at $z = \pm 1$ ensure that particles do not penetrate the boundaries. These conditions

$$\varphi(x, -1) = 1, \quad \varphi(x, 1) = 0 \tag{4.14}$$

physically equate to a layer of all small particles at the bottom and a layer of all large particles at the top (despite an actual system having a free surface at the top) so that mixing and segregation do not occur beyond the boundaries. These conditions are consistent with no-flux boundary conditions $f(\varphi) = 0$, but are easier to use in the numerical code. The boundary conditions (4.14) actually amount to a horizontal stationary shock if $\varphi = 0$ next to $z = -1$ (and respectively $\varphi = 1$ next to $z = 1$). The horizontal, stationary shock remains until the first small particle reaches the bottom (or, respectively, until the first large particle reaches the top $z = 1$). When this occurs, a boundary shock forms and propagates toward the interior. These shocks are not interior shocks characterized in §4.1 and §4.2, but rather just layers of small or large particles accumulating at the bottom or top.

The first set of four simulations uses the initial data given by (4.9) and (4.10) from §4.2. Each simulation corresponds to one quadrant of Figure 4.1 and to a corresponding case (i)-(iv) in §4.2.

In Fig. 4.2, $\nabla\varphi_0 = (v_0, w_0)$ is in the first quadrant. Corresponding to case (i) from §4.2, contours of φ initially spread out, and then steepen as the normal $\nabla\varphi$ rotates clockwise. As the contours reach the boundaries $z = \pm 1$, a layer of small particles grows from $z = -1$, with a sharp shock wave interface propagating upwards. Similarly, a layer of large particles grows from $z = 1$, led by a shock wave propagating downwards. Between these shocks, contours continue to rotate, until $\nabla\varphi$ enters the fourth quadrant. The first contour whose slope enters into the fourth quadrant is the contour at $z = 0$ and the contour becomes vertical at $t \approx 0.157$ (between the first and second frames of Fig. 4.2). Subsequently, the interior contours compress

where they have positive slope, with a corresponding steepening of the graph of φ. At $t \approx 1.169$ (between the fifth and sixth frames) an interior shock has formed at $z = 0$ in between the boundary shocks.

In Fig. 4.3, $\nabla\varphi_0 = (v_0, w_0)$ is in the fourth quadrant everywhere it is non-zero, corresponding to case (ii) from §4.2. Here, two interior shocks form quickly, where the gradient is steepest, which happens to be at the edges $x = \pm 1$ at $t \approx 0.121$ (between the first and second frames). The shocks then propagate toward the center of the domain like two zippers zipping closed the mixed region. Eventually full segregation is achieved at $t \approx 0.855$.

In Fig. 4.4, $\nabla\varphi_0 = (v_0, w_0)$ is in the third quadrant everywhere. The initial data corresponds to that from case (iii) in §4.2. The initial gradient is closer to vertical, i.e., outside the parabola $v_0 = -w_0^2$, towards the lateral boundaries where $|x_0| \gtrapprox 0.732$. In these regions, the gradient quickly blows up, yielding a shock first at the boundaries of the domain $x = \pm 1$ at $t \approx 0.121$ (around the second frame). In the region where $|x_0| \lessapprox 0.732$, the mixed region evolves by first rotating. Contours then tip over at $t \approx 0.157$ (between the second and third frames) and spread as the gradient approaches the origin after crossing the w-axis. The subsequent evolution consists of a pair of shocks trapping a central mixing region.

In Fig. 4.5, $\nabla\varphi_0 = (v_0, w_0)$ is in the second quadrant everywhere. This being case (iv) in §4.2, contours simply rotate and spread out as $\nabla\varphi$ proceeds along a trajectory to the origin. Contours near the upper and lower boundaries quickly touch the boundaries, generating layers of small and large particles. The only shocks in this solution form the boundaries of these layers.

A simple note must be made that in case (iii), a shock appears in the second frame at $t = 0.1$ when the predicted shock formation time is not until $t =\approx 0.121$. This can be attributed to numerical error from the Godunov method used in the z-direction, as a first order method can often result in an unclear placement of shocks visually. Otherwise, each of these simulations strongly support the analytic results from the example in §4.2. The same features described in cases (i)-(iv) are found in the corresponding figures. Additionally, each of the times at which

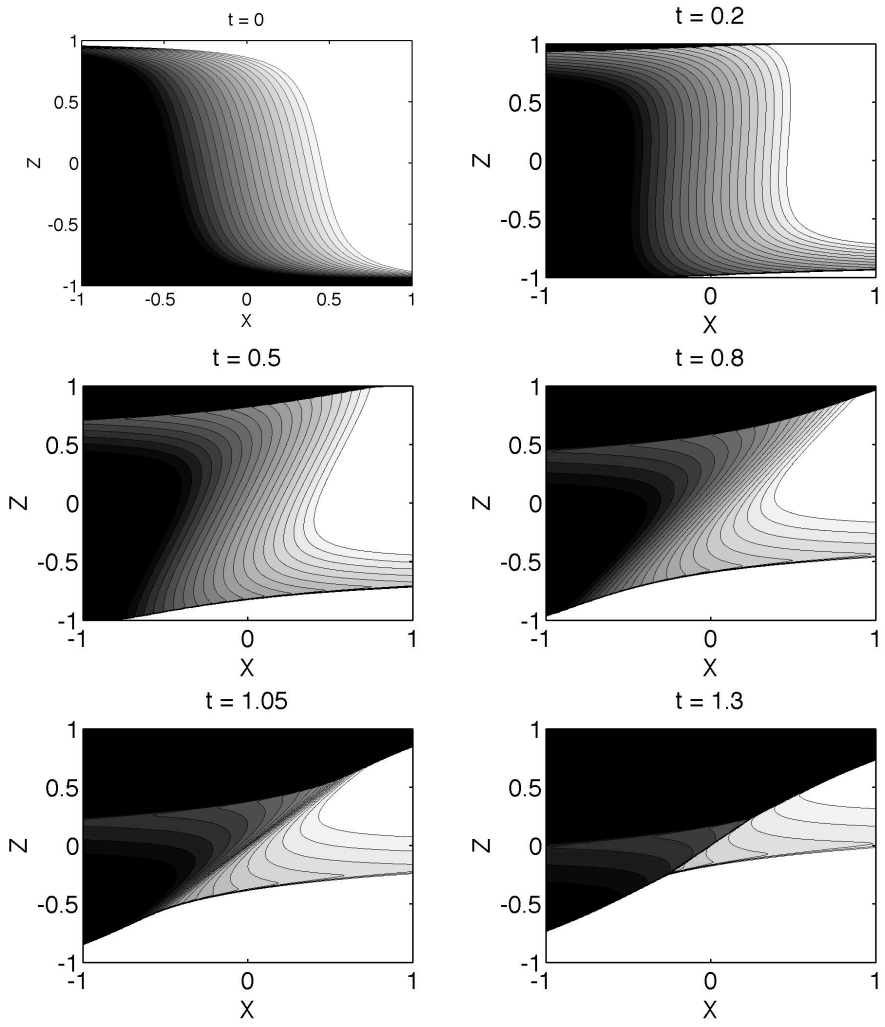

Figure 4.2: Shock formation with $v_0, w_0 > 0$.

shocks form, or trajectories cross into different quadrants correspond to the correct frames.

In the second set of simulations, φ varies inside the unit circle $\{(x, z) : x^2 + z^2 < 1\}$. Outside of the unit circle, a constant value of φ is taken so that the initial condition across the unit circle remains smooth. The two cases are:

(A) The region outside the unit circle consists of all large particles where $\varphi = 0$. Then $\varphi_0(x, z) = 1 - r$ for $x^2 + z^2 = r^2$ with $r \in [0, 1]$. Thus, $\varphi = 0$ at $r = 1$ giving a continuous initial condition across $r = 1$, and $\varphi = 1$ at $r = 0$.

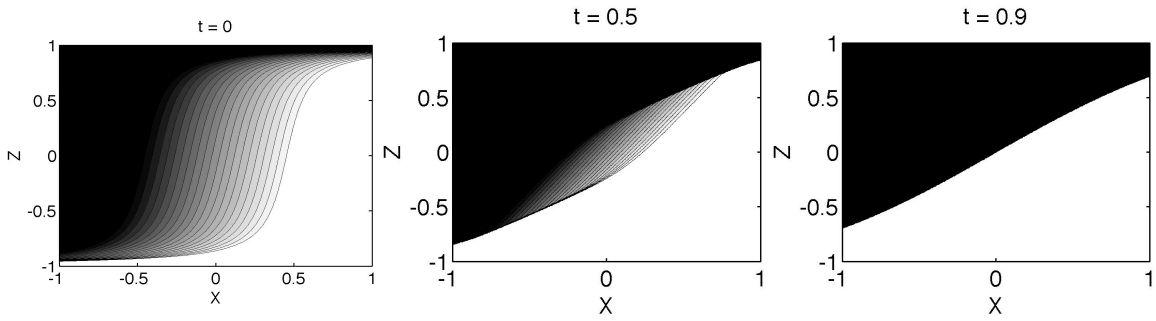

Figure 4.3: Shock formation with $v_0 > 0,\ w_0 < 0$.

(B) The region outside the unit circle consists of all small particles where $\varphi = 1$. Then $\varphi_0(x, z) = r$ for $x^2 + z^2 = r^2$ with $r \in [0, 1]$. Thus, $\varphi = 1$ at $r = 1$ giving a continuous initial condition across $r = 1$, and $\varphi = 0$ at $r = 0$.

In Fig. 4.6 corresponding to (A), $\nabla\varphi_0$ points toward the origin in (x, z). For example, if (x_0, z_0) are both negative, then $\nabla\varphi_0 = (v_0, w_0)$ points toward the first quadrant. Thus, $(v_0, w_0) = \nabla\varphi_0(x_0, z_0)$ is in the quadrant opposite (x_0, z_0). As time progresses, the contours in the upper half of the second frame begin to compress, consistent with $\nabla\varphi_0$ originating in the third or fourth quadrants. The contours on the bottom half of the second frame are spreading out, as $\nabla\varphi$ moves toward the origin. At $t = 0.5$ (which is shown to be exact using Theorem 4.1.1), a shock forms in the upper half of the picture; this is consistent with $\nabla\varphi_0$ lying in the third or fourth quadrant. As t increases, the contours in the bottom half of the fourth frame continue to spread out.

In Fig. 4.7 corresponding to (B), $\nabla\varphi_0$ points away from the origin $(x, z) = (0, 0)$. For example, if (x_0, z_0) are both negative, then $\nabla\varphi_0 = (v_0, w_0)$ points toward the third quadrant. Thus, (v_0, w_0) have the same sign as $(x_{,0}\,, z_0)$ respectively. As time progresses, the contours in the lower half of the second frame begin to compress, consistent with $\nabla\varphi_0$ originating in the third or fourth quadrants. The contours on the top portion of the second frame are spreading out, as $\nabla\varphi$ moves toward the origin. At $t = 0.5$, a shock forms in the upper half of the picture; this is consistent with $\nabla\varphi_0$ lying in the third or fourth quadrant. As t increases, the contours

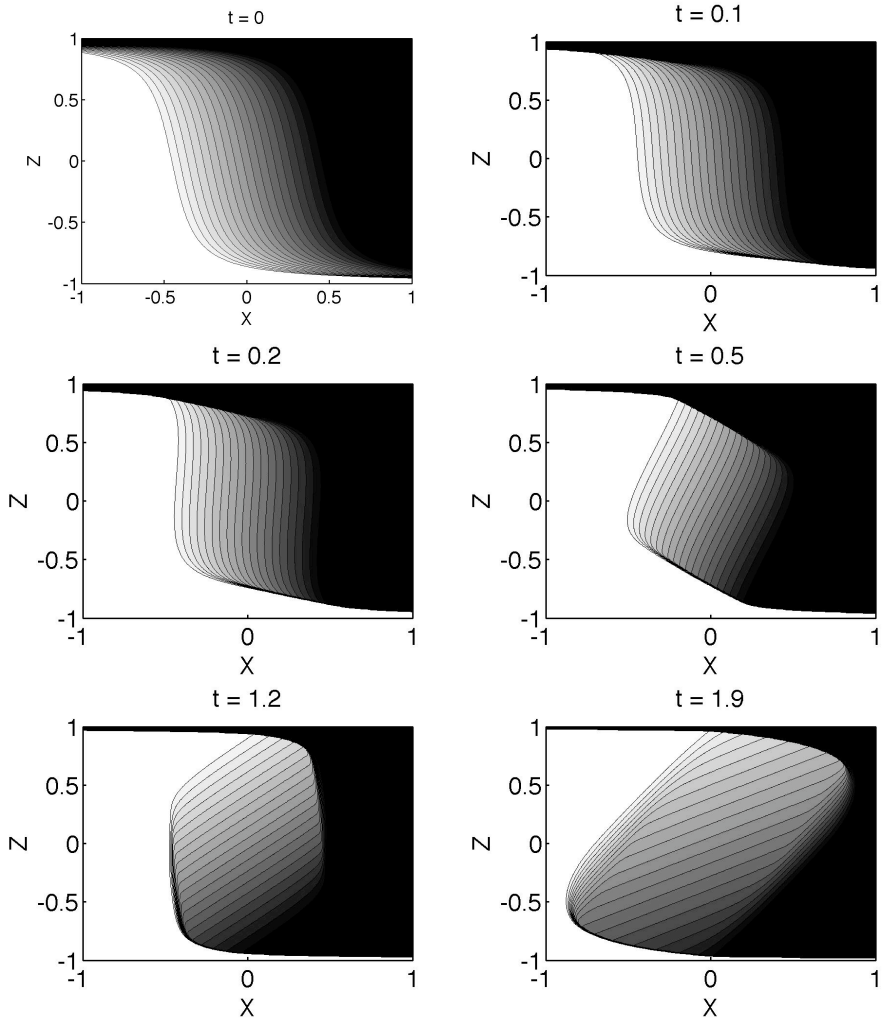

Figure 4.4: Shock formation with $v_0, w_0 < 0$.

in the bottom half of the fourth frame continue to spread out.

In both cases, the shock formation time can be calculated exactly. In case (B), since $\varphi_0(x,z) = \sqrt{x^2+z^2}$ for $x^2+z^2 \leq 1$, then $\nabla\varphi_0 = \left(\dfrac{x}{\sqrt{x^2+z^2}}, \dfrac{z}{\sqrt{x^2+z^2}}\right)$. The infimum of (4.6) occurs when $x_0 = 0$, giving $v_0 = 0$. Thus, $t_+ = -\dfrac{1}{2w_0}$, so for $z_0 = -1$ the shock formation time is $t_+ = \dfrac{1}{2}$. A similar calculation can be made for case (A), with $\varphi_0(x,z) = 1 - \sqrt{x^2+z^2}$. Once again, the shock formation time occurs at $t = \dfrac{1}{2}$ this time stemming from $x_0 = 0,\ z_0 = 1$.

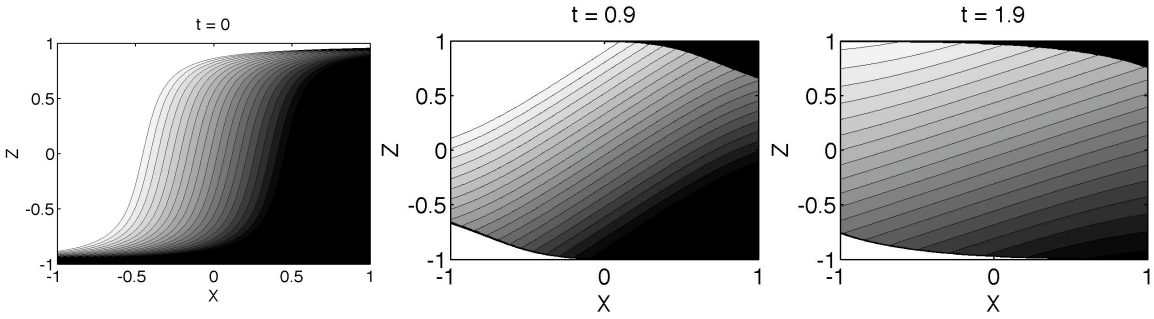

Figure 4.5: No shock formation with $v_0 < 0,\ w_0 <> 0$.

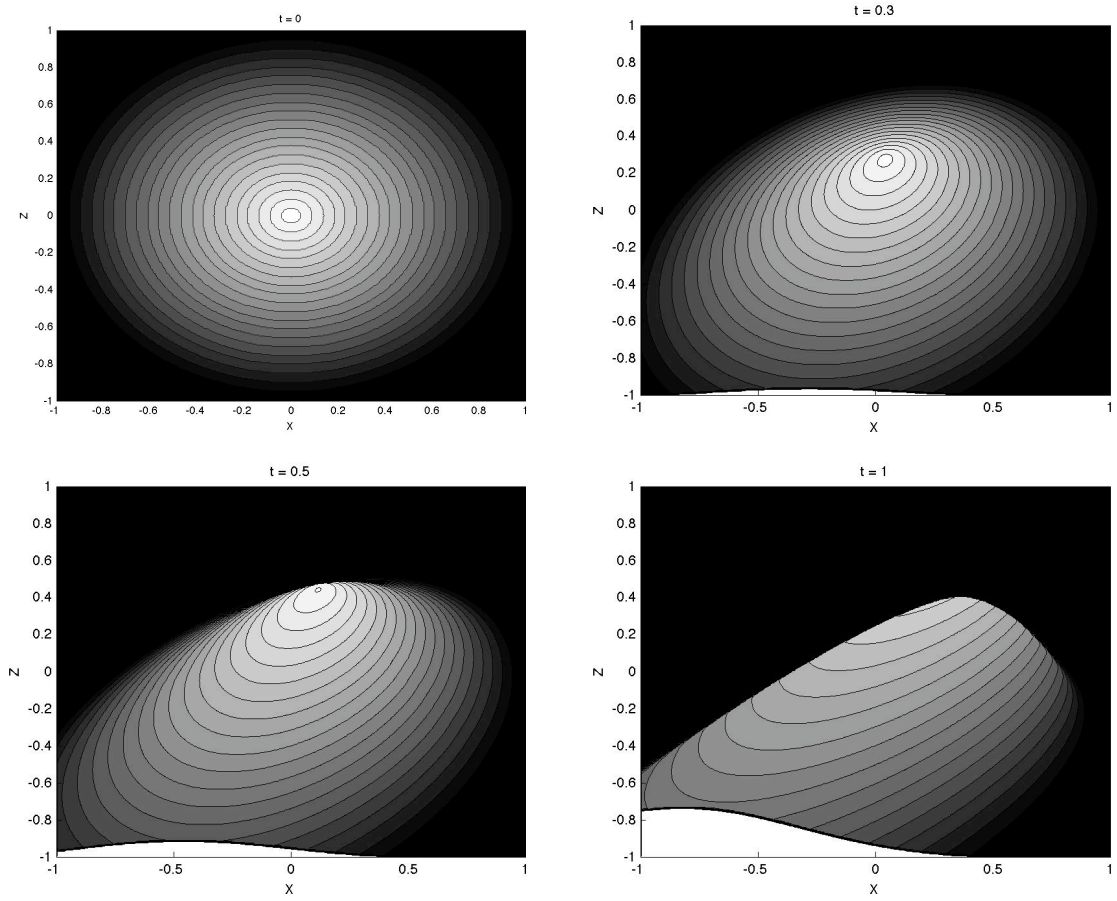

Figure 4.6: Case (A): shock formation from $\nabla\varphi_0(r) = 1 - r$.

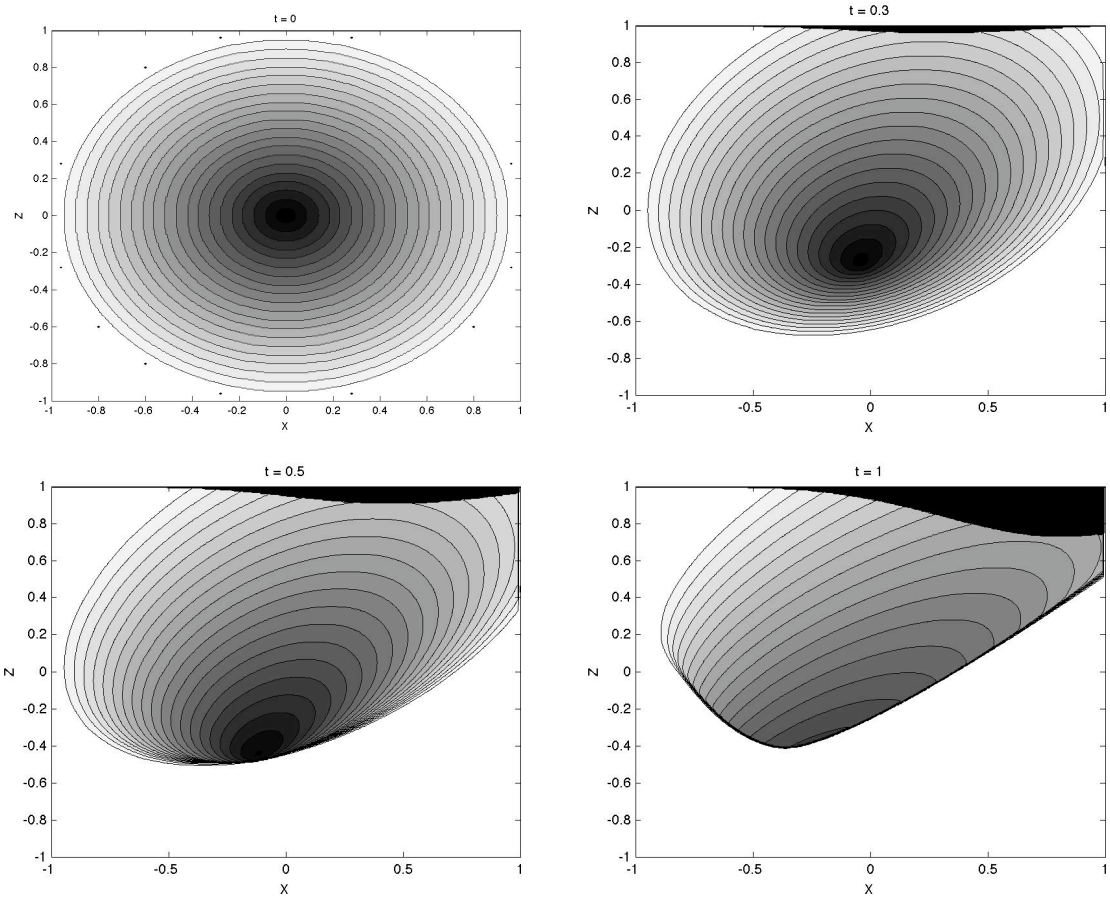

Figure 4.7: Case (B): shock formation from $\nabla\varphi_0(r) = r$.

Chapter 5

Shock Breaking

Consider a shock wave $z = \hat{z}(x,t)$ that separates two constant values of φ. The evolution of this interface is governed by the PDE (3.13). For an increasing parallel bulk velocity $u(z)$, if the shock is stable and decreasing, in that $\hat{z}_x < 0$, then the shock will steepen and eventually break due to shear. In other words, $\min_x \hat{z}_x(x,t) \to -\infty$ in finite time. Subsequently, the interface could evolve by expressing x as a function of z, t and employing the Rankine-Hugoniot condition. However, the resulting piecewise constant solution is unstable because in this weak solution of PDE (4.1a), part of the evolved shock wave is unstable according to Theorem 3.3.1. The unstable part of the evolved interface is replaced by a continuous wave constructed by the method of characteristics. This solution, consisting of the stable parts of the evolved shock interface, and a central mixing zone across which φ varies continuously from φ_- to φ_+ persists typically only for a short time. However, we will show special conditions in which this simple structure persists indefinitely. The subsequent evolution of the stable solution is more complicated, as the stable portion of the evolved shock interface is affected by the mixing zone. The structure undergoes one further change before settling down into a final form. The latter stages of this mixing zone are described in §5.1 and are verified with numerical simulations.

Consider the initial value problem (4.7). It is instructive to first look at the simple case of a vertical initial interface at $x = 0$; the following construction forms part of the solution of an

initial boundary value problem in [44]. Thus, the initial condition considered is

$$\varphi(x,z,0)=\varphi_0(x,z)=\begin{cases}\varphi_-, & \text{if } x<0\\ \\ \varphi_+, & \text{if } x>0\end{cases} \tag{5.1}$$

It is convenient to track the interface in the form $x=x(z,t)$, which evolves according to the Rankine-Hugoniot condition, i.e.,

$$x_t+rx_z=z, \quad r=\varphi_-+\varphi_+-1, \tag{5.2}$$

with initial condition

$$x(z,0)=0. \tag{5.3}$$

Since $0<\varphi_-,\varphi_+<1$, it results that $-1\leq r\leq 1$. Solving (5.2), (5.3) gives

$$x(z,t)=zt-\frac{1}{2}rt^2, \quad t\geq 0. \tag{5.4}$$

If $\varphi_-<\varphi_+$, then the interface (5.4) maintains stability as it evolves since $\partial x/\partial z=t>0$. On the other hand, if $\varphi_->\varphi_+$, then (5.4) is unstable, and is replaced by a rarefaction wave that continues to shear. Contours are found by employing the method of characteristics on (4.7a):

$$z=(2\varphi-1)t+\lambda \tag{5.5a}$$

$$x=\frac{1}{2}(2\varphi-1)t^2+\lambda t+u. \tag{5.5b}$$

The initial location of the interface is given by $x=0,\ z=z_0$, giving $\lambda=z_0,\ \mu=0$. Consequently, there is a one-parameter family of curves parameterized by z_0. Eliminating z_0 shows

the characteristic curves form parallel lines:

$$z = \frac{x}{t} + \frac{1}{2}(2\varphi - 1)t. \tag{5.6}$$

The full solution is given by

$$\varphi(x,z,t) = \begin{cases} \varphi_-, & x < x_-(z,t) \\ \dfrac{1}{2} - \dfrac{x - zt}{t^2}, & x_-(z,t) \le x \le x_+(z,t) \\ \varphi_+, & x > x_+(z,t), \end{cases} \tag{5.7}$$

where $x_\pm(z,t) = zt - \dfrac{1}{2}(2\varphi_\pm - 1)t^2$.

Now consider the more general situation (4.7) with an initial condition with a shock or sharp interface $x = g(z)$ separating two constant values $\varphi_- > \varphi_+$ of φ:

$$\varphi(x,z,0) = \varphi_0(x,z) = \begin{cases} \varphi_-, & \text{if } x < g(z) \\ \varphi_+, & \text{if } x > g(z). \end{cases} \tag{5.8}$$

For any general decreasing $g(z)$, the shock interface will steepen and eventually break. Without loss of generality, let $g(z)$ represent a shock on the verge of breaking with the singularity at $z = 0$. Accordingly, we assume g is at least C^4 with

$$g(0) = 0,\ g'(0) = 0,\ g''(0) = 0,\ g'''(z) < 0 \text{ for all } z. \tag{5.9}$$

Then $g'(z) < 0$ and $zg''(z) < 0$ for all $z \neq 0$. In particular, the interface is initially vertical at $z = 0$ and decreasing elsewhere. As before, the interface $x = x(z,t)$ evolves according to the Rankine-Hugoniot condition (5.2), this time with initial condition $x(z,0) = g(z)$. The method

of characteristics gives the initial value problem:

$$\frac{dx}{dt} = z, \quad \frac{dz}{dt} = r, \quad x(0) = g(z_0);\ z(0) = z_0, \quad r = \varphi_- + \varphi_+ - 1. \tag{5.10}$$

Characteristics are then given by

$$x = \frac{1}{2}rt^2 + z_0 t + g(z_0); \quad z = rt + z_0. \tag{5.11}$$

Eliminating z_0 gives:

$$x(z,t) = -\frac{1}{2}rt^2 + zt + g(z - rt). \tag{5.12}$$

This shock wave (5.12) will be called *the evolved interface*, labeled $S_E(t)$. In particular, at $z = rt$, $\frac{\partial x}{\partial z} = t > 0$ so that the interface has positive slope over some middle portion where φ_- is above φ_+. This corresponds to an unstable portion of the evolved interface.

5.1 The Mixing Zone

Stage 1 - $\mathcal{M}_1(t)$. For fixed $t > 0$, the unstable portion of the evolved interface lies between the two extrema of (5.12) called $P_\pm(t) = (x_\pm(t), z_\pm(t))$. Since g' is concave, the z derivative of (5.12)

$$\frac{\partial}{\partial z}x(z,t) = t + g'(z - rt) = 0 \tag{5.13}$$

has two solutions $z = z_\pm(t)$ with $z_-(t) < rt < z_+(t)$ for $t > 0$. Then $x_\pm(t)$ is determined from (5.12) with $z = z_\pm(t)$. Moreover, differentiating this relation with respect to t and using (5.12) and (5.13) gives $x'_\pm(t) = z_\pm(t)$.

Now the method of characteristics is used to replace the portion of the evolved interface between the extrema $P_\pm(t)$. In Fig. 5.1 the evolved interface $S_E(t)$ is shown along with contours $C^\pm_\varphi(t)$ of $\varphi(x,z,t)$ with $\varphi_+ \le \varphi \le \varphi_-$ that run between the two extrema $P_\pm(t)$ of the curve $S_E(t)$. The contours $C^\pm_\varphi(t)$ are given by the general form of (3.8) with $f(\varphi) = \varphi(\varphi - 1)$ and initial points specified by $P_\pm(t_1) : x_0 = x_\pm(t_1), z_0 = z_\pm(t_1)$, where $t_1 \in [0,t]$ parameterizes each

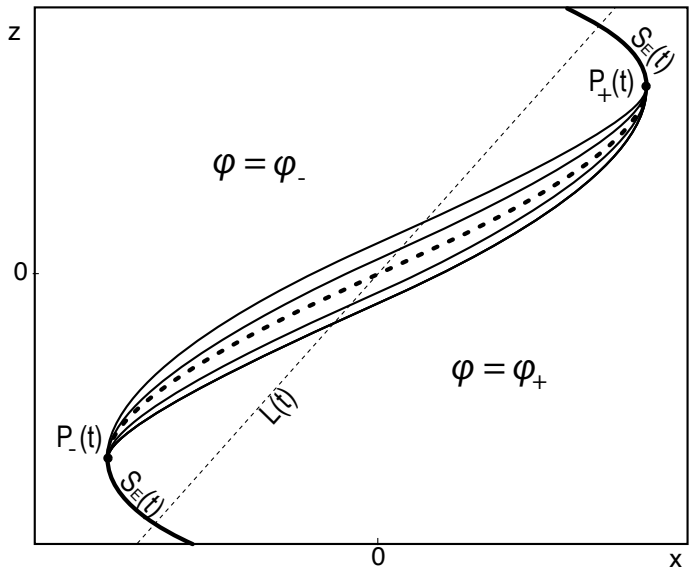

Figure 5.1: Schematic of the mixing zone joining constant values $\varphi_- > \varphi_+$.

curve at a fixed time t. Thus,

$$C_\varphi^\pm(t) = \{(x^\pm(t, t_1, \varphi), z^\pm(t, t_1, \varphi)), \quad 0 \le t_1 \le t\}, \tag{5.14}$$

with

$$x^\pm(t, t_1, \varphi) = \frac{1}{2}(2\varphi - 1)(t - t_1)^2 + z_\pm(t_1)(t - t_1) + x_\pm(t_1), \quad z^\pm(t, t_1, \varphi) = (2\varphi - 1)(t - t_1) + z_\pm(t_1). \tag{5.15}$$

In particular, for $\varphi = \frac{1}{2}(\varphi_+ + \varphi_-)$, $C_\varphi^\pm(t)$ coincides with the unstable part of the evolved interface $S_E(t)$ given by (5.12).

The characteristics $C_\varphi^\pm(t)$ have the following properties, which are verified by differentiating (5.15) and using (5.12), (5.13).

- For each $t > 0$, the characteristics (5.15) all emanate from $P_\pm(t)$, when $t_1 = t$. In other

words, $x^{\pm}(t,t,\varphi) = x_{\pm}(t)$; $z^{\pm}(t,t,\varphi) = z_{\pm}(t)$, for each $\varphi \in [\varphi_+, \varphi_-]$.

- Each $C^{\pm}_{\varphi}(t)$, ends, at $t_1 = 0$, on the same line $L(t) : x = \frac{1}{2}tz :\ x^{\pm}(t,0,\varphi) = \frac{1}{2}tz^{\pm}(t,0,\varphi)$.
- Each $C^{\pm}_{\varphi}(t)$ has the same slope at each $t_1 \in [0,t]$; in particular, they all terminate with the same slope $\dfrac{dx}{dz} = t$ on $L(t)$ (so that the characteristics have half the slope of $L(t)$ where they intersect the line).
- Each $C^{\pm}_{\varphi}(t)$ has $\dfrac{dx}{dt} > 0$ for $0 < t < t^*$ where t^* is found later in §5.1.

Provided $z^+(t,t_1,\varphi)$ is increasing in $t_1 \in (0,t)$ (and likewise $z^-(t,t_1,\varphi)$ decreasing in t_1), the characteristics $C^{\pm}_{\varphi}(t)$ form a mixing zone $\mathcal{M}_1(t)$ between $P_+(t)$ and $P_-(t)$. In this mixing zone, φ varies continuously from $\varphi = \varphi_-$ to $\varphi = \varphi_+$. The boundary of $\mathcal{M}_1(t)$ consists of the four curves $C^{\pm}_{\varphi_{\pm}}(t)$; within these curves the solution is defined implicitly from the equations

$$x = x^{\pm}(t,t_1,\varphi), \quad z = z^{\pm}(t,t_1,\varphi), \quad 0 < t_1 < t, \quad \varphi_+ < \varphi < \varphi_-. \tag{5.16}$$

Outside $\mathcal{M}_1(t)$, the solution $\varphi(x,z,t)$ is φ_- and φ_+ to the left and right respectively of the evolved shock and $\mathcal{M}_1(t)$. The solution, illustrated in Figure 5.1 at a fixed t, is called *the smooth mixing solution.*

Evolutionary Property. The construction of the smooth mixing solution is evolutionary. First, each point of each characteristic $C^{\pm}_{\varphi}$ at time $t > 0$ is evolved from a point $P_{\pm}(t_0)$ at an earlier time $t_0 \geq 0$. Further, the mixing region $\mathcal{M}_1(t)$ relates properly to characteristics evolved from the initial condition. For $\varphi_+ \leq \varphi \leq \varphi_-$, and $t \geq 0$, let $S_{\varphi}(t)$ denote the curve obtained by evolving (x,z) along characteristics $\varphi =$ constant starting at points $(x_0 = g(z_0), z_0)$ on the initial interface:

$$S_{\varphi}(t): \quad \begin{cases} x_s(\varphi,t;z_0) = \dfrac{1}{2}(2\varphi-1)t^2 + z_0 t + g(z_0) \\ \\ z_s(\varphi,t;z_0) = (2\varphi-1)t + z_0 \end{cases} \tag{5.17}$$

Now consider all the characteristics $\varphi = \varphi_-$ evolving from the initial condition, i.e., with $x \le g(z)$. The intersection of the characteristics with a plane $t =$ constant is a region in the (x, z) plane, bounded on the right by $S_{\varphi_-}(t)$. Similarly, the region $x \ge g(z)$, where $\varphi = \varphi_+$ initially, is evolved to a region bounded on the left by $S_{\varphi_+}(t)$. If $\varphi(x, z, t)$ is the weak solution that is evolutionary, then any point (x, z) to the right of $S_{\varphi_-}(t)$ must have $\varphi(x, z, t) < \varphi_-$, and any point to the left of $S_{\varphi_+}(t)$ must have $\varphi(x, z, t) > \varphi_+$. The construction for $\mathcal{M}_1(t)$ can be checked for consistency with these observations by showing that $C_{\varphi_+}(t)$ is to the right of $S_{\varphi_+}(t)$ for each $t > 0$ (or similarly $C_{\varphi_-}(t)$ is to the left of $S_{\varphi_-}(t)$). Recall that the points (x^+, z^+) on $C_{\varphi_+}(t)$ are given in (5.15) and consider a point $(x_s, z_s) \in S_{\varphi_+}$ with the same value of z so that $z^+ = z_s$. Then, to prove the evolutionary property of the smooth mixing solution, it suffices to show $x^+ > x_s$:

Lemma 1 *$z^+(t, t_1, \varphi_+) = z_s(\varphi_+, t, z_0)$ implies $x^+(t, t_1, \varphi_+) > x_s(\varphi_+, t, z_0)$.*

Proof: Suppose

$$z^+(t, t_1, \varphi_+) = z_s(\varphi_+, t, z_0).$$

Then, the definitions (5.15), (5.17) of z^+, z_s give

$$z_0 = z_+(t_1) - (2\varphi_+ - 1)t_1.$$

Using equation (5.12) for $x_+(t)$, the difference between x^+ and x_s becomes

$$x^+(t, t_1, \varphi_+) - x_s(\varphi_+, t, z_0) = \frac{1}{2}(\varphi_+ - \varphi_-)t_1^2 + g(z_+(t_1) - (\varphi_+ + \varphi_- - 1)t_1) - g(z_+(t_1) - (2\varphi_+ - 1)t_1).$$

Using the fact that $g'(z_+(t_1) - (\varphi_+ + \varphi_- - 1)t_1) = -t$, then $z_+(t_1) - (\varphi_+ + \varphi_- - 1)t_1 > 0$ (since $g'(z) < 0$ if and only if $z > 0$). The Taylor expansion of $g(z_+(t_1) - (2\varphi_+ - 1)t_1)$ about $z = z_+(t_1) - (\varphi_+ + \varphi_- - 1)t_1$ completes the argument:

$$x^+(t, t_1, \varphi_+) - x_s(\varphi_+, t, z_0) = \frac{1}{2}(\varphi_- - \varphi_+)t_1^2 - \frac{1}{2}g''(\xi)(\varphi_- - \varphi_+)t_1^2,$$

for some $\xi \in (z_+(t_1) - (\varphi_+ + \varphi_- - 1)t_1, (2\varphi_+ - 1)t_1)$. But $g''(\xi) < 0$ for $\xi > 0$, and $\varphi_- > \varphi_+$, so that $x^+(t, t_1, \varphi_+) - x_s(\varphi_+, t, z_0) > 0$. This completes the proof. ■

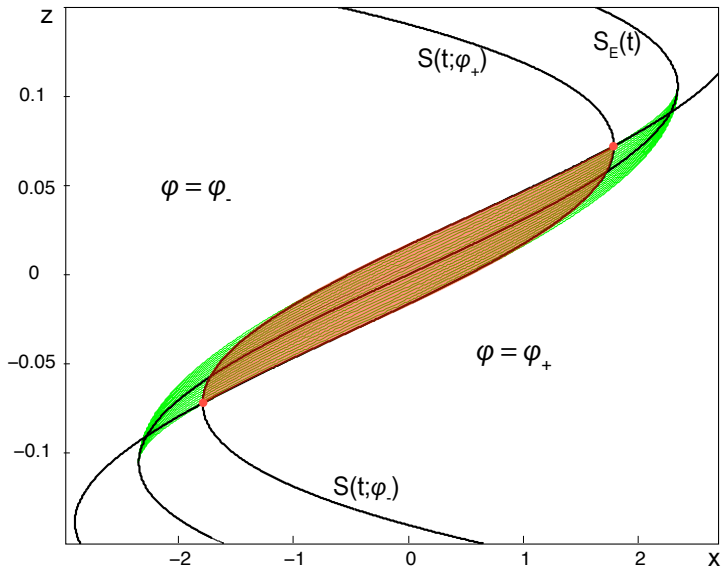

Figure 5.2: The mixing zone and the region bounded by $S(t;\varphi_-)$ and $S(t;\varphi_+)$.

Figure 5.2 shows the characteristics $C_\varphi(t)$ in the mixing zone $\mathcal{M}_1(t)$ and the contours $S_{\varphi_\pm}(t)$ (labeled $S(t;\varphi_\pm)$ in the figure) evolved from the initial interface. The evolved shock $S_E(t)$ is the same as the curve $S_\varphi(t)$, with $\varphi = \frac{1}{2}(\varphi_+ + \varphi_-)$; in the figure, the stable and unstable portions are shown. As the theorem shows, the mixing zone contains the shaded region bounded by the curves $S(t;\varphi_-)$ and $S(t;\varphi_+)$. The calculation for Figure 5.2 uses $\varphi_+ = 0, \varphi_- = 1$.Note that the x and z scales have been expanded in order to visualize the computed solution.

Breakdown of the smooth mixing solution. The smooth mixing solution depends on $z^+(t, t_1, \varphi)$ being an increasing function of t_1 (and z^- decreasing in t_1). When $z^+(t, t_1, \varphi)$ becomes a decreasing function of t_1, the characteristics C_ϕ overlap the evolved interface, leading to multiple

values for φ. In such a circumstance, the solution includes an interaction between the characteristics and the evolved shock, leading to a structure in which there is a shock wave with non-constant φ on one side. In general, the smooth mixing solution becomes singular in this way after a finite time.

Without loss of generality, attention is restricted to the solution near $P_+(t)$; calculations for the solution near $P_-(t)$ are similar. Differentiating the z equation in (5.15) with respect to t_1 gives

$$\frac{\partial z^+}{\partial t_1}(t, t_1, \varphi) = -(2\varphi - 1) + z'_+(t_1). \tag{5.18}$$

Differentiating again gives

$$\frac{\partial^2 z^+}{\partial t_1^2}(t, t_1, \varphi) = z''_+(t_1). \tag{5.19}$$

To see that $z''_+(t_1) < 0$, differentiate (5.13):

$$g''(z_+(t) - rt)(z'_+(t) - r) + 1 = 0. \tag{5.20}$$

Differentiating again, and using (5.13) gives

$$g'''(z_+(t) - rt)(z'_+(t) - r)^2 = tz''_+(t). \tag{5.21}$$

It now follows from $g''' < 0$ (see (5.9)) that $\dfrac{\partial^2 z^+}{\partial t_1^2}(t, t_1, \varphi) = z''_+(t_1) < 0$. Consequently,

$$\frac{\partial z^+}{\partial t_1}(t, t_1, \varphi) \geq \frac{\partial z^+}{\partial t_1}(t, t, \varphi), \quad \text{for all } t_1 \in (0, t).$$

Therefore, if a singularity develops, it corresponds to $\dfrac{\partial z^+}{\partial t_1}$ first becoming zero at $t_1 = t$, for some t. That is, the singularity occurs at $P_+(t)$. Moreover, since $\dfrac{\partial z^+}{\partial t_1}(t, t_1, \varphi)$ is decreasing as a function of φ, this must first occur at $\varphi = \varphi_-$. Thus, from (5.18), the construction breaks

down in the physical domain $-1 < z < 1$ if there is a first $t = t^*$ such that

$$\frac{\partial z^+}{\partial t_1}(t^*, t^*, \varphi_-) = -(2\varphi_- - 1) + z'_+(t^*) = 0 \quad \text{and} \quad z_+(t^*) < 1. \tag{5.22}$$

Although this argument has focused on the characteristics emanating from $P_+(t)$, it is just as likely that the singularity develops first due to similar behavior at $P_-(t)$. It is also possible that $\frac{\partial z^\pm}{\partial t_1}(t, t, \varphi_\pm)$ remain non-zero as t increases, and that the construction breaks down due to $z_\pm(t)$ reaching the boundary $z = \pm 1$, at some $t = \bar{t}$. The following summary includes all possibilities of how the smooth mixing solution breaks down.

SUMMARY: *The smooth mixing solution given by (5.15) can develop a finite time singularity in one of two ways. Either the contours given by (5.15) generate a multivalued function, or $P_\pm(t)$ reaches the boundary $z = \pm 1$.*

To further characterize the breakdown of the smooth mixing solution, the following formulation of equations for the breakdown time is useful. Without loss of generality, consider the upper part of the construction (5.15). Recall that $\varphi_- > \varphi_+$ are constants in the initial condition (5.8) and let t^* denote the first time that the smooth mixing solution develops a singularity. Then $z'_+(t^*) = 2\varphi_- - 1$ from (5.22), and (5.20) becomes

$$g''(z_+ - rt) = -\frac{1}{\varphi_- - \varphi_+}, \tag{5.23}$$

(where $r = \varphi_+ + \varphi_- - 1$). The assumption (5.9) that $g'''(z) < 0$, implies $g''(z)$ is a decreasing function of z. Consequently, either

(1) There exists a $t = t^*$ such that $g''(z_+(t^*) - rt^*) = -\dfrac{1}{\varphi_- - \varphi_+}$ and $z_+(t^*) < 1$, or

(2) $g''(z_+(t) - rt) > -\dfrac{1}{\varphi_- - \varphi_+}$ for all $t > 0$ such that $z_+(t) \leq 1$, in which case there may be

a time $t = \bar{t}$ with $z_+(\bar{t}) = 1$. In this case, a shock develops as a reflection off the boundary $z = 1$.

Example - cubic interface. To study cases (1) and (2) above further, consider the example in which the initial interface is a pure cubic

$$g(z) = -kz^3, \quad \text{with } k > 0.$$

The goal here is to describe regions of parameter values $(\varphi_-, \varphi_+, k)$ for which the smooth mixing solution breaks down at $t = t^*$, (case (1)) and parameter values for which the breakdown is at $t = \bar{t}$ (case (2)). The calculation is simplified somewhat by the observation that the initial value problem is symmetric about $z = 0$. With $g(z) = -kz^3$, equation (5.23) for $t = t^*$ becomes

$$-6k(z_+(t) - rt) = -\frac{1}{\varphi_- - \varphi_+}, \tag{5.24}$$

so that $z_+(t^*) = \dfrac{1}{6k(\varphi_- - \varphi_+)} + rt^*$. Substituting $z_+(t^*)$ back into (5.13), and solving for t^* gives

$$t^* = \frac{1}{12k(\varphi_- - \varphi_+)^2}.$$

Then $t^* > \bar{t}$, when $z_+(t^*) < 1$, for which $\varphi_+ + \varphi_- - 1 < 12k(\varphi_- - \varphi_+)^2 - 2(\varphi_- - \varphi_+)$. The boundary case (i.e., $t^* = \bar{t}$) yields the inequality

$$\varphi_+ + \varphi_- - 1 < 12k(\varphi_- - \varphi_+)^2 - 2(\varphi_- - \varphi_+). \tag{5.25}$$

This is a quadratic inequality in the variables $(\varphi_- - \varphi_+)$ and $(\varphi_- + \varphi_+)$ with $0 \le \varphi_+ \le \varphi_- \le 1$. Figure 5.3 shows the three different cases for how the boundary parabola sits in the interior triangle $0 < \varphi_+ < \varphi_- < 1$. In each case, if (φ_-, φ_+) lies in the region labeled I, then a shock forms in the interior of the domain. On the other hand, if the pair (φ_-, φ_+) lies in the region labeled B, then the points $P_\pm(t)$ have reached the boundary $z = \pm 1$ before the interior shock has formed. Figure 5.3 shows the classification of the breakdown based on φ_- and φ_+ for three

different values of k. In particular, since $z_{\pm}(t)$ are monotonically increasing and decreasing (respectively), the points $P_{\pm}(t)$ reach the boundary in finite time, so a singularity in the mixing zone solution always develops in finite time. To summarize, either a singularity develops from the interior breakdown at a time t^*, or from the point $P_{\pm}(t)$ reaching the boundary at a finite time $\bar{t}$.

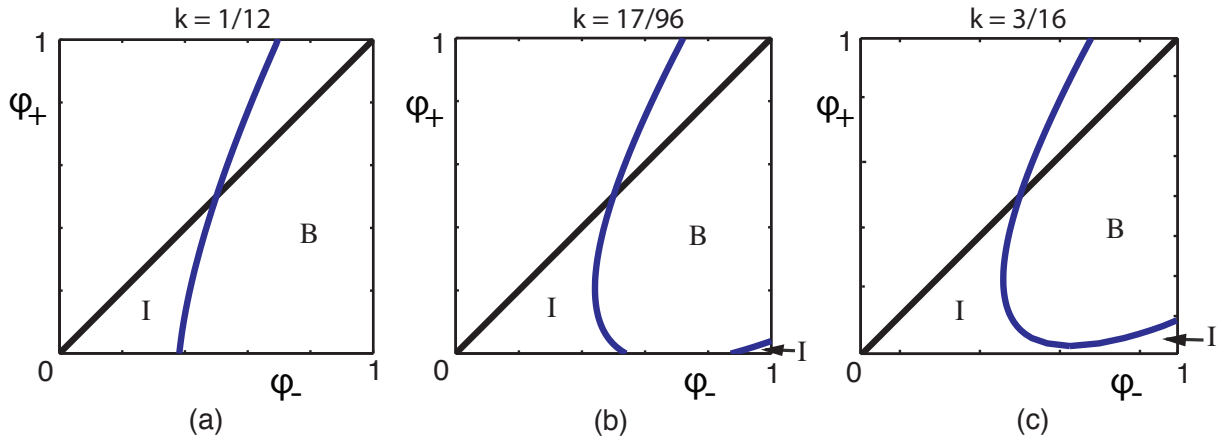

Figure 5.3: Cubic Case: classifying breakdown of $\mathcal{M}_1(t)$.

In the special case where $\varphi_- = 1,\ \varphi_+ = 0$ and $g(z) = -kz^3$, the curvature of the evolved initial interface solely determines where the breakdown occurs. For a higher curved $g(z)$ where $k > 1/6$, the smooth mixing solution develops a singularity in the interior at time $t^* = \dfrac{1}{12k}$. For an initial interface with smaller curvature, the maximum and minimum points ($P_{\pm}(t)$) of the evolved initial interface move apart at a faster rate, thus sending them to the boundary sooner. In this case, with $0 < k < 1/6$, the singularity develops at the boundary at time $\bar{t} = 3k$. Note that for $k = 1/6$, the breakdown times are equal, with $t^* = \bar{t} = \dfrac{1}{2}$. The curvature of the initial interface plays an important role in determining how a singularity develops, and this is also seen in an example later on in section §5.2, where the initial interface is piecewise quadratic.

Stage 2 - $\mathcal{M}_2(t)$ and $\mathcal{M}_3(t)$. The structure of the mixing zone $\mathcal{M}_1(t)$ is maintained until a finite time singularity forms as described from cases (1) and (2) earlier. Assuming the singularity forms in the interior of the region (case (1)), this breakdown time occurs at $t = t^*$ given by (5.22). For $t > t^*$, the characteristic surfaces begin to cross near $P_\pm(t)$ generating a multi-valued solution. Consequently, the weak solution must include additional shocks with φ non-constant on one side. The solution for the mixing zone with $t > t^*$ is highly implicit, so the new solution is constructed numerically.

This new solution, $\mathcal{M}_2(t)$ is constructed from the solution $\mathcal{M}_1(t)$ at $t = t^*$ by using characteristics and shock fitting. Referring to figure 5.4(b), the difficulty is that both the shocks $S_I(t)$ and the solution φ in regions $\Phi_S(t)$ and $\Phi_P(t)$ evolve together. The construction of $S_I(t)$ depends on $\varphi(x, z, t_1)$ in the region $\Phi_S(t)$ for each $t^* < t_1 < t$, but this in turn depends on $S_I(t_1)$. Similarly, $\varphi(x, z, t)$ in region $\Phi_P(t)$ depends on the locations of $P_+(t_1)$ for $t^* < t_1 < t$, which forms the end points of $S_I(t_1)$.

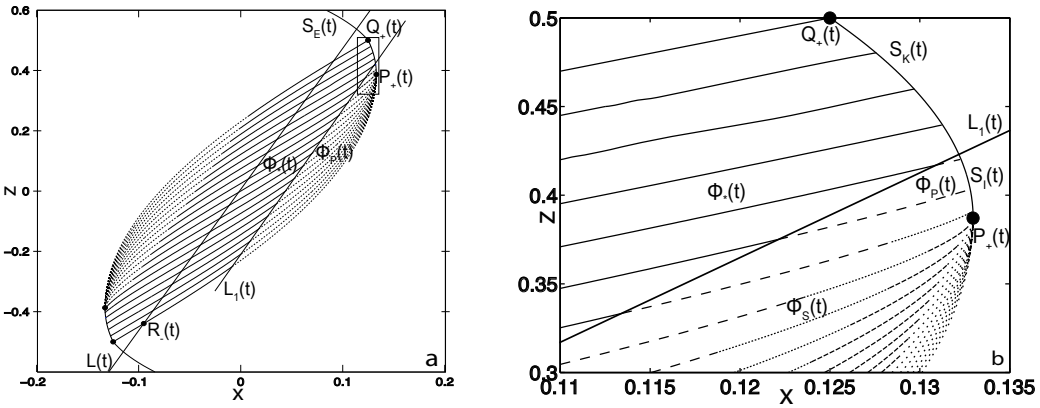

Figure 5.4: Cubic case: (a) The solution for $\mathcal{M}_2(t)$. (b) Zoomed in around $P_+(t)$.

Focusing on the portion of the mixing zone where $x > 0$, let $L_1(t)$ be the line given by (5.15)

with $t_1 = t^*$. To the left of $L_1(t)$, the contours in the region $\Phi_*(t)$ are simply evolved from $\mathcal{M}_1(t^*)$. In other words, for each (x_0, z_0) in $\mathcal{M}_1(t^*)$, the characteristics (3.8) give the contours in $\Phi_*(t)$ parametrically. However, $\varphi = \tilde{\varphi}(x, z, t)$ is then known only implicitly in this region, and has to be found by eliminating the parameter t_0 from the equations in (3.8). The shock $S_K(t) \;:\; x = x_K(z, t)$ is then determined numerically from the method of characteristics to solve (5.2) with initial condition

$$x(t_2; t_2) = x_{Q_+}(t_2); \quad z(t_2; t_2) = z_{Q_+}(t_2) \tag{5.26}$$

with $\varphi_- = \tilde{\varphi}(x_K(t)-, z, t)$ calculated by root finding in $\Phi_*(t)$ and where the points $Q_\pm(t) = (x_{Q_\pm}(t), z_{Q_\pm}(t))$ are given by the intersection of the evolved initial interface $S_E(t)$ with the $\varphi_\mp$ contours. The shock $S_K(t)$ is calculated this way until it intersects $L_1(t)$ where $\varphi = \varphi_F(t)$, the value of $\varphi(x, z, t)$ corresponding to the contour that passes through the point of intersection of $S_K(t)$ with $L_1(t)$.

The shock $S_K(t)$ continues across $L_1(t)$ as $S_I(t)$. However, to calculate $S_I(t)$ from (5.2), φ_- must be known in the region $\Phi_P(t)$. To find φ_- in this region, first note that the construction $\mathcal{M}_2(t)$ given in Figure 5.4 is valid up until some time $t = \hat{t} > t^*$. This time is determined by solving (5.12) and replacing z with z^+ from (5.15) with $t_1 = 0$ and $\varphi = \varphi_+$. In the cubic example earlier in this section $\hat{t} = \dfrac{1}{2k}$. The strategy to compute $S_I(t)$ over n small intervals $[t_j, t_j + dt]$ with $j = 0, \ldots, n-1$ where $t_j = t^* + jdt$, $t_0 = t^*$, and $dt = (\hat{t} - t^*)/n$.

In the region Φ_P, φ is approximated over N subintervals $[t_j + l\delta t, t_j + (l+1)\delta t]$ with $l = 0, \ldots, N-1$ where $\delta t = dt/N$. Since the construction is similar for each j, it suffices to describe it only for $j = 0$. First, let $(x_0, z_0) \in S_E(t^*)$ and evolve these characteristics to get $\varphi = \bar{\varphi}(x, z, t)$ given implicitly by (5.17) near $L_1(t)$. It should be noted that the transition of φ from Φ_P to $\Phi_*(t)$ is continuous across $L_1(t)$ and the contours are C^1.

The shock $S_I(t)$ can now be constructed for $t^* < t < t^* + \delta t$ from (5.2) with φ_+ constant and $\varphi_- = \bar{\varphi}(x_I(z, t)-, z, t)$. $S_I(t)$ can be numerically computed to any desired accuracy with an ODE solver such as ODE45 in MATLAB (as used to construct figure 5.4). To find the point

$P_+(t)$, the end point of $S_I(t)$, simply find where $\dfrac{\partial x_I}{\partial z} = 0$. This process of calculating $S_I(t)$ and finding $P_+(t)$ on the intervals $[t^* + k\delta t, t^* + (k+1)\delta t]$ is repeated until $k = N - 1$. At this point, $P_+(t^* + k\delta t)$ is known for each $k = 0, \ldots, N-1$ meaning φ can be computed in the regions $\Phi_P(t^* + dt)$ and $\Phi_S(t^* + dt)$ from equation (5.15) using these calculated values of $P_+(t)$ and interpolating between them. In particular, the contour $C_{\varphi_+}(t)$ terminates on $L(t)$ at a point labeled $R_-(t)$ in Figure 5.4. The construction of the second stage solution $\mathcal{M}_2(t)$ at time $t = t^* + dt$ is now complete, and the process is repeated for each $t = t^* + jdt$.

Figure 5.4(a) shows the structure of the solution for $t > t^*$ close to t^* as computed in MATLAB with $n = 4,\ N = 61,\ t = \dfrac{1}{2k},\ k = 1$. Figure 5.4(b) zooms in around $P_+(t)$ to show $S_I(t),\ \Phi_S(t)$, and $\Phi_P(t)$ more clearly.

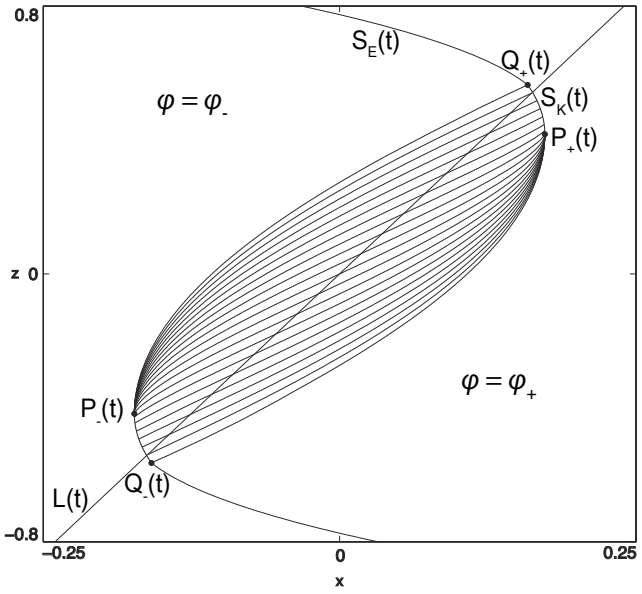

Figure 5.5: Cubic case: The solution $\mathcal{M}_3(t)$.

This numerical scheme will take the solution from t^* to $\hat{t}$ when the construction to the solution once again changes. At $t = \hat{t}$ occurs when $Q_\pm(\hat{t})$ is located on the line $L(\hat{t})$ providing

a continuous location for $Q_{\pm}(t)$ from $\mathcal{M}_2(t)$ to $\mathcal{M}_3(t)$. The new location of $Q_{\pm}(t)$ is where the $\varphi_{\mp}$ contour intersects $S_E(t)$, which now occurs when

$$x = g(z) + zt \tag{5.27}$$

with x and z given by (5.15) for some $0 < t_1 < t$. To find this exact value, solve (5.27) for $t_1(t) > 0$ and plug back into (5.15), giving the point $Q_{\pm}(t) = \big(x_{Q_{\pm}}(t), z_{Q_{\pm}}(t)\big)$. This can be done exactly, provided the point of intersection between $S_E(t)$ and $\varphi_{\mp}$ respectively falls within the $\Phi_*(t)$ region, since these contours are the known evolution of the exact solution given in $\mathcal{M}_1(t)$.

However, at a time $t = \hat{t}$, $Q_{\pm}(t)$ must be numerically calculated since the $\varphi_{\pm}$ contour intersects $S_E(t)$ at the line $L_1(t)$, where the solution has been numerically calculated in $\mathcal{M}_2(t)$, putting the contour in the $\Phi_S(t)$ region. For the cubic case with $g(z) = --kz^3$, this time can be explicitly calculated, as the $\varphi = 0$ contour at $t_1 = 0$ from (5.15) intersects $S_E(t)$ given by $x(z,t) = zt - kz^3$. Equating the two lets us solve for $t = \hat{t}$ exactly: $\hat{t} = \dfrac{1}{2k}$. Now let each point in the φ_+ (and similarly for φ_-) contour $(x_i(t), z_i(t))$ be distinguished as the pair $i = 0, \ldots, (nN) - 1$. To find the point $Q_-(t)$, simply rewrite (5.27) as

$$q_i(t) = x_i(t) - g(z_i(t)) - z_i(t)t \tag{5.28}$$

and find the first value of i for which $q_i(t)q_{i+1}(t) < 0$. Interpolating linearly between the two points $(x_i(t), z_i(t))$ and $(x_{i+1}(t), z_{i+1}(t))$ gives $Q_-(t)$. From here, the shock is calculated using the same procedure as in $\mathcal{M}_2(t)$, the only difference being the new location of $Q_{\pm}(t)$.

Figure 5.5 shows the location of $Q_{\pm}(t)$ is different from $\mathcal{M}_2(t)$, since the outermost contours $C_{\varphi_{\pm}}$ have now reached the evolved initial interface before reaching the line $L(t)$ where $t_1 = 0$. The numerical calculation in Figure 5.5 uses the same values as in Figure 5.4.

The construction for the third stage of the solution $\mathcal{M}_3(t)$ will persist for as long as the mixing region remains away from the boundary $z = \pm 1$. Thus, the complete structure of the

mixing region solution of (4.7) with initial condition (5.8) is given by the continuous evolution of the three stages: $\mathcal{M}_1(t)$ for $0 < t \leq t^*$, $\mathcal{M}_2(t)$ for $t^* < t < \hat{t}$, and $\mathcal{M}_3(t)$ for $t > \hat{t}$ provided the solution stays away from the boundary.

5.2 A Special Mixing Zone

A smooth, stable, monotonically decreasing interface separating small particles from large particles subject to shear will eventually break assuming the parallel bulk velocity $u(z)$ is monotonically increasing. The point at which the interface becomes unstable will be cubic to leading order. As shown in §5.1, the evolutionary mixing region that results is at first smooth in φ, with no shocks having developed in the unstable region. After a finite time, this smooth mixing solution gives way to a second, more complicated structure where a shock has formed near the local extrema of the evolved initial interface.

However, this secondary structure does not necessarily develop if the initial interface $g(z)$ is not at least of cubic order in z. In some instances, the initial structure of the mixing solution $\mathcal{M}_1(t)$ will persist indefinitely (in an unbounded domain) in one of two ways:

(1) The mixing solution will be smooth between the local extrema of the evolved initial interface. No shocks will exist other than the stable portion of the evolved initial interface. It will be similar to $\mathcal{M}_1(t)$ from §5.1.

(2) The mixing solution involves shocks and rarefaction waves whose precise locations depend on each other. This solution will be similar to $\mathcal{M}_3(t)$ from §5.1.

To show the indefinite persistence of this type of solution, consider the Gray-Thornton model given by:

$$\varphi_t + mz\varphi_x + S(\varphi(\varphi-1))_z = 0, \quad -\infty < x, z < \infty, \ t > 0 \tag{5.29a}$$

$$\varphi(x, z, 0) = \varphi_0(x, z) \quad -\infty < x, z < \infty. \tag{5.29b}$$

Here, the parallel bulk velocity $u(z) = mz$ is linear with $m > 0$. The segregation rate is set by the parameter $S > 0$. Consider an initial interface given by (5.8) where

$$g(z) = -\text{sgn}(z)kz^2 \tag{5.30}$$

with $k > 0$. Then, for φ constant on either side of the initial interface with $\varphi_- > \varphi_+$, the initial condition is given by:

$$\varphi(x, z, 0) = \varphi_0(x, z) = \begin{cases} \varphi_-, & \text{if} \quad x < g(z), \\ \\ \varphi_+, & \text{if} \quad x > g(z). \end{cases} \tag{5.31}$$

The initial interface given by $g(z)$ is only C^1; the interface is still vertical at the origin, but there is a jump in the concavity. As the system begins to evolve, the bulk velocity introduces shear into the system, and the interface evolves according to

$$x(z, t) = mzt - \text{sgn}(z)kz^2. \tag{5.32}$$

The extrema $P_\pm(t)$ of these curves are given by

$$P_\pm(t): \quad x_\pm(t) = \pm\frac{m^2}{4k}t^2; \quad z_\pm(t) = \pm\frac{m}{2k}t. \tag{5.33}$$

Therefore, the points $P_\pm(t)$ lie on the line $L(t)$:

$$L(t): \quad x = \frac{m}{2}tz. \tag{5.34}$$

Thus, the characteristics

$$C_{\varphi}^{\pm}(t): \quad \begin{cases} x^{+}(t,t_1,\varphi) = \dfrac{mS}{2}(2\varphi-1)(t-t_1)^2 + \dfrac{m^2}{2k}t_1(t-t_1) + \dfrac{m^2}{4k}t_1^2 \\ \\ z^{+}(t,t_1,\varphi) = S(2\varphi-1)(t-t_1) + \dfrac{m}{2k}t_1, \qquad 0 \le t_1 \le t, \end{cases} \tag{5.35}$$

begin (with $t_1 = t$) and end (with $t_1 = 0$) on $L(t)$.

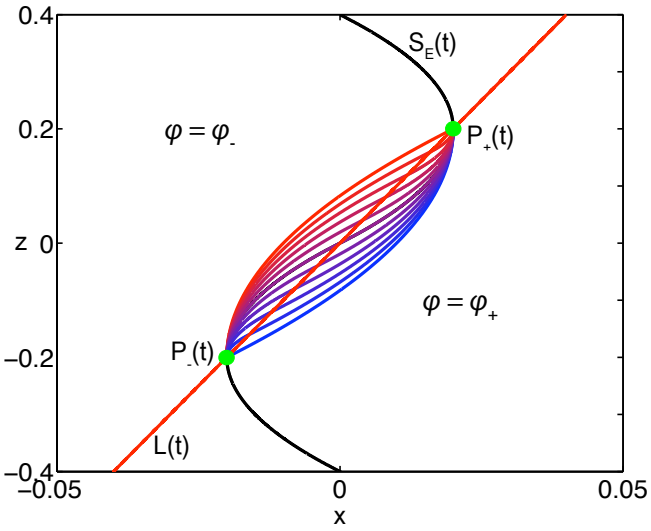

Figure 5.6: Quadratic Case: $k = \frac{1}{4}, m = 1, S = 1, \varphi_+ = 0, \varphi_- = 1, t = 0.1$

To check whether the smooth mixing solution with these contours is valid, simply check the sign of $\dfrac{\partial z}{\partial t_1}$ at $P_{\pm}(t)$, i.e., at $t_1 = t$. Taking $\dfrac{\partial}{\partial t_1}$ of the z equation from (5.35) gives

$$\left.\frac{\partial z}{\partial t_1}\right|_{t_1=t} = -S(2\varphi-1) + \frac{m}{2k}. \tag{5.36}$$

Notice $\dfrac{\partial z}{\partial t_1}$ is independent of time, whereas the similar calculation (5.22) for the cubic case in §5.1 is time dependent. The independence of time in (5.36) is the reason the mixing solution

persists indefinitely, as no breakdown time exists.

For initial condition (5.31), this quantity is smallest for $\varphi = \varphi_-$, and equals zero when

$$\frac{m}{Sk} = 2(2\varphi_- - 1). \tag{5.37}$$

Consequently, for $\varphi_- > 1/2$, a smooth mixing zone persists indefinitely if $\frac{m}{Sk} \geq 2(2\varphi_- - 1)$. On the other hand, if $\frac{m}{Sk} < 2(2\varphi_- - 1)$, a shock appears immediately, but this structure also persists indefinitely.

By solving (5.37) for k, the behavior of the solution can be determined by the curvature of the initial interface, as it was in §5.1. If

$$k < \frac{m}{2S(2\varphi_- - 1)} \tag{5.38}$$

then the mixing solution is smooth for all time. Otherwise, if (5.38) is violated, then a shock appears immediately. Thus, for a given initial curvature k, if the particles move relatively faster horizontally (from the shear rate proportional to m) than vertically (due to the segregation rate S), no shock will form and a smooth solution will persist. The case where (5.38) holds is shown in Figure 5.6.

Chapter 6

Scaling the Gray-Thornton Model

In this chapter, we scale the Gray-Thornton model when considering a linear velocity profile. We then impose a piecewise quadratic initial condition as in §5.2 to find a variable that plays an important role in determining the structure to the solution for the shock wave breaking problem. This variable presents a balance between how fast particles are moving downslope against the flux of particles normal to the downslope direction. As a result, if particles move relatively faster downslope than normal to the slope, no shock forms in the solution. Additionally, we find spatial scalings that give us a similarity solution for the mixing zone.

Consider the Gray-Thornton model

$$\varphi_t + u(z)\varphi_x + S(\varphi(\varphi-1))_z = 0, \ \ -\infty < x < \infty, \ \ -1 < z < 1, \ t > 0 \tag{6.1}$$

where $u(z) = mz, \ m > 0$ is the parallel bulk velocity and $S > 0$ is a proportionality constant setting the segregation rate. By taking $\psi = \varphi - \frac{1}{2}$, (6.1) becomes

$$\psi_t + mz\psi_x + S(\psi^2)_z = 0. \tag{6.2}$$

Introducing the scaling

$$t = aT, \ x = bX, \ z = cZ, \ \psi = d\Psi \tag{6.3}$$

and substituting back into (6.2) produces a PDE in X, Z, T, Ψ

$$\frac{d}{a}\Psi_T + \frac{mcd}{b} Z\Psi_X + \frac{Sd^2}{c}\left(\Psi^2\right)_Z = 0. \tag{6.4}$$

Balancing the terms gives three equations:

$$\frac{d}{a} = \frac{mcd}{b} = \frac{Sd^2}{c}. \tag{6.5}$$

From here, the scalings for time and volume fraction can be written as proportional to the length scales (and vice versa). Solving for a, b, c, and d gives

$$a = \frac{b}{mc}, \quad b = mSa^2 d, \quad c = Sad, \quad d = \frac{mc^2}{Sb}. \tag{6.6}$$

However, solving for a, b, c, and d in terms of m and S is not possible without another equation.

Example: Consider (6.1) with initial condition given by (5.8) where $g(z) = -\text{sgn}(z)kz^2$, the same initial condition given in the piecewise quadratic example in §5.2. The evolved initial interface is given by (5.32). Looking at the case where $z > 0$ and using the scaling given by (6.3), equation (5.32) can be rewritten

$$bX = mcZaT - kc^2 Z^2. \tag{6.7}$$

Balancing the terms here gives three equations

$$\frac{1}{k} = \frac{c^2}{b}, \quad m = \frac{b}{ac}, \quad \frac{m}{k} = \frac{c}{a} \tag{6.8}$$

the first of which can be used to substitute into the equation for d in (6.6). This gives

$$d = \frac{m}{Sk} \tag{6.9}$$

which is exactly the variable in (5.37) that determines the structure of the mixing zone in §5.2.

To find a, b and c, note from the x equation of (5.35) that $\frac{x}{t^2} = const.$ Since $\frac{x}{X} = b$ (from(6.3)) then $\frac{X}{t^2} = const.$ Thus, at $x = x_P(t)$, $\frac{bX}{t^2} = \frac{m^2}{4k}$ and since $\frac{X}{t^2} = const.$ is arbitrary and can be set to 1, thus $b = \frac{m^2}{4k}$. Similarly, this procedure gives $c = \frac{m}{2k}$ and using the third equation from (6.7), $a = 1/2$.

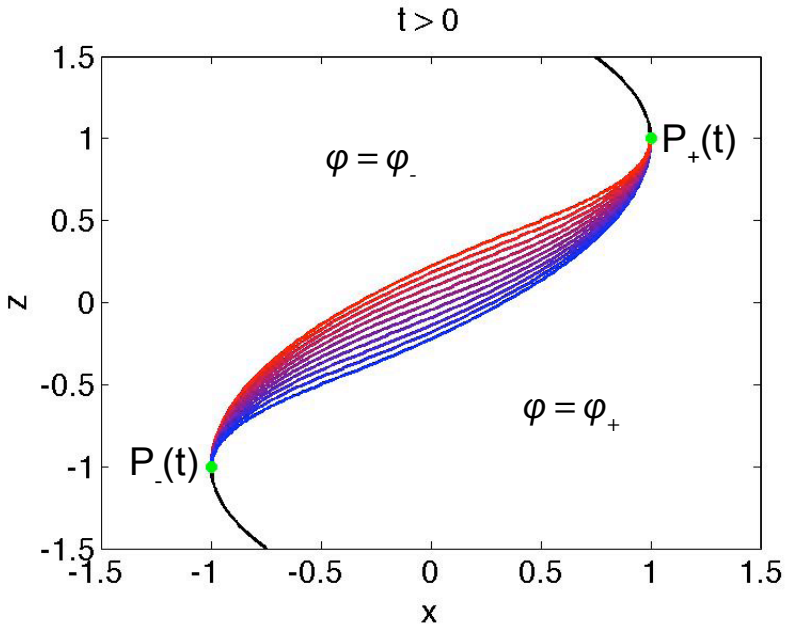

Figure 6.1: Scaled solutions for $t = \frac{N}{10}$ for $N = 1, \ldots, 10$.

Notice, that $x = x_P(t) = \frac{m^2}{4k}t^2 = bt^2$ and $z = z_P(t) = \frac{m}{2k}t = ct$. By dividing (x, z) by $(x_P(t), z_P(t))$ respectively, the new solution (X, Z) is independent of time. With (5.37) satisfied, the solution is just a fixed region with endpoints at $(X_{P_\pm}, Z_{P_\pm}) = (\pm 1, \pm 1)$ for all $t > 0$. Thus, for all $t > 0$, the solutions lie on top of each other, as can be seen in Figure 6.1 with $k = \frac{1}{4}, m = 1, S = 1, \varphi_+ = 0, \varphi_- = 1$ and $X = \frac{x}{x_P(t)}, Z = \frac{z}{z_P(t)}$.

Chapter 7

Modifications to the Gray-Thornton Model

Up to this point, all calculations, examples, theorems, and results used a linear parallel bulk velocity $u(z) = mz,\ m > 0$. Under situations where the parallel bulk velocity is approximately linear, as in granular avalanche flow down a smooth incline, these results are useful. However, there are cases where a nonlinear velocity profile must be considered. Granular avalanches down an extremely rough bed [**?**] and granular flow in a Couette cell geometry [41, 42, 43] are two scenarios in which a linear velocity profile no longer applies.

Assuming that the velocity is no longer linear, then a modification to the model must be made. The first modification is simply to use a general monotonically increasing parallel bulk velocity $u(z)$. In addition to the generalization of the velocity profile, another generalization is to assume the flux function for particles in the z-direction is any convex function $f(\varphi)$ with $f(0) = f(1) = 0$. Although prior results in this thesis used the specific flux function derived by Gray and Thornton $f(\varphi) = \varphi(\varphi - 1)$ [23], it is important in the context of nonlinear hyperbolic conservation laws to consider the general case. In this case, the model simply becomes

$$\varphi_t + u(z)\varphi_x + f(\varphi)_z = 0, \quad -\infty < x < \infty, \quad a < z < b, \quad t > 0. \tag{7.1}$$

where the constant segregation rate $S_r > 0$ is in the flux function $f(\varphi)$. Shock wave breaking is explored using this model with $\varphi_- > \varphi_+$ both constant in §7.2.1.

However, to generalize (7.1) further, we must account for the fact that with a nonlinear velocity profile, shear within the material is no longer constant at all heights, and thus, the segregation rate becomes depth dependent. Hence, the z-term from (7.1) is modified to allow for this change. The Gray-Thornton model only needs to be modified slightly to include this change:

$$\varphi_t + u(z)\varphi_x + (S(z)f(\varphi))_z = 0, \quad -\infty < x < \infty, \quad a < z < b, \quad t > 0. \tag{7.2}$$

Here, $S(z)$ describes the depth-dependent segregation rate.

Equation (7.2) leads to a couple of interesting observations. First, φ is no longer constant along characteristics. This makes analysis of (7.2) the system much more complicated than analysis of either (2.16) or (7.1). Since φ is not constant along characteristics, the method of characteristics no longer yields a system of two ordinary differential equations as it does in (2.16) and (7.1). The system is now three differential equations:

$$\frac{dx}{dt} = u(z), \quad \frac{dz}{dt} = S(z)f'(\varphi), \quad \frac{d\varphi}{dt} = -S'(z)f(\varphi). \tag{7.3}$$

Since the final two ODE are independent of x, they form a vector field in the (z, φ)-plane with a first integral

$$S(z)f(\varphi) = const. \tag{7.4}$$

The (φ, z) phase portrait to (7.3) is shown in Figure 7.1 using (7.4) with $S(z)$ decreasing. In Figure 7.1, $S(z) = se^{-z/\lambda}$ with $s, \lambda > 0$, $f(\varphi) = \varphi(\varphi - 1)$ and $0 \le z \le 1$. Note, $\varphi \to 0$ as $t \to \infty$. On the other hand, if $S(z)$ is increasing, then the phase portrait (not shown) is similar, but the trajectories are flipped upside-down and $\varphi \to 1$ as $t \to \infty$. In either case, $f(\varphi) \to 0$ as $t \to \infty$.

We use (7.2) to generalize the shock formation problem in §7.1, and to generalize the shock wave breaking problem in §7.2 with $\varphi_- = 1$ and $\varphi_+ = 0$. A complete generalization of shock

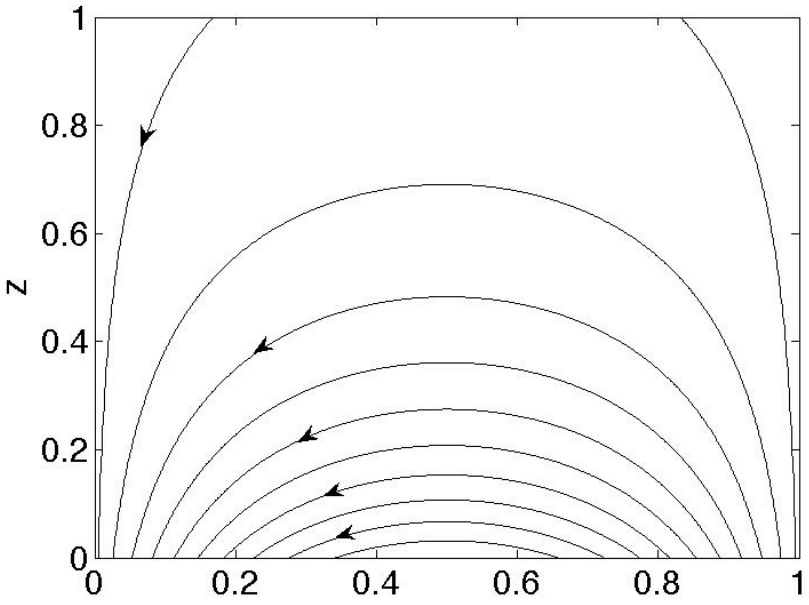

Figure 7.1: (φ, z) phase portrait for (7.3)

formation where $\varphi_- > \varphi_+$ are constant proves to be extremely difficult since these constants are not necessarily solutions to (7.2) (although they are solutions if $\varphi = 0, 1$). In this case, φ_- and φ_+ will actually evolve along with the mixing zone, rather than remain constant as they do for (2.16), (7.1) with $\varphi_- > \varphi_+$, or for (7.2) with $\varphi_- = 1$ and $\varphi_+ = 0$. A discussion of the full generalization of shock wave breaking takes place at the end of §7.3.

However, to obtain some understanding of how $\varphi \neq 0, 1$ evolves in (7.2), we note that for $\varphi_0(z)$ uniform in x, the solution $\varphi_(z, t)$ remains uniform in x. Thus, we can eliminate the x-term in (7.2) to get the one dimensional model

$$\varphi_t + (S(z)f(\varphi))_z = 0, \quad -\infty < x < \infty, \quad a < z < b, \quad t > 0. \tag{7.5}$$

Using (7.5), we analyze the evolution of $\varphi_0(z)$ uniform in x in §7.3.

7.1 Shock Formation

Consider (7.2) with initial condition

$$\varphi(x,z,0) = \varphi_0(x,z), \quad -\infty < x < \infty, \quad a < z < b \tag{7.6}$$

with $\varphi_0(x,z)$ smooth, $u(z)$ an increasing function, and $f(\varphi)$ convex. The goal, much like §4.1 is to characterize the initial data to determine if a shock will form in the interior of the spatial domain. As before, showing that the solution involving the gradient $\nabla\varphi$ becomes unbounded will indicate the formation of a jump in the concentration of small particles. Thus, a similar setup to §4.1, but with a more complex analysis, will help resolve the shock formation question.

Let $(v,w) = (\varphi_x, \varphi_z)$ be the gradient of φ. Differentiating (7.2) successively with respect to x and z gives two equations

$$\frac{dv}{dt} = -S(z)f''(\varphi)vw - S'(z)f'(\varphi)v \tag{7.7a}$$

$$\frac{dw}{dt} = -u'(z)v - S(z)f''(\varphi)w^2 - 2S'(z)f'(\varphi)w - S''(z)f(\varphi) \tag{7.7b}$$

where $\frac{d}{dt} = \partial_t + u(z)\partial_z + S(z)f'(\varphi)\partial_z$ is the convective derivative along characteristics. Since φ is not constant along characteristics for a depth dependent segregation rate, these ODE are coupled with the z and φ ODE from (7.3). From these four ODE, shock formation can be determined in quadrants I, II and IV of the (v,w) phase-plane. Experimentally, velocity profiles are observed to either be approximately linear, or approximately exponential [41, 43]. Since we have already studied shock formation under a linear velocity profile, we restrict ourselves to an exponential profile:

$$S(z) = se^{\beta(z-a)}, \quad a \le z \le b, \tag{7.8}$$

with $s > 0$ and β constant.

Theorem 7.1.1 *Suppose (7.8) holds and consider (7.2) with $u'(z) > 0$ and $f(\varphi)$ convex with*

$f(0) = f(1) = 0$. *If either (a)* $\varphi_x^0(x_0, z_0) > 0$, *or (b)* $\varphi_x^0(x_0, z_0) = 0$ *and* $\varphi_z^0(x_0, z_0) < 0$, *then either a shock forms in finite time, or the characteristic emanating from* (x_0, z_0) *reaches a boundary* $z = a$ *or* $z = b$ *before* $\nabla\varphi$ *becomes singular.*

Proof: First, observe that the w-axis, i.e. $v = 0$, is invariant for equation (7.7a). In case (a), it follows from the assumption $v(0) = \varphi_x^0(x_0, z_0) > 0$ that $v(t) > 0$ for all $t > 0$ for which the solution of (7.7) remains bounded. This is the only information needed concerning v in case (a) in order to analyze finite time blow-up of w in equation (7.7b).

Differentiating (7.4) gives

$$S'(z)f'(\varphi)w = -\frac{S'(z)^2}{S(z)}f(\varphi). \tag{7.9}$$

Substituting into equation (7.7b) gives

$$\frac{dw}{dt} = -u'(z)v - S(z)f''(\varphi)w^2 + \left(2\frac{S'(z)^2}{S(z)} - S''(z)\right)f(\varphi) < -S(z)f''(\varphi)w^2, \tag{7.10}$$

since $v > 0$, $2\dfrac{S'(z)^2}{S(z)} - S''(z) = s\beta^2 e^{\beta(z-a)}$ and $f(\varphi) \leq 0$. Although z and φ are evolving along the characteristic emanating from (x_0, z_0), both $S(z) > 0$ and $f''(\varphi) > 0$ are bounded from below by positive constants in the physical domain $a < z < b$, $0 \leq \varphi \leq 1$. Thus, there is a constant $\alpha > 0$ such that

$$\frac{dw}{dt} < -\alpha w^2, \tag{7.11}$$

at least until the characteristic reaches the boundary.

If $w(0) = \varphi_z^0(x_0, z_0) < 0$, then (7.11) implies that $w(t) \to -\infty$ in finite time since

$$w(t) \leq \frac{w(0)}{1 + \alpha w(0)t}. \tag{7.12}$$

If $w(0) > 0$, then it must be shown that $w(t^*) = 0$ for some finite time $t = t^*$ in order to show

that $w(t) \to -\infty$. To do this, first observe that

$$\frac{dw}{dv} = \frac{-u'(z)v - S''(z)f(\varphi) - 2S'(z)f'(\varphi)w - S(z)f''(\varphi)w^2}{-S'(z)f'(\varphi)v - S(z)f''(\varphi)vw} \tag{7.13}$$

$$= \frac{w}{v} + \frac{-u'(z)v - S''(z)f(\varphi) - S'(z)f'(\varphi)w}{-S'(z)f'(\varphi)v - S(z)f''(\varphi)vw}. \tag{7.14}$$

Using (7.9) and substituting into (7.14) gives

$$\frac{dw}{dv} = \frac{w}{v} + \frac{-u'(z)v + \left(\frac{S'(z)^2}{S(z)} - S''(z)\right) f(\varphi)}{-S'(z)f'(\varphi)v - S(z)f''(\varphi)vw}, \tag{7.15}$$

and since $\dfrac{S'(z)^2}{S(z)} - S''(z) = 0$, (7.15) becomes

$$\frac{dw}{dv} = \frac{w}{v} + \frac{-u'(z)}{\frac{S'(z)^2}{S(z)w} f(\varphi) - S(z)f''(\varphi)w} > \frac{w}{v}. \tag{7.16}$$

Thus $\dfrac{dw_0}{dv_0} > \dfrac{dw}{dv}$, so for $v < v_0$

$$w = w_0 + \int_{v_0}^{v} \frac{dw}{dv'} dv' = w_0 - \int_{v}^{v_0} \frac{dw}{dv'} dv'. \tag{7.17}$$

Therefore, $w(v) < w_0 - \dfrac{w_0}{v_0}(v_0 - v) = \dfrac{w_0}{v_0} v$, giving that $w(\bar{v}) = 0$ for some $\bar{v} > 0$ in finite time. Thus, the gradient $\nabla\varphi$ has now entered the fourth quadrant and is subject to (7.11).

In summary, for any $\nabla\varphi_0$ that starts in the first or fourth quadrants will develop a finite time singularity unless the characteristic reaches the boundary first. All that remains is case (b) in which $v(t) = 0$. Thus the estimate (7.11) applies on the w-axis. Consequently, $w(0) < 0$ leads to finite time blow-up of $w(t)$, completing the proof. ■

For initial data that starts in the second quadrant (i.e $v < 0,\ w > 0$), we show that all solutions tend to the origin $(v, w) = (0, 0)$ as $t \to \infty$. The equations are still given by (7.7), so considering (7.7a) we see the term $-S(z)f''(\varphi)vw > 0$ but the term $-S'(z)f'(\varphi)v$ could be

positive or negative. Referring to Figure 7.1 we see that if $S'(z) < 0$ that $\varphi \to 0$ as $t \to \infty$, thus the term $-S'(z)f'(\varphi)v \to S'(z)v > 0$, giving $\dfrac{dv}{dt} > 0$. If $S'(z) > 0$ then $\varphi \to 1$ as $t \to \infty$. As a result, the term $-S'(z)f'(\varphi)v \to -S'(z)v$, which still gives $\dfrac{dv}{dt} > 0$. So in both cases, $\dfrac{dv}{dt}$ eventually becomes positive, meaning v is always tending toward the w-axis after some time $t = \bar{t}$. We claim $v \to 0$ as $t \to \infty$:

Theorem 7.1.2 *Consider (7.2) with $S(z)$ given by (7.8), $u'(z) > 0$ and $f(\varphi)$ convex with $f(0) = f(1) = 0$. If $v_0 = \varphi_x^0(x_0, z_0) < 0$ and $w_0 = \varphi_z^0 > 0$ then $v \to 0$ as $t \to \infty$.*

Proof : Assume for contradiction that $v \to \varepsilon < 0$ as $t \to \infty$. Since $S(z)f(\varphi) = const.$ and $S,\ f$ and their derivatives are bounded, we know that z must have a maximum (see Figure 7.1) and φ is either increasing to $\varphi = 1$ or decreasing to $\varphi = 0$. Thus, no oscillations or blow up occur in v or w, so one of two cases are possible:
(I) $(v, w) \to (\varepsilon, 0)$ as $t \to \infty$
(II) $(v, w) \to (\varepsilon, w*)$ as $t \to \infty$.
For case (I), since $w > 0$ then as $w \to 0^+$ as $t \to \infty$, the trajectory decreases toward $w = 0$ from the positive direction meaning $\dfrac{dw}{dt} < 0$ at $(v, w) = (\varepsilon, 0)$. However, as $t \to \infty,\ w \to 0$ by assumption, and $f(\varphi) \to 0$ (see equation (7.4) and Figure 7.1), thus from (7.7b) $\dfrac{dw}{dt} \to -u'(z)v > 0$. This contradicts the fact that $\dfrac{dw}{dt} < 0$ if $(v, w) \to (\varepsilon, 0)$, eliminating case (I) as a possibility.

Case (II) is the only possibility left, so assume $(v, w) \to (\varepsilon, w^*)$ as $t \to \infty$. Since $w_0 > 0$ and $w \to w^* > 0$, then $w > w_{\min} > 0$ for all time t. Additionally $S(z),\ f(\varphi)$ and their respective derivatives are bounded away from zero on $a < z < b,\ 0 < \varphi < 1$, so after $t = \bar{t}$, equation (7.7a) becomes the inequality

$$\frac{dv}{dt} \geq -Kw_{\min}v \tag{7.18}$$

with $K = \delta_1\delta_2 > 0$ given by $S(z) \geq \delta_1 > 0$ and $f''(\varphi) > \delta_2 > 0$. By comparison, the solution v satisfies

$$v \geq v_0 e^{-Kw_{\min}t}. \tag{7.19}$$

Since $v_0 < 0$, then $v \to 0$ as $t \to \infty$ contradicting the assumption that $v \to \varepsilon < 0$ as $t \to \infty$. Thus, by contradiction for both case (I) and (II), $v \to 0$ as $t \to \infty$. ■

Now that we have established $v \to 0$, we show that $w \to 0$ as $t \to \infty$. Since $v \to 0$ and $f(\varphi) \to 0$ as $t \to \infty$, then from (7.7b)

$$\frac{dw}{dt} \to -S(z)f''(\varphi)w^2 \leq -Cw^2 \text{ as } t \to \infty, \tag{7.20}$$

where $C > 0$ is a bound due to the fact that $S(z)$ and $f''(\varphi)$ are bounded on $a < z < b,\ 0 < \varphi < 1$. Thus, by comparison

$$w \leq \frac{w_0}{1 + Cw_0 t}, \tag{7.21}$$

showing that $w \to 0$ as $t \to \infty$ since $w_0 > 0$. Therefore, for $v_0 < 0,\ w_0 > 0$, no interior shock forms since $(v, w) \to (0, 0)$, meaning φ tends toward a constant.

In summary, for initial data in the first and fourth quadrants of the (v, w) plane, we have shown that an interior shock forms in finite time. In the second quadrant, the solution remains smooth aside from the shocks that propagate in from the boundary. We have fully characterizde the problem of interior shock formation in the first, second and fourth quadrants of the (v, w) plane, but characterization of the third quadrant remains an open problem. The difficulty of characterizing the third quadrants stems from the fact that solutions in (v, w) can either blow up or head toward the origin. For initial data close to the v-axis but away from the w-axis, solutions will remain bounded and head to $(v, w) = (0.0)$. Initial that are close to the w-axis but away from the v-axis will blow up. However, in between, there is some separating curve or region that is currently unknown that separates initial data that blow up from initial data that remain bounded.

7.2 Generalized Shock Wave Breaking

7.2.1 Constant Segregation Rate, $\varphi_- > \varphi_+$

Consider an interface $x = g(z)$ separating two constant values $\varphi_- > \varphi_+$ of φ, with the same initial condition as (5.8). As in §5, for any monotonically decreasing $g(z)$, the interface will steepen and eventually break at a single point as long as $u(z)$ is a monotonically increasing function (i.e. $u'(z) > 0$). Thus, without loss of generality, we can assume conditions (5.9) hold for $g(z)$, giving $g'(z) < 0$ and $zg''(z) < 0$ for all $z \neq 0$. In particular, the $g'(0) = 0$ at $z = 0$ and decreasing elsewhere.

Assuming a constant segregation rate throughout the material (not depth-dependent), and any convex flux $f(\varphi)$ with $f(0) = f(1) = 0$, the Gray-Thornton model becomes

$$\varphi_t + u(z)\varphi_x + f(\varphi)_z = 0, \quad -\infty < x < \infty, \quad -1 < z < 1, \quad t > 0. \tag{7.22}$$

The interface $x = x(z,t)$ with $x(z,0) = g(z)$ evolves according to the Rankine-Hugoniot condition

$$x_t + rx_z = u(z) \tag{7.23}$$

where $r = \dfrac{f(\varphi_+) - f(\varphi_-)}{\varphi_+ - \varphi_-}$ is constant. Employing the method of characteristics on (7.23) gives

$$\frac{dx}{dt} = u(z), \quad \frac{dz}{dt} = r. \tag{7.24}$$

Solving for (x, z) gives us a parametric curve in (x, z) parameterized by z_0:

$$z(t; z_0) = rt + z_0 \tag{7.25a}$$

$$x(t; z_0) = \int_0^t u(r\tilde{t} + z_0)d\tilde{t} + g(z_0). \tag{7.25b}$$

Eliminating z_0 from (7.25) gives a curve $x = x(z,t)$ which we call the *evolved initial interface.*

Theorem 7.2.1 *The evolved initial interface $x = (z, t)$ has a local maximum $(x, z) = (x_+(t), z_+(t))$ and a local minimum $(x, z) = (x_-(t), z_-(t))$ up to a short time $t = T < \infty$.*

Proof: To show $x = x(z, t)$ has local extrema, we must find solutions z_-, z_+ to $\dfrac{\partial}{\partial z}x(z, t) = 0$. Applying the chain rule and using (7.25a) we see $\dfrac{\partial}{\partial z} = \dfrac{\partial}{\partial z_0}\dfrac{\partial z_0}{\partial z} = \dfrac{\partial}{\partial z_0}$. Hence, we take $\dfrac{\partial}{\partial z_0}$ of $x(t; z_0)$ and set it equal to zero:

$$\frac{\partial}{\partial z_0}x = \int_0^t u'(r\tilde{t} + z_0)d\tilde{t} + g'(z_0) = 0. \tag{7.26}$$

Evaluating the integral gives

$$f(z_0, t) = g'(z_0) + \frac{1}{r}(u(rt + z_0) - u(z_0)) = 0. \tag{7.27}$$

By employing the Implicit Function Theorem on $f(z_0, t)$, we can show that $t = \hat{t}(z_0)$ near $z_0 = 0$. We note $f(0, 0) = 0$ and $\dfrac{\partial}{\partial t}f(z_0, t) = ru'(z_0 + rt)$. Letting $t = 0, z_0 = 0$ we get

$$\frac{\partial}{\partial t}f(0, 0) = ru'(0) > 0 \tag{7.28}$$

thus showing $t = \hat{t}(z_0)$ in a neighborhood of $z_0 = 0$.

Next, we show that $t = \hat{t}(z_0) \geq 0$ by showing $\hat{t}'(0) = 0$ and $\hat{t}''(0) > 0$ showing that t is concave up with a minimum at $\hat{t}(0) = 0$ near $z_0 = 0$. Since $f(z_0, \hat{t}(z_0)) = rg'(z_0) + u(z_0 + r\hat{t}) - u(z_0) = 0$, then

$$\frac{\partial f}{\partial z_0} = rg''(z_0) + u'(z_0 + r\hat{t})(1 + r\hat{t}') - u'(z_0) = 0. \tag{7.29}$$

At $z_0 = 0$, (7.29) becomes $\hat{t}'(0) = 0$. Taking one more z_0 derivative of f gives

$$\frac{\partial^2 f}{\partial z_0^2} = rg'''(z_0) + u''(z_0)(1 + r\hat{t}(z_0))^2 + u'(z_0)r\hat{t}''(z_0) - u''(z_0) = 0. \tag{7.30}$$

Evaluating at $z_0 = 0$ gives $\hat{t}''(0) = \dfrac{-g'''(0)}{u'(0)} > 0$, meaning the solution to (7.27) is a function $t = \hat{t}(z_0)$ that is concave up and has a minimum $\hat{t} = 0$ at $z_0 = 0$. Thus, for each time $\hat{t}$ up

to some short time T, two values of z satisfy (7.27). In other words, (7.27) has two solutions $z_{0_+}(t)$ and $z_{0_-}(t)$. Using the z equation from (7.25), we get that the evolved initial interface has a maximum $z_+(t)$ and a minimum $z_+(t)$ where $z_\pm(t) = rt + z_{0_\pm}(t)$. To find $x_\pm(t)$ simply substitute $z_\pm(t)$ into the x equation in (7.25). ■

The portion of the evolved initial interface between the local extrema is now unstable since in this region φ_- is above φ_+, which is the unstable case in Theorem 3.3.1 (with φ_- and φ_+ reversed). From here, we can construct the mixing zone $\mathcal{M}_a(t)$ similar to §5.1. Using the method of characteristics on (7.22), we get

$$\frac{dx}{dt} = u(z), \quad \frac{dz}{dt} = f'(\varphi). \tag{7.31}$$

Since φ is constant on characteristics, the solution to (7.31) is

$$z = f'(\varphi)t + \lambda, \quad x = \int_0^t u(f'(\varphi)\tilde{t} + \lambda)d\tilde{t} + \mu. \tag{7.32}$$

To resolve the constants of integration, we parameterize each curve at a fixed time t by t_1 with $P_\pm(t_1) = (x_\pm(t_1), z_\pm(t_1))$ where $t_1 \in [0, t]$. Thus, (7.32) becomes $C_\varphi^\pm(t) = \{(x^\pm(t, \varphi; t_1), z^\pm(t, \varphi; t_1)),\ 0 \leq t_1 \leq t\}$ with:

$$\begin{aligned} z^\pm(t, \varphi; t_1) &= f'(\varphi)(t - t_1) + z_\pm(t_1) \\ x^\pm(t, \varphi; t_1) &= \int_{t_1}^t u\left(f'(\varphi)(\tilde{t} - t_1) + z_\pm(t_1)\right) d\tilde{t} + x_\pm(t_1). \end{aligned} \tag{7.33}$$

At $t_1 = t$, each curve $C_\varphi^\pm(t)$ is at the point $(x^\pm, z^\pm) = P_\pm(t) = (x_\pm(t), z_\pm(t))$, and at $t_1 = 0$, each curve $C_\varphi^\pm(t)$ lies on another curve (in the linear case in §5 this is the line $L(t)$) given by $x = \int_0^t u(z^\pm(\tilde{t}, \varphi; 0))d\tilde{t}$.

Figure 7.2 shows $\mathcal{M}_a(t)$ with $g(z) = -z^3,\ \varphi_- = 1,\ \varphi_+ = 0,\ u(z) = -e^{-z},\ S = 1$. Figure 7.2a is a numerical PDE simulation using Godunov's method on equation (7.22) whereas Figure 7.2b is a numerical solution of the ODE system (7.31). Notice the similarities between the PDE

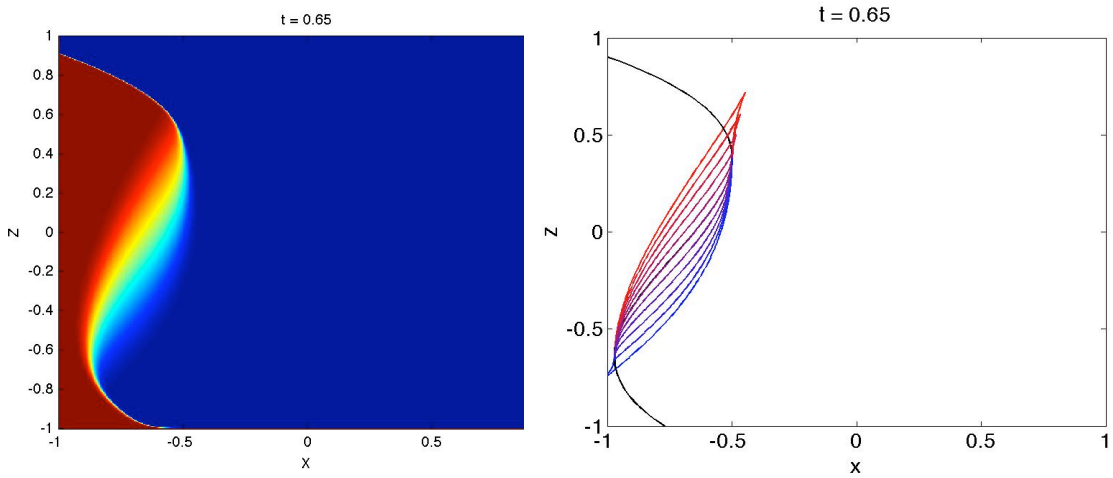

Figure 7.2: (a) PDE simulation for $\mathcal{M}_a(0.65)$ (b) Numerical solution to (7.31) for $\mathcal{M}_a(0.65)$

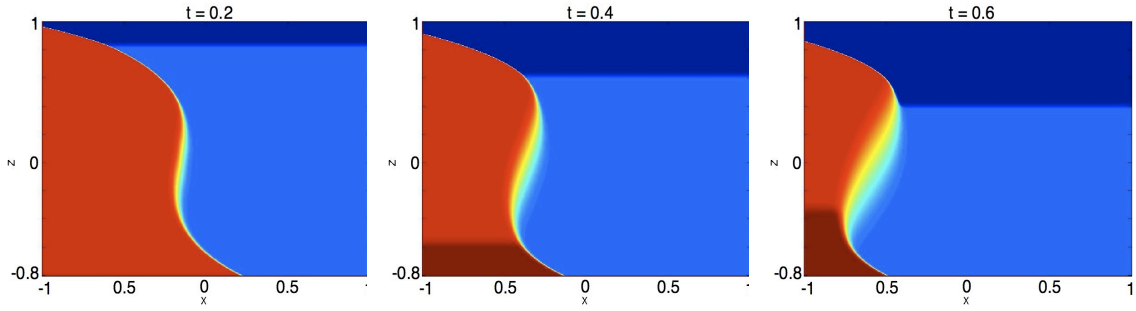

Figure 7.3: PDE simulation for the evolution of $\mathcal{M}_a(t)$ with $\varphi_+ = 0.1$.

simulation in Figure 7.2a and the numerical solution in Figure 7.2b. However, due to the fact that the starting points for each contour are unknown at later times (equivalent to $\mathcal{M}_3(t)$ from §5), we simply choose these points to be at the extrema of the evolved initial interface when finding the numerical ODE solution. These chosen points are slightly incorrect, accounting for the slight visual differences between figure 7.2a and 7.2b. Figure 7.3 shows the evolution of $\mathcal{M}_a(t)$ with $g(z) = -z^3,\ \varphi_- = 1,\ \varphi_+ = 0.1,\ u(z) = -e^{-z},\ S = 1$.

In summary, for a short time $t < T$, we have shown that the evolved initial interface has a local maximum and minimum $P_\pm(t)$. Between these points, a smooth mixing region replaces

the unstable portion of the evolved initial interface with the curves $C_{\varphi}^{\pm}(t)$ given by (7.33).

7.2.2 Depth-Dependent Segregation Rate, $\varphi_- = 1,\ \varphi_+ = 0$

Consider a monotonically decreasing initial interface $x = g(z)$ separating a region of small particles $\varphi_- = 1$ on the left from a region of large particles $\varphi_+ = 0$ on the right. Assume $g(z)$ has conditions given by (5.9) giving $g'(z) < 0$ and $zg''(z) < 0$ for all $z \neq 0$. As we have already seen, for a monotonically increasing parallel bulk velocity $u(z)$, the interface will steepen and eventually break at a single point.

Assuming a segregation rate proportional to the derivative of the velocity (i.e., $S(z) = s|u'(z)|,\ s > 0$), the Gray-Thornton model becomes:

$$\varphi_t + u(z)\varphi_x + (S(z)f(\varphi))_z = 0, \quad -\infty < x < \infty, \quad -1 < z < 1, \quad t > 0. \tag{7.34}$$

Note φ_- and φ_+ are solutions to (7.34). The interface evolves according to the Rankine-Hugoniot condition derived from the divergence theorem [63]

$$x_t = u(z) \tag{7.35}$$

meaning the evolved initial interface $x = x(z,t)$ is given by

$$x(z,t) = u(z)t + g(z). \tag{7.36}$$

To show $x(z,t)$ has a maximum and minimum with respect to z, we simply take

$$\frac{\partial}{\partial z}x(z,t) = u'(z)t + g'(z) = 0. \tag{7.37}$$

Since g' is concave and $u' > 0$, then for short time there are two solutions near $z = 0$ to (7.37), denoted $z_{\pm}(t)$. Substituting $z_{\pm}(t)$ into (7.36) gives the maximum and minimum of the evolved interface $P_{\pm}(t) = (x_{\pm}(t), z_{\pm}(t))$.

The portion of the evolved initial interface between the local extrema is now unstable since in this region all small particles lie above all large particles. From here, the analysis becomes more complex than in §7.2.1 since φ is not constant along characteristics. Instead, the method of characteristics applied to (7.34) gives

$$\frac{dx}{dt} = u(z), \quad \frac{dz}{dt} = S(z)f'(\varphi), \quad \frac{d\varphi}{dt} = -S'(z)f(\varphi), \tag{7.38}$$

showing φ is non-constant on characteristics. The region $\mathcal{M}_b(t)$ between the endpoints $P_\pm(t)$ must be calculated numerically, as (7.38) proves too difficult to find an analytic solution. Figure 7.4 shows the mixing zone $\mathcal{M}_b(t)$ that results from $g(z) = -z^3$ with $\varphi_- = 1,\ \varphi_+ = 0,\ u(z) = -e^{-z},\ S(z) = e^{-z}$. Note the only difference between Figure 7.2 and Figure 7.4 is the segregation rate ($S = 1$ in the former and $S(z) = e^{-z}$ in the latter). Due to the difference, we also see a difference between the two mixing regions. In Figure 7.4 the outermost contour $\varphi_+ = 0$ comes much lower toward $(x, z) \approx (-0.7, -0.95)$, whereas in Figure 7.2 the $\varphi_+ = 0$ contour only reaches the evolved interface at $(x, z) \approx (-0.8, -0.8)$. The differences between the two figures for $x > -0.5$ are much less noticeable, as the segregation rate $S(z) = e^{-z}$ is closer to $S = 1$ than for $x < -0.5$.

Figure 7.4a is a numerical PDE simulation of (7.34) while Figure 7.4b is a numerical solution for $\varphi(x, z, t)$ from the ODE system (7.38). Note at the points where the φ contours intersect the evolved initial interface, shocks form. These points correspond to $Q_\pm(t)$ from $\mathcal{M}_3(t)$ in §5. Also, notice the similarities between the PDE simulation in Figure 7.4a and the numerical solution to (7.38) in Figure 7.4b. However, due to the fact that the starting points for each contour are unknown at later times (equivalent to $\mathcal{M}_3(t)$ from §5), we simply choose these points to be at the extrema of the evolved initial interface when finding the numerical ODE solution. These chosen points are slightly incorrect, accounting for the slight visual differences between figure 7.4a and 7.4b.

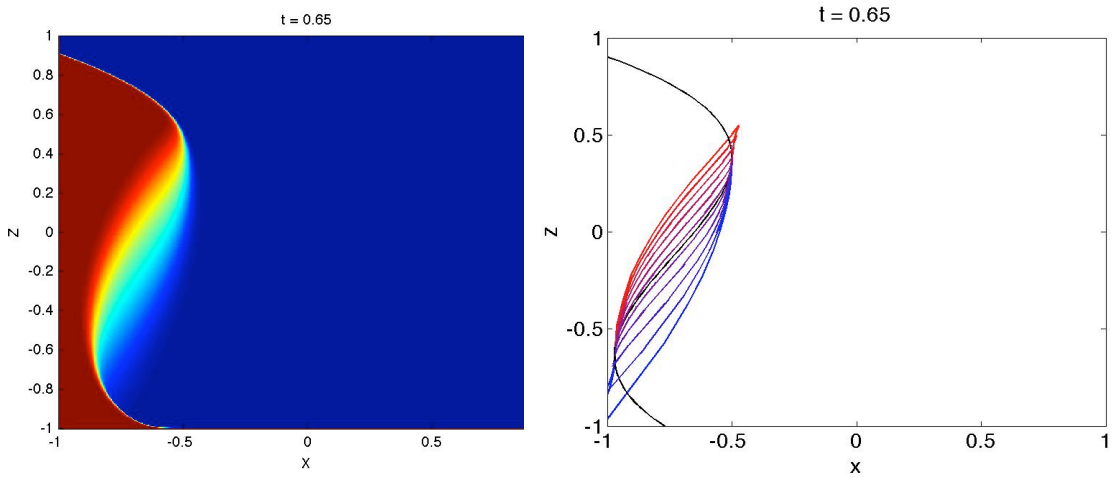

Figure 7.4: (a) PDE simulation for $\mathcal{M}_b(0.65)$ (b) Numerical solution to (7.38) for $\mathcal{M}_b(0.65)$

7.3 Depth-Dependent Segregation Rate, $\varphi_- > \varphi_+$

Consider a monotonically decreasing initial interface $x = g(z)$ separating a region with a higher concentration of small particles φ_- on the left from a region with a higher concentration of large particles φ_+ on the right, i.e., $\varphi_- > \varphi_+$. Assume $g(z)$ has conditions given by (5.9) giving $g'(z) < 0$ and $zg''(z) < 0$ for all $z \neq 0$. Then for a monotonically increasing parallel bulk velocity $u(z)$, the interface will steepen and eventually break at a single point.

The evolution of this system is governed by equation (7.34). However, since φ_- and φ_+ no longer consist only of all small or all large particles respectively, they are not solutions to (7.34), and thus, evolve along with the rest of the breaking interface. The interface evolves according to the Rankine-Hugoniot condition

$$x_t + r(x, z, t)x_z = u(z) \tag{7.39}$$

where $r(x, z, t) = S(z)\dfrac{f(\varphi_+(x, z, t)) - f(\varphi_+(x, z, t))}{\varphi_+(x, z, t) - \varphi_-(x, z, t)}$. Thus, by the method of characteristics,

the evolved initial interface $x = x(z,t)$ evolved according to

$$\frac{dz}{dt} = r(x,z,t), \quad z(0) = z_0 \tag{7.40a}$$

$$\frac{dx}{dt} = u(z(t)), \quad x(0) = x_0 = g(z_0). \tag{7.40b}$$

Here, due to the fact that φ_- and φ_+ evolve rather than remain constant, even showing that the evolved interface has a maximum and minimum becomes too cumbersome. The best we can do is to note that

$$x(z,t) = \int_0^t u\bigg(\int_0^{t'} r(x,z,t'')dt'' + z_0\bigg)dt' + x_0. \tag{7.41}$$

The mixing region evolves according to (7.38) where the evolved initial interface is unstable. We again use numerical simulations to show that a mixing region $\mathcal{M}_c(t)$ indeed occurs between two points $P_\pm(t)$. In Figure 7.5 we see the mixing region $\mathcal{M}_c(t)$ with $g(z) = -z^3$, $\varphi_- = 1$, $\varphi_+ = 0.35$, $u(z) = -e^{-z}$, $S(z) = e^{-z}$. In Figure 7.6 $\mathcal{M}_c(t)$ has the same conditions but with $\varphi_- = 0.9$. In both instances, it is clear that φ_+ evolves, and in Figure 7.6 φ_- evolves as well.

Without loss of generality, we consider the evolution of φ_+ (the same will apply to $\varphi_- < 1$). We see from Figure 7.5 that the φ_+ region is uniform in x away from the mixing zone. However, close to the mixing zone, an interaction between the mixing zone itself and the uniform φ_+ region occurs. Contours bend toward the mixing zone and down toward the evolved initial interface. The difficulty in fully understanding this region is that we do not have explicit formulae for the contours in the mixing region. Thus, there is no way to understand how the mixing region interacts with the region that is uniform in x.

However we can study the region that is uniform in x and develop an exact theory. Consider an inclined two dimensional plane with x as the downslope direction and z normal to the surface. By employing an initial condition φ_0 that is constant throughout the plane, the problem becomes one-dimensional, since the flow is uniform in the x-direction. Here, we consider

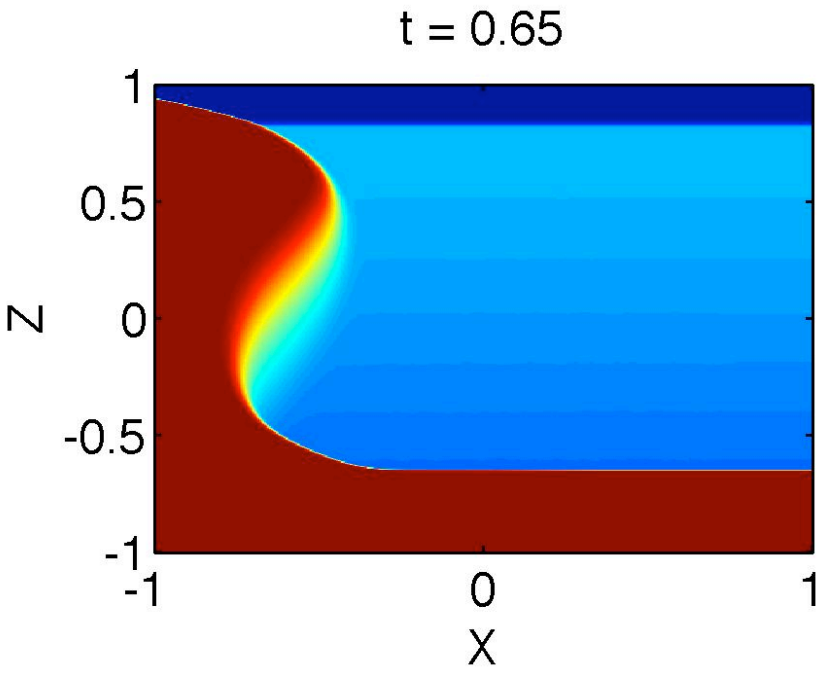

Figure 7.5: $\mathcal{M}_c(t)$ at $t = 0.65$ with $\varphi_- = 1$

a nonlinear, monotonically increasing parallel bulk velocity, implying the segregation rate is depth-dependent. The segregation rate $S(z)$ will be taken to be either increasing, decreasing or constant. We consider the flux $f(\varphi) = \varphi(\varphi - 1)$ introduced by Gray and Thornton.

Under these assumptions, the modified Gray-Thornton model becomes

$$\varphi_t + (S(z)\varphi(\varphi - 1))_z = 0, \quad a < z < b, \quad t > 0 \tag{7.42}$$

where the x term has been dropped due to the uniformity in that direction. In this equation, $S(z)$ should be proportional to the shear rate $|u'(z)|$. For simplicity, we consider $0 < z < 1$. Although (7.42) is a one dimensional conservation law, calculating an explicit solution is complicated by the observation that φ is not constant along characteristics. The goal is to characterize the evolution of φ from constant initial data $\varphi_0(z)$, including the shocks that propagate inward from the boundary due to an accumulation of small and large particles at the

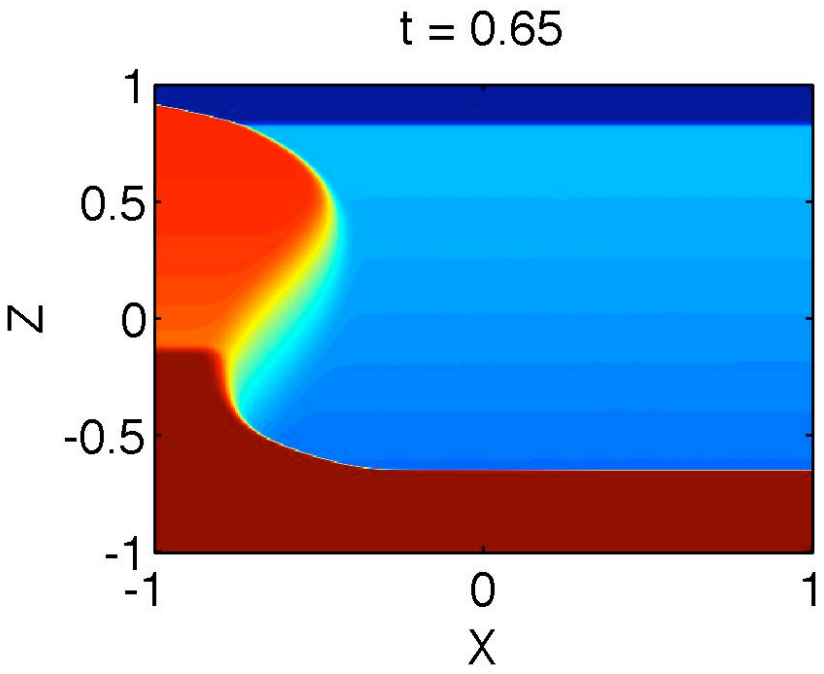

Figure 7.6: $\mathcal{M}_c(t)$ at $t = 0.65$ with $\varphi_- = 0.9$

bottom and top respectively.

7.3.1 Interior Solution

The method of characteristics applied to (7.42) is:

$$\frac{dz}{dt} = S(z)(2\varphi - 1) \tag{7.43a}$$

$$\frac{d\varphi}{dt} = -S'(z)\varphi(\varphi - 1), \tag{7.43b}$$

with initial data $z(0) = z_0, \varphi(z, 0) = \varphi_0(z)$. Solving (7.43b) for φ gives

$$\varphi = \frac{1}{2}\frac{\frac{dz}{dt} + S(z)}{S(z)} \tag{7.44}$$

meaning if $z(t)$ is known, then $\varphi(z(t),t)$ is known, and given by (7.44). System (7.43) has a first intergral (see (7.4)):

$$S(z)\varphi(\varphi-1)=c \tag{7.45}$$

with c an arbitrary constant. Solving (7.45) for φ gives

$$\varphi=\pm\frac{1}{2}\sqrt{\frac{c_1}{S(z)}+1}+\frac{1}{2} \tag{7.46}$$

where $c_1=4c$. Note, since $0<\varphi<1$ and $S(z)>0$, we get the conditions

$$S(z)\geq -c_1, \quad c_1\leq 0. \tag{7.47}$$

Rearranging (7.46), we get

$$(2\varphi-1)=\begin{cases}\sqrt{\dfrac{c_1}{S(z)}+1}, & \text{if } \dfrac{dz}{dt}>0\\[2ex] -\sqrt{\dfrac{c_1}{S(z)}+1}, & \text{if } \dfrac{dz}{dt}<0.\end{cases} \tag{7.48}$$

Note, since $f(\varphi)=\varphi(\varphi-1)$, $\dfrac{dz}{dt}>0 \iff \varphi>\dfrac{1}{2}$ and $\dfrac{dz}{dt}<0 \iff \varphi<\dfrac{1}{2}$ (see Figure 7.1). Substituting (7.48) into the z equation from (7.43) gives a differential equation solely in z:

$$\frac{dz}{dt}=\pm\sqrt{S(z)(c_1+S(z))}. \tag{7.49}$$

Therefore, $(z(t),\varphi(z(t),t))$ is found by solving (7.44) and (7.49) together.

7.3.2 Boundary Shocks

For $t>0$, two boundary shocks form, one at the top ($z=1$) and one at the bottom ($z=0$) due to an accumulation of large and small particles respectively. The shocks propagate inward, i.e. away from the boundaries, according to the Rankine-Hugoniot jump condition [63] for a

shock $z = \tilde{z}(t)$ applied to (7.42):

$$\tilde{z}_t = S(\tilde{z})(\varphi_- + \varphi_+ - 1). \tag{7.50}$$

At the bottom, $\varphi_- = 1$ (a region of small particles accumulate at the bottom) and $\varphi_+ = \varphi(z(t), t)$ from (7.44). This gives the ODE

$$\frac{dz_-}{dt} = S(z_-)\varphi(z_-(t), t); \quad z_-(0) = 0 \tag{7.51}$$

where $z = z_-(t)$ is the shock propagating inward initially from $z = 0$.

Similarly, at the top, $\varphi_- = \varphi(z(t), t)$ and $\varphi_+ = 0$ (a region of large particles accumulate at the top). The ODE for the shock $z = z_+(t)$ propagating inward initally from $z = 1$ is

$$\frac{dz_+}{dt} = S(z_+)(\varphi(z_+(t), t) - 1); \quad z_+(0) = 1. \tag{7.52}$$

The time to complete segregation, where a region of only large particles has formed on top of a region of only small particles is found by setting the solutions to (7.51) and (7.52) equal and solving for t. In other words, $t = t^*$ is the time to complete segregation found by setting $z^* = z_-(t) = z_+(t)$ and solving for t. The solution for $t > t^*$ is $\varphi = 0$ for $z > z^*$ and $\varphi = 1$ for $z < z^*$.

7.3.3 Examples

Two examples illustrate the complete solution to (7.42) with initial condition $\varphi(z_0, 0) = \varphi_0(z_0)$. In the first example we consider simple shear with constant segregation rate; in the second example we consider a depth-dependent segregation rate that is exponential in height z. In both examples, $\varphi = \varphi(z(t), t)$ can be solved completely in the region between the two boundary shocks, with exact equations for the boundary shocks given as well.

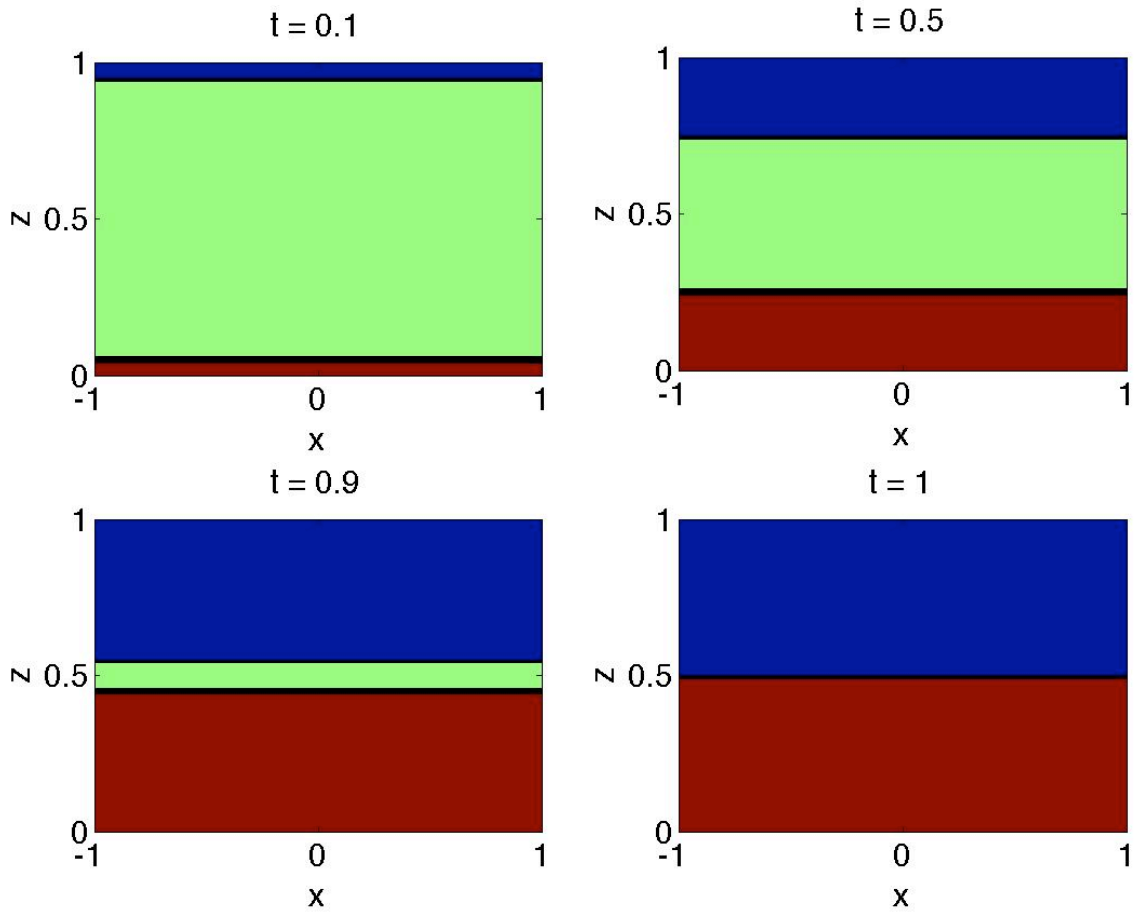

Figure 7.7: Contour plots of the evolution of $\varphi(z(t),t)$ from equation (7.42) with $S(z)=1$ and initial condition $\varphi(z(0),0)=\varphi_0(z_0)=\dfrac{1}{2}$.

Example 1: $S(z)=1$.

In this example, we take the segregation rate to be constant. Equation (7.43b) becomes $\dfrac{d\varphi}{dt}=0$, meaning $\varphi=\varphi_0(z_0)$ for all t. Equation (7.43a) becomes $\dfrac{dz}{dt}=2\varphi_0(z_0)-1$, with solution

$$z=(2\varphi_0(z_0)-1)t+z_0. \tag{7.53}$$

Equation (7.53) can be solved for $z_0=\tilde{z}_0(z,t)$ using the Implicit Function Theorem. Thus, $\varphi=\varphi_0(z_0)=\varphi_0(\tilde{z}_0(z,t))$.

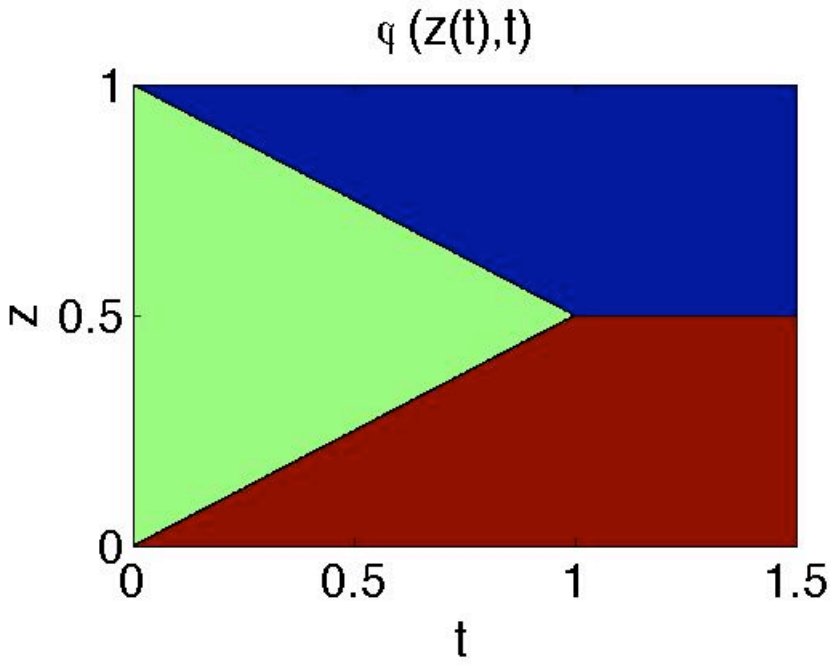

Figure 7.8: Solution of (7.44) and (7.49) with boundary shocks given by (7.51-7.52) for the case where $S(z) = 1,\ \varphi_0(z_0) = \dfrac{1}{2}$.

The boundary shock equations given by (7.51) and (7.52) become

$$\frac{dz_-}{dt} = \varphi_0(\tilde{z}_0(z_-, t)), \quad z_-(0) = 0; \qquad \frac{dz_+}{dt} = \varphi_0(\tilde{z}_0(z_+, t)) - 1, \quad z_+(0) = 1. \tag{7.54}$$

For the case where $\varphi_0(z_0) = \varphi_0 = const.$, the solutions are $z_-(t) = \varphi_0 t$ and $z_+(t) = (\varphi_0 - 1)t + 1$. Setting $z_- = z_+$ gives $t = t^* = 1$ and $z = z_-(t^*) = z_+(t^*) = z^* = \varphi_0$. In other words, the boundary shocks propagate inward, and meet at $t = t^* = 1$ at a height $z = z^* = \varphi_0$. If $\varphi_0 = \dfrac{1}{2}$, then complete segregation would occur at $t = 1$ with the shock at $z = \dfrac{1}{2}$. Note that the time to complete segregation, $t = t^*$ is independent of φ_0, but the height where segregation occurs $z = z^*$ is not. The solution with $\varphi_0 = \dfrac{1}{2}$ is shown in Figure 7.7 with the evolution of the solution through time shown in Figure 7.8.

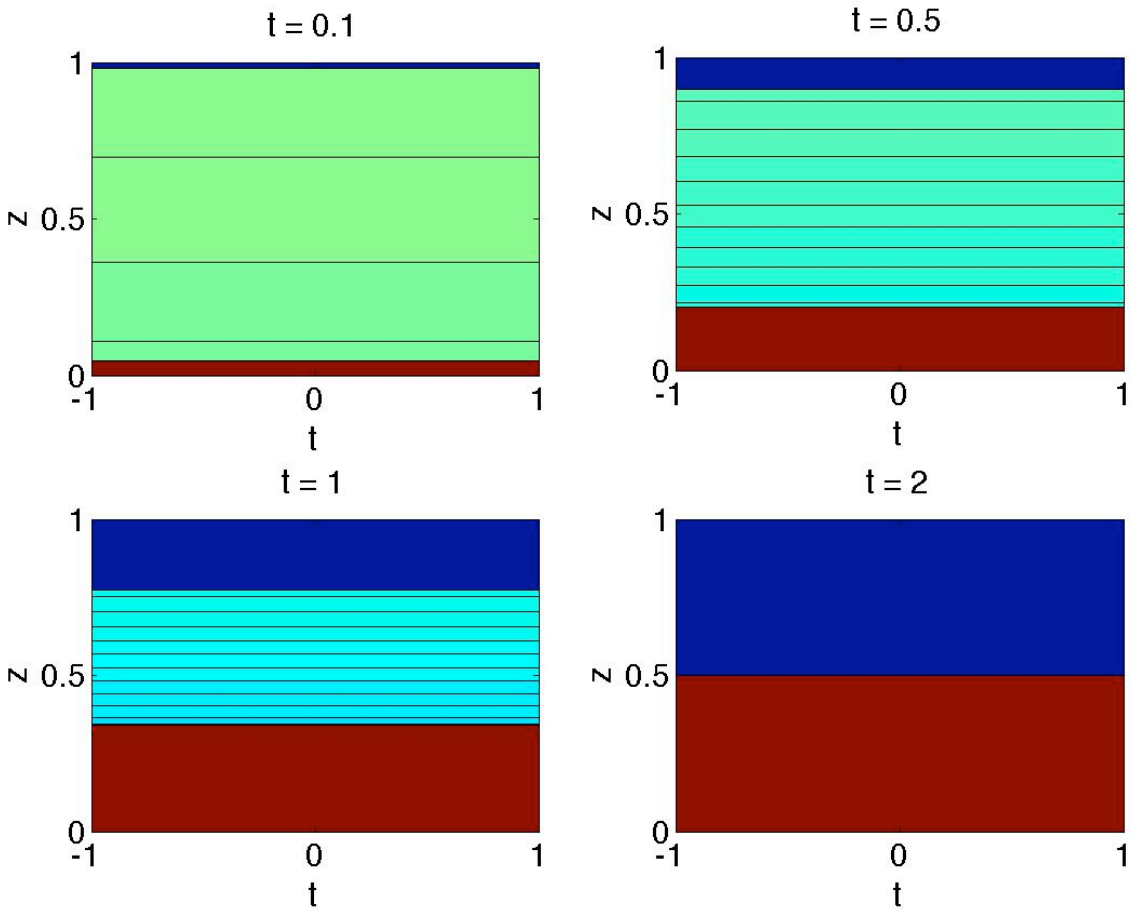

Figure 7.9: Contour plots of the evolution of $\varphi(z(t), t)$ from equation (7.42) with $S(z) = e^{-z}$ and initial condition $\varphi(z(0), 0) = \varphi_0(z_0) = \dfrac{1}{2}$. The contour lines are at intervals of 0.005.

Example 2: $S(z) = e^{-z}$

In this example we consider a depth-dependent segregation rate that is exponential in height. The ODE (7.49) becomes

$$\frac{dz}{dt} = \pm\sqrt{e^{-z}(c_1 + e^{-z})}, \quad z(0) = z_0 \tag{7.55}$$

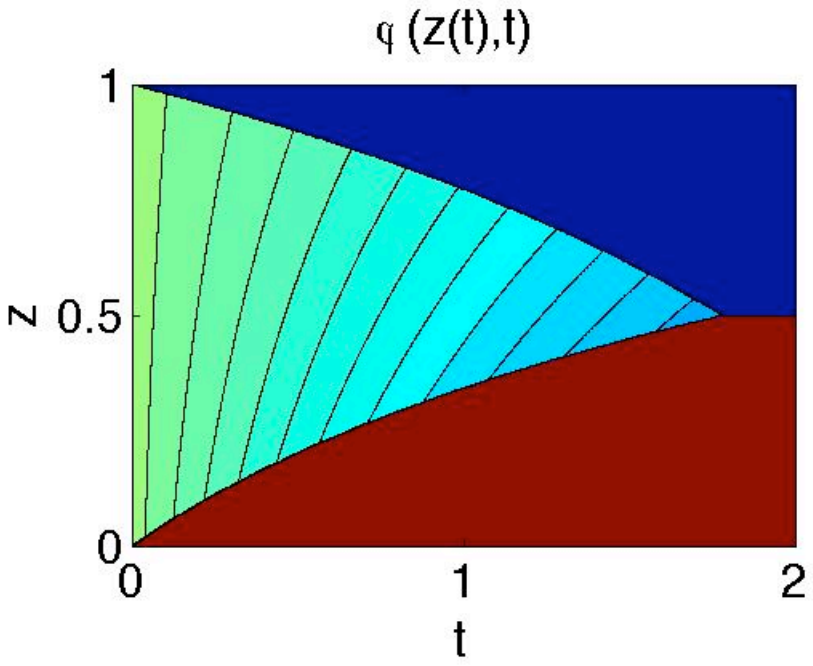

Figure 7.10: Solutions of (7.44) and (7.49) with boundary shocks given by (7.51-7.52) for the case where $S(z) = e^{-z},\ \varphi_0(z_0) = \frac{1}{2}$. The contour lines represent intervals of 0.02.

and has solution

$$z(t) = \ln\left(\frac{c_1^2 t^2 + 2c_1^2 c_2 t + c_1^2 c_2^2 - 4}{4c_1}\right) \tag{7.56}$$

with (7.44) giving

$$\varphi(z(t), t) = \varphi(t) = \frac{1}{2}c_1 t + \frac{1}{2}c_1 c_2 + 1. \tag{7.57}$$

After applying the initial conditions $z(0) = z_0, \varphi(0) = \varphi_0(z_0)$, the solution becomes

$$z(t) = \ln\left(e^{-z_0}t^2(\varphi_0(z_0)^2 - \varphi_0(z_0)) + t(2\varphi_0(z_0) - 1) + e^{z_0}\right), \tag{7.58}$$

$$\varphi(z_0, t) = e^{-z_0}t(\varphi_0(z_0)^2 - \varphi_0(z_0)) + \varphi_0(z_0). \tag{7.59}$$

By eliminating z_0 from (7.58-7.59), we obtain $\varphi = \varphi(z, t)$; in other words, the solution φ only depends on the height z at time t. In the specific case where $\varphi_0(z_0) = \varphi_0 = const.$, the solution

for $\varphi(z,t)$ is

$$\varphi(z,t) = \frac{2t(\varphi_0^2 - \varphi_0)}{e^z - t(2\varphi_0 - 1) + \sqrt{e^{2z} - 2e^z t(2\varphi_0 - 1) + t^2}} + \varphi_0, \tag{7.60}$$

with the positive square root chosen so that at $t = 0,\ z = z_0$ in equation (7.58). The solution (7.60) gives the solution on the interior between the boundary shocks.

To find the shock that propagates inward initially from $z = 0$, we use equation (7.51):

$$\frac{dz_-}{dt} = e^{-z_-}\varphi(z_-(t), t), \quad z_-(0) = 0. \tag{7.61}$$

Similarly, for the shock propagating inward initially from $z = 1$, equation (7.52) gives the ODE

$$\frac{dz_+}{dt} = e^{-z_+}(\varphi(z_+(t), t) - 1), \quad z_+(0)1. \tag{7.62}$$

The solutions $z_-(t)$ and $z_+(t)$ are calculated numerically from (7.61) and (7.62) using ODE45 in MATLAB.

The two shocks meet when $z_-(t) = z_+(t)$. If $\varphi_0 = \frac{1}{2}$, there must be an equal amount of small and large particles, meaning $z = z^* = \frac{1}{2}$. Calculating the time to segregation numerically gives $t = t^* \approx 1.781$. In other words, complete segregation occurs after $t = t^* \approx 1.781$ with $\varphi = 0$ if $z > z^* = \frac{1}{2}$ and $\varphi = 1$ if $z < z^* = \frac{1}{2}$. The solution at $t = 0.1, 0.5, 1, 2$ is shown in Figure 7.9 with the evolution of the solution over time shown in Figure 7.10.

Understanding the evolution of $\varphi = \varphi_0 = const.$ with a depth-dependent segregation rate $S(z)$ helps in understanding the full shock wave breaking problem in §7.2 where $\varphi_- > \varphi_+$ on either side of an interface $x = g(z)$

7.3.4 1D Shock Formation

We can also completely determine whether a shock will form in the interior of the domain, much as we have done in §4 and §7.1. Consider (7.5) with initial condition $\varphi(z,0) = \varphi_0(z)$.

Differentiating (7.5) with respect to z gives us an ODE in $\varphi_z = w$,

$$\frac{dw}{dt} = -S''(z)f(\varphi) - 2S'(z)f'(\varphi) - S(z)f''(\varphi)w^2, \tag{7.63}$$

where $\frac{d}{dt} = \partial_t + S(z)f'(\varphi)\partial_z$ is the convective derivative along characteristics. Using (7.9) and substituting into (7.63), we get

$$\frac{dw}{dt} = \left(2\frac{S'(z)^2}{S(z)} - S''(z)\right) f(\varphi) - S(z)f''(\varphi)w^2. \tag{7.64}$$

As in §7.1, if we consider $S(z) = se^{\beta(z-a)},\ a < z < b$, then $2\dfrac{S'(z)^2}{S(z)} - S''(z) > 0$. Since $f(\varphi) < 0$ for $0 < \varphi < 1$, (7.64) becomes the inequality

$$\frac{dw}{dt} \leq -S(z)f''(\varphi)w^2. \tag{7.65}$$

Since $S(z),\ f''(\varphi)$ are bounded away from zero on a finite domain, $\dfrac{dw}{dt} \leq -Kw^2$ with $K = \min|S(z)f''(\varphi)| > 0$. Thus, by comparison, the solution for w satisfies the inequality

$$w \leq \frac{w_0}{1 + Kw_0 t}. \tag{7.66}$$

From here, we see that if $w_0 < 0$, then $w = -\infty$ at the latest when $t = -\dfrac{1}{Kw_0}$; a shock forms on the interior of the domain. If $w_0 > 0$, then $w \to 0$ as $t \to \infty$; the solution remains smooth on the interior of the domain for all time until the boundary shocks meet and form a completely segregated material. These results coincide with the two dimensional shock formation problem from §4 and §7.1 where $v = 0$ along the w-axis. This makes sense, since $v = \varphi_x = 0$ along the w-axis, and thus the two dimensional problem simply becomes the one dimensional problem.

Chapter 8

Conclusions

In this thesis, we have studied granular segregation using the Gray-Thornton PDE model. Specifically, we have investigated the formation and breaking of concentration shocks in the two dimensional version of the model. We considered both linear and nonlinear parallel bulk velocity profiles (and thus constant and depth-dependent segregation rates) in shock formation and breaking.

In the case of a linear parallel bulk velocity profile with smooth initial data, we can completely determine the formation of concentration shocks away from the boundaries by characterizing the initial data. We found an explicit solution to the ODE system for the gradient of the concentration of small particles derived from the Gray-Thornton model. Additionally, we provided a theorem that determines the exact time a concentration shock forms. A specific example, along with numerical simulations verify the analysis for this case. Since that analysis for the formation of shocks in nonlinear hyperbolic systems in multiple dimensions has mainly been restricted to scalar equations with constant coefficients, one of the novelties of our approach is the fact that the coefficient for the downslope transport term (the parallel bulk velocity $u(z)$) is non-constant.

The analysis of the shock formation problem is more complicated for a nonlinear parallel bulk velocity with a depth-dependent segregation rate. This results from the fact that φ is no longer

constant on characteristics, and we get an ODE system in four variables that reduces to two under a linear parallel bulk velocity. In this case, an explicit solution for $\nabla\varphi = (\varphi_x, \varphi_z) = (v, w)$ cannot be found. Instead, we consider the four quadrants of the (v, w) plane; for three of the quadrants, we can determine whether a shock will form or not, but no determination can be made about the exact time a shock starts to form. Determining if a shock forms in the last quadrant remains an open problem.

It is important to know what happens to a shock after it has formed. We proved a theorem that determines the stability of the shock; if the shock is stable, it simply propagates and evolves according to the PDE model. However, if a stable shock loses stability, a mixing region will result. Under an increasing linear parallel bulk velocity, a stable monotonically decreasing shock (in the height) that separates two constant values of φ will have a singularity form at one point. As the shock evolves further, a portion of the shock becomes unstable and a mixing region forms. We found an explicit solution for the structure of the resulting mixing zone for short time. This initial structure for the mixing region then develops singularities at the endpoints; shocks form near these endpoints and the structure of the mixing region changes. The solution to the new structure cannot be determined exactly; instead, we presented a numerical approximation to the solution. The mixing zone undergoes one further change to its structure, where the solution was found using the same numerical procedure.

When the parallel bulk velocity is nonlinear, and monotonically increasing, a singularity in the shock still forms typically at one point, but analysis of the resulting short time mixing zone becomes more complicated. All results for the mixing zone employed a general convex flux function $f(\varphi)$ with $f(0) = f(1) = 0$. In the case where the shear rate was still assumed to be constant, we showed that the evolved shock has a maximum and minimum (in x) near the point of singularity that determined the endpoints of the mixing region. Since φ is still constant along characteristics, the method of characteristics let us determine explicit formulae for the contours of the mixing region between the endpoints.

If the segregation rate is depth-dependent (i.e. non-constant), we consider two cases. In the

first case, the constant values of φ on either side of the initially stable shock are taken to be $\varphi_- = 1$ and $\varphi_+ = 0$. Here, φ_- and φ_+ remain the same, since they satisfy the appropriately modified Gray-Thornton model. As a result, analysis is somewhat simplified by the fact that φ can be explicitly determined on either side of the evolved interface. However, determining an explicit solution for the structure of the mixing zone is impossible, but it can be shown that a smooth mixing zone exists for short time. Numerical simulations verify the existence of the mixing region.

Finally, when the velocity profile is nonlinear and increasing with a depth-dependent segregation rate, and for φ_- and φ_+ are constant with $\varphi_- > \varphi_+$, we rely solely on numerical simulations to show the existence of the mixing zone. Analysis becomes extremely difficult due to the fact that φ_- and φ_+ evolve along with the mixing zone. Thus, finding φ along either side of the evolved interface and on the boundaries of the mixing region is extremely difficult at this point.

However, some headway in understanding the evolution of these initially constant regions is made when we consider a two dimensional inclined plane, where the initial data is uniform in the downslope direction. We considered a depth-dependent segregation rate, first with constant initial data φ_0 (to understand the φ_- and φ_+ constant case in shock breaking), and then with general initial data that is uniform in the downslope direction. An explicit solution is found in both cases, including propagation of the shocks that form near the boundaries.

8.1 Future Directions

The work in this thesis can be extended in several different ways. Some two dimensional extensions in shock breaking include considering a completely vertical initial interface, an infinite segregation rate or multiple singularities in the initial interface. See [22, 44, 66] for preliminary results on these issues. Additionally, when considering the simplest case of the shock breaking problem, we have only explored up to the point where the mixing region reaches the boundary. However, the problem could be extended beyond that time, and the structure of the mixing zone

could be explored. The ultimate goal would be to determine if the mixing region settles down to a steady state [23, 58]. This could be applied to the generalizations of the mixing zone problem from §7.2 as well. We could also consider the problem of shock formation for the full three dimensional model. Similar techniques would likely apply when analyzing shock formation, but the analysis would certainly be more complicated. Finally, in any amount of dimensions we can consider problems where the bulk velocity is time-dependent. Some initial investigations into a non-local rheology for granular flows for a sample with only a single particle size suggests that the bulk velocity ($u(z)$ in the two dimensional case) may actually be dependent on the volume fraction of the sample [50] . Thus, as the concentration of small particles φ is changing, the volume fraction of the sample is changing, meaning the bulk velocity is changing over time. As the volume fraction increases, the bulk velocity increases proportional to the square root of the volume fraction and similarly for decreasing volume fraction.

In the case of a vertical interface separating two constant values of φ, an exact solution for the mixing region has already been determined when the velocity profile is an increasing linear function, the segregation rate is constant, and $\varphi_- = 1,\ \varphi_+ = 0$ [44]. However, no work has been done to find the short time solution for the mixing region resulting from a vertical interface when any or all of the following modifications to the problem are made:

- The flux function is generalized to any convex flux with $f(0) = f(1) = 0$
- The velocity profile is any increasing, nonlinear velocity profile
- The segregation rate is depth-dependent
- The values on either side of the interface are general constants, with $0 < \varphi_+ < \varphi_- < 1$.

In the case of a Couette cell configuration as in [41, 42, 43], we could consider two of these modifications at once: an exponential velocity profile and a corresponding depth-dependent segregation rate. Additionally, we could assume the flux function is generalized. It would be important to study this particular solution since it is experimentally possible to observe this

using the Couette cell in [41, 43], where comparisons could be made between the analytic or numerical solution and the experiment itself.

For the case of infinite segregation rate where an interface η separates all small particles on the left of the interface from all large particles on the right, the problem is shown to be one dimensional [22]. The interface transport equation is given by

$$\frac{\partial \eta}{\partial t} + u(\eta)\frac{\partial \eta}{\partial x} = 0 \tag{8.1}$$

where $u(\eta)$ is the non-dimensional downslope velocity, taken to be increasing and linear. Gray and Kokelaar go on to show that the decreasing interface steepens, becomes vertical, and remains vertical and is transported (much like a decreasing shock in Burger's equation) at the same speed as the two dimensional mixing region [66]. However, they do not consider other increasing velocity profiles, or different constant values of φ on either side of the interface, which would be important to compare to the lens speeds from the corresponding two dimensional, finite segregation rate problem.

Additionally, Gray and Kokelaar consider a piecewise constant interface, where each piece is separated by a vertical shock. They show that the propagation speeds of the shocks correspond to the propagation speeds in the multiple lens interaction studied in [66]. However, once again, they can generalize by considering other velocity profiles, concentrations of φ on either side of the shocks, and in the multiple lens problem from [66], generalized segregation rates. The reason it is important to consider the multiple lens interaction, is that in real avalanches, it is certainly possible that the decreasing interface is not solely given by $g(z)$ with conditions (5.9). Instead, each lens in the multiple lens interaction problem will satisfy (5.9) locally.

For the shock breaking problem in §5, the solution is only given up until $Q_\pm$ reach the boundary. However, it should be possible to determine the structure past this time. The shocks that start at $Q_\pm$ will change due to the interactions with the boundaries; the point $Q_\pm$ will travel along the boundary back toward the center of the lens, making the lens appear as if it is trying to tilt in a new direction. Simulations show the lens wobbles back and forth, and it

is an interesting question as to whether the wobbling will continue indefinitely, or if the solution will settle down to a steady state.

The full three dimensional model considers an avalanche flowing down a hillside, where the bulk velocity is in the x-direction and depends on both the height z and the width y. Segregation will occur in both the lateral and normal directions (y and z), with possibly different fluxes ($f_1(\varphi)$ and $f_2(\varphi)$) in each direction. The three dimensional PDE model then becomes

$$\frac{\partial \varphi}{\partial t} + u(y,z)\frac{\partial \varphi}{\partial x} + S_y \frac{\partial}{\partial y}\left(\left|\frac{\partial}{\partial y}u(y,z)\right| f_1(\varphi)\right) + S_z \frac{\partial}{\partial z}\left(\left|\frac{\partial}{\partial z}u(y,z)\right| f_2(\varphi)\right) = 0 \tag{8.2}$$

with no flux boundary conditions in y and z. For the problem of shock formation, we would consider a smooth initial condition $\varphi(x,y,z,0) = \varphi_0(x,y,z)$. The goal would be to apply similar techniques as used in §4 and §7.1 to classify from what initial data an interior shock forms.

To generalize the two dimensional model with a time-dependent parallel bulk velocity, one must simply change the velocity profile, which in turn will have an affect on the segregation as well. Since the volume fraction of the material may be different at different locations downslope, the velocity will not only change in time, but may change in x as well:

$$\varphi_t + (u(x,z,t)\varphi)_x + (S(x,z,t)f(\varphi))_z = 0. \tag{8.3}$$

In many cases, the material will proceed from mixed to segregated, meaning the volume fraction of the material is generally decreasing in time (as it is more packed in the fully mixed state). Thus, a simple assumption can be made that the velocity will decrease, i.e., $\dfrac{\partial}{\partial t}u(x,z,t) < 0$. However, if the material has not fully been mixed yet, then we assume the volume fraction increases until some time $t = T$ when the sample is most mixed. In this case, $\dfrac{\partial}{\partial t}u(x,z,t) > 0$ for $t < T$ and $\dfrac{\partial}{\partial t}u(x,z,t) < 0$ for $t > T$. For problems where the material is uniform in x, we simply drop of the x term in (8.3) and $S(x,z,t) = S(z,t)$ becomes independent of x as well.

A possible three imensional model could accompany this as well. There would be small stress fluctuations in the y-direction, meaning some velocity is present in the y-direction. The

model then becomes

$$\begin{aligned}
&\frac{\partial \varphi}{\partial t} + \frac{\partial}{\partial x}(u(x,y,z,t)\varphi) + \varepsilon \frac{\partial}{\partial y}(v(x,y,z,t)\varphi) \\
&+S_y \frac{\partial}{\partial y}\left(\left(\left|\frac{\partial}{\partial y}u(x,y,z,t)\right| + \varepsilon \left|\frac{\partial}{\partial y}v(x,y,z,t)\right|\right) f_1(\varphi)\right) \\
&+S_z \frac{\partial}{\partial z}\left(\left(\left|\frac{\partial}{\partial z}u(x,y,z,t)\right| + \varepsilon \left|\frac{\partial}{\partial z}v(x,y,z,t)\right|\right) f_2(\varphi)\right) = 0
\end{aligned} \tag{8.4}$$

where $\varepsilon << 1$ indicating the fluctuations in the y-direction are small in relation to the velocity downslope. Ignoring the transverse fluctuations (i.e., $\varepsilon = 0$), the model becomes similar to (8.2), but with $u = u(x,y,z,t)$ instead of $u = u(y,z)$.

REFERENCES

[1] C. Ancey, P. Coussot, and P. Evesque. Examination of the possibility of a fluid-mechanics treatment of dense granular flows. *Mech. Cohesive-Frictional Materials*, 1:385–403, 1996.

[2] I. S. Aranson and L. s. Tsimring. Patterns and collective behavior in granular media: Theoretical concepts. *Reviews of Modern Physics*, 78:641–692, 2006.

[3] P. Bertran. The rock-avalanche of February 1995 at Claix (French Alps). *Geomorphology*, 54:339–346, 2003.

[4] J. Bridgewater. Fundamental powder mixing mechanisms. *Powder Techol.*, 15:215–236, 1976.

[5] J. Bridgewater, W. S. Foo, and D. J. Stephens. Particle mixing and segregation in failure zons - theory and experiment. *Powder Techol.*, 41:147–158, 1985.

[6] E. S. Calder, R. S. J. Sparks, and M. C. Gardeweg. Erosion, transport and segregation of pumice and lithic clasts in pyroclastic flows inferred from ignimbrite at Lascar Volcano, Chile. *J. Volcan. and Geotherm. Res.*, 104:201–235, 2000.

[7] E. D. Conway. The formation and decay of shocks for a conservation law in several dimensions. *Arch. Rat. Mech. Anal.*, 64:47–57, 1977.

[8] M. H. Cooke, D. J. Stephens, and J. Bridgewater. Powder mixing - a literature survery. *Powder Techol.*, 15:1–20, 1976.

[9] J. E. Costa and G. Williams. Debris flow dynamics. *U.S. Geological Survey, Open-File Report*, pages 84–606, 1984.

[10] D. M. Cruden and O. Hungr. The debris of the Frank slide and theories of rock slide avalanche mobility. *Canadian Journal of Earth Science*, 33(3), 1986.

[11] A. Daerr. Dynamical equilibrium of avalanches on a rough plane. *Phys. Fluids*, 13, 2115-2124.

[12] A. Daerr and S. Douady. Two types of avalanche behaviour in granular media. *Nature*, 399, 241-243.

[13] A. J. C. de Saint-Venant. Théorie du mouvement non-permanent des eaux, avec application aux crues des rivières et à l'introduction des marées dans leur lit. *C. R. Acad. Sc.*, 73:147–154, 1871.

[14] J. A. Drahun and J. Bridgewater. The mechanisms of free surface segregation. *Powder Technol.*, 36, 39-53.

[15] J. Duran. *Sand, Powders, and Grains: An Introduction to the Physics of Granular Materials.* Springer, New York, 2000.

[16] T. Erismann. Flowing, rolling, bouncing, sliding: Synopsis of basic mechanisms. *Acta Mech.*, 64:101–110, 1986.

[17] S. K. Godunov. A difference scheme for numerical solutions of discontinuous solutions of hydrodynamic equations. *Math. Sbornik*, 47:271–306, 1959.

[18] J. Goguel. Scale dependent rock slide mechanisms. *Rockslides and Avalanches*, 1:167–180, 1978.

[19] L. A. Golick and K. E. Daniels. Mixing and segregation rates in sheared granular materials. *Physical Review E.*, 80:042301, 2009.

[20] J. M. N. T. Gray. Granular flow in partially filled slowly rotating drums. *J. Fluid Mech.*, 441:1–29, 2001.

[21] J. M. N. T. Gray and V. A. Chuganov. Particle-size segregation and diffusive remixing in shallow granular avalanches. *J. Fluid Mech.*, 569:365–398, 2006.

[22] J. M. N. T. Gray and B. P. Kokelaar. Large particle segregation, transport, and accumulation in granular free-surface flows. *J. Fluid Mech.*, 652:105–137, 2010.

[23] J. M. N. T. Gray and A. R. Thornton. A theory for particle size segregation and shallow granular free-surface flows. *Proc. Roy. Soc. A*, 461:1447–1473, 2005.

[24] Gotechnique. Experiments on the flow behavior of granular materials at high velocity in an open channel. *Ind. Engeng. Chem. Fundam.*, 34:405–413, 1984.

[25] A. Heim. Der Bergsturz von Elm. *Deutsch Geol. Gesell. Zeitschrift*, 34:74–115, 1882.

[26] A. Heim. Bergsturz und Menscheleben. *Beiblatt zur Vierteljahresschrift der Natf. Ges. Zurich*, 20:1–218, 1932.

[27] K. Hsu. Albert Heim: Observations on landslides and relevance to modern interpretations. *Rockslides and Avalanches*, 1:69–93, 1978.

[28] R. M. Iverson. The physics of debris-flows. *Reviews in Geophysics*, 35:245–296, 1997.

[29] R. M. Iverson. The debris-flow rheology myth. *Debris-Flow Hazards Mitigation: Mechanics, Prediction, and Assessment*, pages 303–314, 2003.

[30] R. M. Iverson. Debris-flow mechanics. *Debris-Flow Hazards and Related Phenomena*, pages 105–134, 2005.

[31] R. M. Iverson and J. W. Vallance. New views of granular mass flows. *Geology*, 29(2):115–118, 2001.

[32] H. M. Jaeger, S. R. Nagel, and R. P. Behringer. Granular solids, liquids, and gases. *Reviews of Modern Phys.*, 68(4):1259–1273, 1996.

[33] J. T. Jenkins and F. Mancini. Balance laws and constitutive relations for plane flows of a dense, binary mixture of smooth nearly elastic circular disks. *J. Appl. Mech.*, 54:27–34, 1987.

[34] F. John. Formation of singularities in one-dimensional nonlinear wave propagation. *Comm. Pure Appl. Math*, 27:277–405, 1974.

[35] V. Jomelli and P. Bertran. Wet snow avalanche deposits in the French Alps: Structure and sedimentology. *Geografiska Annaler. Series A, Physical Geography*, 83(1/2):15–28, 2001.

[36] P. Jop, Y. Forterre, and O. Pouliquen. A constitutive law for dense granular flows. *Nature*,

441:727–730, 2006.

[37] P. E. Kent. The transport mechanism in catastrophic rock falls. *J. Geol.*, 74:79–83, 1965.

[38] P. D. Lax. Hyperbolic systems of conservation laws II. *Comm. Pure Appl. Math*, 10:537–566, 1957.

[39] R. J. LeVeque. *Finite Difference Methods for Ordinary and Partial Differential Equations*. 2007, publisher=SIAM.

[40] A. Majda. *Compressible Fluid Flow and Systems of Conservation Laws in Several Space Dimensions*. Springer-Verlag, 1984.

[41] L. B. H. May. Shear-Driven Particle Size Segregation: Models, Analysis, Numerical Solutions, and Experiments. 2009.

[42] L. B. H. May, K. Phillips, L. A. Golick, M. Shearer, and K. E. Daniels. Shear-driven particle-size segregation of granular materials: comparison of theory, modeling, and experiment. 2009.

[43] L. B. H. May, M. Shearer, and K. E. Daniels. Scalar conservation laws with nonconstant coefficients with application to particle size segregation in granular flow. *J. Nonlinear Science*, 2010.

[44] M. McIntyre, E. L. Rowe, M. Shearer, J. M. N. T. Gray, and A. R. Thornton. Evolution of a mixing zone in granular avalanches. *Appl. Math Res. Express*, 2007:12 pages, 2007.

[45] G. Metcalfe, T. Shinbrot, J. J. McCarthy, and J. M. Ottino. Avalanche mixing of granular solids. *Nature*, 374:39–41, 1995.

[46] L. W. Morland. Flow of viscous fluids through a porous deformable matrix. *Surv. Geophys.*, 13:209–268, 1992.

[47] T. C. Pierson. Flow behavior of channelized debris flows, Mount St. Helens, Washington. *Hill Slope Processes, A. D. Abrahams (ed.)*, pages 269–296, 1986.

[48] O. Pouliquen. Scaling laws in granular flows down rough inclined planes. *Phys. of Fluids*, 11(3):542–548, 1999.

[49] O. Pouliquen and Y. Forterre. Friction law for dense granular flows: application to the motion of a mass down a rough iclined plane. *J. Fluid Mech.*, 453:133–151, 2002.

[50] O. Pouliquen and Y. Forterre. A non-local rheology for dense granular flows. *Phil. Trans. R. Soc. A*, 367:5091–5107, 2009.

[51] W. Rankine. On the stability of loose earth. *Phil. Trans. of the Royal Soc. of London*, 147:9–27, 1857.

[52] H. Roethlisberger. Destructive power of glaciers. *Switzerland and Her Glaciers, From the Ice Age to the Present*, pages 128–165, 1981.

[53] E. L. Rowe. Application of Godunov's method to particle-size segregation in granular avalanches. 2005.

[54] S. B. Savage. The mechanics of rapid granular flows. *Advances in Appl. Mech.*, 24:289–366, 1984.

[55] S. B. Savage and K. Hutter. The motion of a finite mass of granular material down a rough incline. *J. Fluid Mech.*, 199:177–215, 1989.

[56] S. B. Savage and C. K. K. Lun. Particle size segregation in inclined chute flow of dry cohesionless granular solids. *J. Fluid Mech.*, 189:311–335, 1988.

[57] D. Serre. *Systems of Conservation Laws. 2. Geometric Structures, Oscillations, and Initial-Boundary Value Problems*. Cambridge Univ. Press, 2000.

[58] M. Shearer, J. M. N. T. Gray, and A. R. Thornton. Stable solutions of a scalar conservation law for particle size segregation in dense granular avalanches. *European Journal of Appl. Math*, 19:61–86, 2008.

[59] T. Shinbrot, A. Alexander, and F. J. Muzzio. Spontaneous chaotic granular mixing. *Nature*, 397:675, 1999.

[60] T. Shinbrot and F. J. Muzzio. Nonequilibrium patterns in granular mixing and segregation. *Phys. Today*, March:25–30, 2000.

[61] R. L. Shreve. Sherman landslide, Alaska. *Science*, 154:1639–1643, 1966.

[62] R. L. Shreve. The Blackhawk landslide. *Geol. Soc. Am., Spec. Paper*, 108:47, 1968.

[63] W. R. Strauss. *Partial Differential Equations: An Introduction*. John Wiley & Sons, Inc., 1992.

[64] A. Suzuki and T. Tanaka. Measurement of flow properties of powders along an inclined plane. *Ind. Engeng. Chem. Fundam.*, 10:84–91, 1971.

[65] Diamondback Technology. Process manufacturing: Practical steps to reduce particle segregation. `http://www.chemicalprocessing.com/articles/2005/482.html`.

[66] A. R. Thornton and J. M. N. T. Gray. Breaking size segregation waves and particle recirculation in granular avalanches. *J. Fluid Mech.*, 596:261–284, 2008.

[67] C. Truesdell. *Rational Thermodynamics*. Berlin: Springer, 1984.

[68] J. W. Vallance. Experimental and field studies related to the behavior of granular mass flows and the characteristics of their deposits. 1994.

[69] J. W. Vallance. Encyclopedia of Volcanoes. *Lahars*, pages 601–616, 2000.

[70] B. A. Wills. *Mineral Processing Technology*. New York: Pergamon, 1979.

[71] H. Xu, M. Louge, and A Reeves. Solutions of the kinetic theory for bounded collisional flows. *Contin. Mech. Thermodyn.*, 15:321–349, 2003.